This is to certify that the

thesis entitled

DEHYDRATION OF D-GLUCITOL USING
Ca Y AND Pt/Ca Y ZEOLITE CATALYSTS

presented by

Gregory Alan Kudlac

has been accepted towards fulfillment
of the requirements for

M.S. degree in CHE

Dennis J Miller
Major professor

Date 7/21/88

DEHYDRATION OF D-GLUCITOL USING Ca Y AND Pt/Ca Y ZEOLITE CATALYSTS

By

Gregory Alan Kudlac

A Thesis

Submitted to
Michigan State University
in partial fulfillment of the requirements
for the degree of

MASTER OF SCIENCE

Department of Chemical Engineering

1988

ABSTRACT

DEHYDRATION OF D-GLUCITOL USING
Ca Y AND Pt/Ca Y ZEOLITE CATALYSTS

By

Gregory A. Kudlac

A process has been developed for the catalytic dehydration of D-glucitol. This dehydration is achieved using Ca Y and Pt/Ca Y zeolite catalysts. The advantage of using these catalysts is that essentially complete conversions of D-glucitol were obtained. In addition, the shape selectivity of the catalysts limited the number of products formed.

Several batch reactions were carried out with decahydronaphthalene as a solvent under varying conditions which included a temperature range of 180-260 ^{o}C and a H_2 pressure range of 160-900 psi.

The catalytic activity observed was primarily dehydration and dehydrogenation, with some isomerization. Main products formed were 1,4:3,6-dianhydro-D-glucitol, 1,4-anhydro-D-glucitol and 3,5,6-trihydroxy-3-hexen-2-one.

To my parents, John and Patricia Kudlac, for their undying and boundless support throughout my education, and to my fianceé, Maureen Dorsey, whose emotional support has been instrumental in my success.

ACKNOWLEDGEMENTS

The author wishes to thank Dr. Dennis J. Miller for his support and guidance during all aspects of this project; Miss Lynn Frostman for her excellent HPLC analyses; and especially Mr. Douglas Gage and Ms. Betty Baltzer for their immeasurable assistance interpreting the mass spectrometry data.

TABLE OF CONTENTS

LIST OF TABLES

LIST OF FIGURES

CHAPTER 1

BACKGROUND AND INTRODUCTION

A. BIOMASS CONVERSION PATHWAYS

Investigation into the use of biomass materials as a potential source of energy has been both widespread and varied, and can be divided into two main areas of interest: 1) the direct use of biomass as an energy source, and 2) converting or thermally upgrading the biomass to a fuel which can be used as a substitute for fossil fuels.

Combustion is the primary method in which biomass is directly converted to energy and simply involves burning the biomass, using air as the oxidant. The chemistry of complete oxidation of materials containing mainly carbon, oxygen and hydrogen is:

$$C_xH_yO_z \text{ (biomass)} + (x + y/4 - z/2)\ O_2 \text{ ------->}$$

$$x\ CO_2 + y/2\ H_2O$$

where x, y and z represent the mean elemental composition of the biomass [1]. Incomplete oxidation of the biomass

yields carbon, carbon monoxide, hydrocarbons, and other gases as by-products and the heat of the reaction is reduced. Nitrogen and other impurities present in the biomass are converted to gases and ash.

Conversion or thermal upgrading of biomass by a combination of heat and partial combustion yields a variety of solids, liquids and gases with at least some of the properties of coal, oil and natural gas. Major processes in this area include pyrolysis, gasification, liquefaction and hydrolysis. These processes, with the exception of hydrolysis, are related to each other as can be seen in Figure 1.

Pyrolysis involves the heating of the biomass in the absence of an oxidizing agent such as O_2 or air. Above 100 ^{o}C, the biomass begins to decompose and between 250 and 600 ^{o}C the main products are charcoal and an oily acidic mixture of tar and variable quantities of methanol, acetic acid, acetone and traces of other organic molecules. An empirical example of a pyrolysis reaction scheme is given below [1]:

Charring reaction

$$(C_6H_{10}O_5)n \text{ ------> } 6n\ C + 5n\ H_2O$$

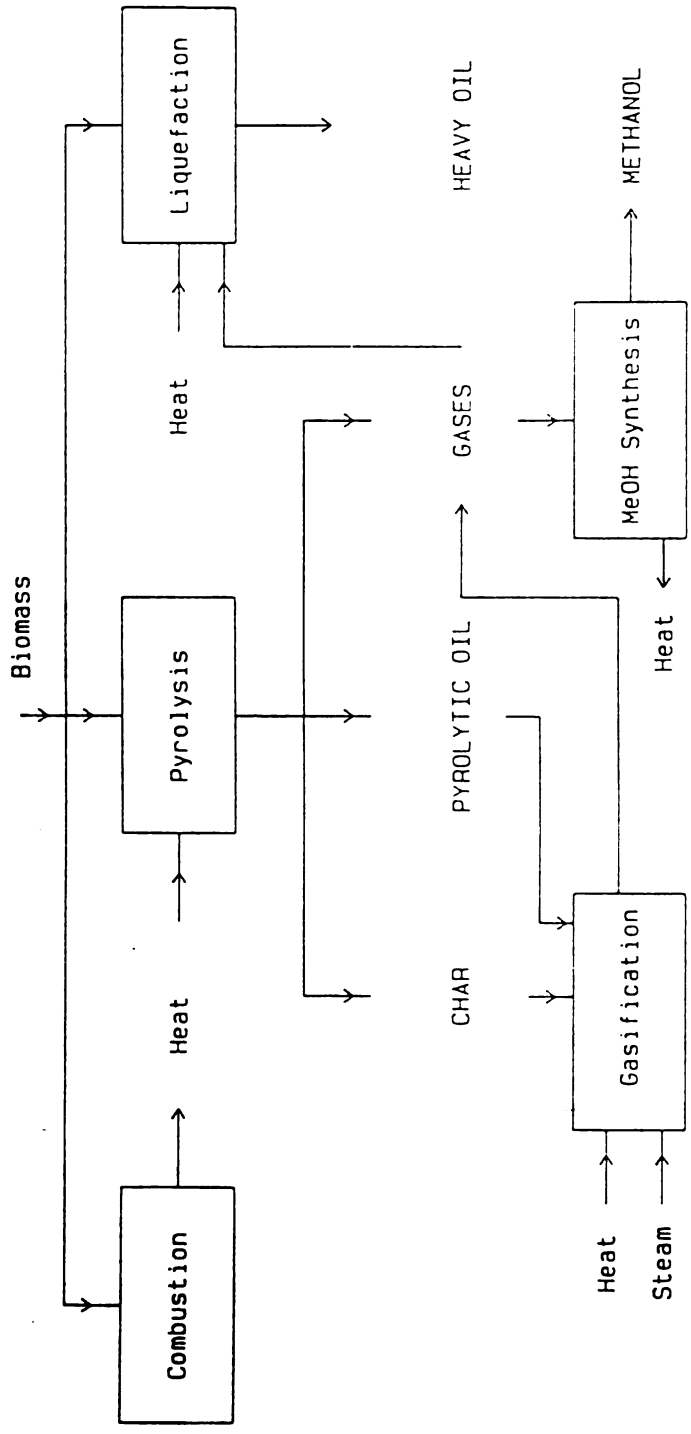

Figure 1. Biomass Conversion Pathways [1]

Oil Formation

$$(C_6H_{10}O_5)n \text{ ------> } 0.8n\ C_6H_8O + 1.8n\ H_2O + 1.2n\ CO_2$$

(where C_6H_8O is assumed as a mean composition of the oil)

In a "flash pyrolysis" system, the biomass is heated rapidly and produces olefins

$$(C_6H_{10}O_5)n \text{ ------> } 2n\ C_2H_4 + n\ H_2O + 2n\ CO_2. \quad [1]$$

Gasification of biomass with oxygen yields a medium energy gas containing mainly carbon monoxide and hydrogen. The chemistry of gasification involves the reaction of pyrolysis char with steam or carbon dioxide to form synthesis gas [1]:

$$C + H_2O \text{ ------> } CO + H_2$$

$$C + CO_2 \text{ ------> } 2CO$$

Above 1000 ^{o}C, the only stable products are carbon monoxide and hydrogen whereas at lower temperatures ethylene, methane and other low molecular weight molecules are stable.

In liquefaction processes, the biomass is converted to a liquid similar to heavy fuel oil by reacting it with carbon monoxide and hydrogen (generally obtained from a

separate pyrolysis or gasification process) in the presence of a catalyst under high temperatures and pressures. A typical liquefaction process is given by the Pittsburgh Energy Center [1]:

$$0.61(C_6H_{9.13}O_{4.33}) + 0.23\ CO + 0.08\ H_2 \text{ ------>}$$

biomass

$$H_2O + 0.64\ CO_2 + 0.53\ (C_6H_{6.93}O_{1.22})$$

liquefaction oil

The final process, hydrolysis, differs from the previous methods in that biomass materials such as cellulose, hemicellulose and starch are reacted only to monosaccharides such as glucose, fructose and xylose. This reaction proceeds according to the following stoichiometry:

$$-(C_6H_{10}O_5)_n- + n\ H_2O \text{ ------> } n\ C_6H_{12}O_6.$$

The ease of this hydrolysis reaction varies considerably depending on the material used. Starches and pentosans (hemicelluloses) require relatively mild conditions using dilute acids and medium temperatures, whereas cellulose needs higher temperatures, stronger acids and pressurized reactors [1]. These monomeric sugars may then be fermented to ethanol and carbon dioxide using a variety of microorganisms.

As will be shown in the next section, these monomeric sugars may be further reacted to form polyols, or alditols, which represent the starting material for the proposed scheme of forming hydrocarbons from biomass materials.

B. PROPOSED REACTION SEQUENCE

The following reactions represent the proposed pathway for converting biomass materials to hydrocarbons via inorganic heterogeneous catalysts:

Sugar Formation

$$\text{Biomass (cellulose)} \xrightarrow[\text{hydrolysis}]{} \text{Sugars and Oligomers} \quad (1)$$

Alditol Formation

$$\text{Sugars (e.g. D-Glucose)} \xrightarrow[\text{metal catalyst}]{H_2} \text{Alditols (D-Glucitol)} \quad (2)$$

Dehydration Reaction

$$\text{Alditol} \xrightarrow[\text{acid catalyst}]{-H_2O} \text{"Polyhydroxylated Olefin"} \quad (3)$$

Hydrogenation Reaction

$$\text{"Polyhydroxylated Olefin"} \xrightarrow[Pt]{H_2} \text{"Lower Polyol"} \quad (4).$$

Reactions (3) and (4) are carried out successively and can be summarized as follows:

$$\text{"Polyhydroxylated Olefin"} \xrightarrow[\text{hydrogenation}]{\text{dehydration}} \text{Hydrocarbons} \quad (5).$$

In reactions (3), (4) and (5), "polyhydroxylated olefin" simply refers to a compound with the formula $C_6H_{12}O_5$ with the departure of one water molecule generating a carbon-carbon double bond or ring structure. In reaction (4), "lower polyol" refers to a compound with the formula $C_6H_{14}O_5$ and is the saturated form of the corresponding "polyhydroxylated olefin".

The next two sections review literature dealing with the direct inorganic catalytic conversion of biomass and the various reactions occurring in the proposed pathway, except for the hydrolysis reaction which has been previously discussed.

C. DIRECT CONVERSION

The papers reviewed in this section present processes in which the starting carbohydrate material is reacted directly to hydrocarbons in the presence of a catalyst.

United States Patent 4,430,253 [2] describes a process in which a hydrogenation catalyst and a sulfide-modified

ruthenium catalyst are used sequentially under batch conditions. The first stage involves hydrogenating the starting material, such as glucose, to the polyol corresponding to the same chain length, i.e. sorbitol, in the presence of the hydrogenation catalyst. The second stage is carried out in the presence of the sulfide-modified ruthenium catalyst. This hydrogenolysis reaction results in the formation of shorter chain length polyols such as ethylene glycol and 1,2-propylene glycol. It is reported that by using the sulfide-modified ruthenium catalyst a greater range of temperatures and a higher degree of selectivity is possible when compared with a traditional hydrogenation catalyst.

In United States Patent 4,401,823 [3] a catalyst comprising of "a carbonaceous pyropolymer possessing recurring units containing at least carbon and hydrogen atoms" and impregnated with a transition metal is used for the hydrogenolysis of carbohydrates to a variety of products. In this process the catalyst used is prepared by treating an inorganic support material such as alumina with an organic pyrolyzable compound at high temperatures. This results in the decomposition and polymerization of the organic material on the surface of the inorganic support. This inorganic support material is then chemically leached from the pyropolymer. The pyropolymer is then impregnated with an aqueous solution of one of several transition metals. Use of this catalyst in reacting carbohydrate

compounds such as sucrose, glucose and lactose under batch conditions resulted in the formation of a variety of products including alcohols, acids, ketones, ethers, and hydrocarbons.

Finally, United States Patent 4,503,278 [4] presents a process in which carbohydrates such as starch, cellulose and glucose are converted into hydrocarbons using a crystalline zeolite catalyst such as ZSM-5. These catalysts, obtained directly from the manufacturer, were used to react the carbohydrates in a fluidized bed reactor and resulted in the formation of carbon monoxide, carbon dioxide, water, and a variety of hydrocarbons, primarily short chain alkanes and alkenes.

In each of these patents, the carbohydrate feed consisted of an aqueous solution of the particular carbohydrate, except for [4] which employed both aqueous solutions of the carbohydrate itself and an aqueous mixture of the carbohydrate and methanol.

D. HYDROGENATION OF CARBOHYDRATES

The papers reviewed in this section discuss processes in which carbohydrates such as glucose and fructose are hydrogenated to the corresponding alditol (e.g. sorbitol).

In United States Patent 4,380,679 [5] the "carbonaceous pyropolymer" discussed in [3] (in this case the impregnated metal is limited to a Group VIII metal) is used

to convert glucose to sorbitol and mannitol. In a series of experiments, this group of catalysts provided very high conversion of the glucose in addition to a high selectivity to sorbitol versus mannitol.

United States Patent 4,380,680 [6] presents a method for hydrogenating carbohydrates in which ruthenium, when dispersed on α-alumina, yields a hydrothermally stable hydrogenation catalyst. The use of this catalyst in the hydrogenation of glucose not only provided high conversion and selectivity of glucose to sorbitol, but also suffered minimal leaching of either the metal or support.

United States Patent 4,382,150 [7] presents a catalyst for the hydrogenation of carbohydrates similar to that in [6] except that the support material used is titanium dioxide and the Group VIII metal is nickel. This catalyst provides the same conversion, selectivity and leaching characteristics as in [6]. In this method, however, it is also shown that the reduction temperature used in the preparation of the catalyst has an affect on the product distribution. For example, when a reduction temperature of 250 ^{o}C is used, 98 percent of the glucose used in the experiment reacted to yield 95 percent sorbitol and 3 percent mannitol. However, when a reduction temperature of 450 ^{o}C is used, only 63 percent of the glucose reacted yielding a product distribution of 44 percent sorbitol, 4 percent mannitol and 27 percent fructose.

Finally, in United States Patent 4,413,152 [8] a

catalyst is presented similar to that used in [6] except that the support material in this case is titanated alumina. This catalyst also affords the same conversion and selectivity characteristics as those in [6] and [7]. In addition, the use of ruthenium instead of nickel results in a lower metal leaching level under hydrogentation condition.

As in section 1.3, all of the carbohydrates used in [5-8] are in aqueous solution and are reacted over fluidized beds except for [5] where the experiments are conducted under batch conditions.

E. DEHYDRATION

The next two reactions in the proposed sequence, dehydrating the alditol and hydrogenating the resulting product(s), represents both the major step in the proposed reaction sequence and the starting point of this research. The papers reviewed in this section discuss the dehydration of alcohols over solid catalysts, and in particular, zeolites. Since the hydrogenating capabilities of Group VIII metals such as platinum is well-documented in the literature, it will be discussed only briefly.

As can be seen in Table 1 [9], numerous studies have been done concerning the dehydration alcohols and diols over solid catalysts. The general reaction scheme for the dehydration of alcohols is given below [10]:

TABLE 1

TYPES OF DEHYDRATION REACTIONS AND CORRESPONDING CATALYSTS [9]

Reactants	Catalysts	Products
Alcohols		
Methanol	Al_2O_3 . Also SiO_2 or Cr_2O_3 or Al_2O_3 activated with oxides of groups 1, 6, 7 & 8	dimethyl ether
2(Alcohol)	synthetic methanol catalyst	higher primary or secondary alcohols
Ethanol	Al_2O_3 . Also Al_2O_3-SiO_2 ; TiO_2 ; Cr_2O_3; W_2O_3 ; SiO_2 ; ZrO_2	ether
Ethanol	Al_2O_3 ; SiO_2 . Also P_2O_5 ; ZrO_2 ; W_2O_3 ; TiO_2 ; K_2CO_3 ; Al_2O_3 with CuO, NiO or Cr_2O_3 ; ThO_2 ; $Mg_3(PO_4)_2$ on coke; H_3PO_4 ; molybdites	ethylene
1-Propanol (propyl alcohol)	Al_2O_3	dipropyl ether
1-Propanol	Al_2O_3	propylene
2-Propanol (isopropyl alcohol)	Al_2O_3 . Also ZnO; $Ca_3(PO_4)_2$; ascanite clay	isopropyl ether + propylene
2-Methyl-1-propanol (isobutyl alcohol)	pumice. Also Al_2O_3	2-methyl-propene (isobutylene) + 1-butene
2-Methyl-2-propanol (tert-butyl alcohol)	pumice. Also $AlPO_4$; Al silicate; $Al_2(SO_4)_3$	2-methyl-propene
1-Butanol	Al_2O_3 . Also Fe_2O_3 + Al_2O_3 ; SiO_2 + TiO_2 ; Na_2PO_3 + bauxite	1-butene (α-butylene)
1-Butanol	H_3PO_4 + Al_2O_3	2-methylpropene
1-Butanol	Al_2O_3	1-butene + *cis*-2-butene + *trans*-2-butene (pseudobutylenes)
2-Butanol (sec-butyl alcohol)	Al_2O_3	1-butene + *cis*-2-butene
Methyl butanols	Al_2O_3	methyl butenes
2-Methyl-2-butanol (tert-amyl alcohol)	Al_2O_3	3-methyl-2-butene (β-isoamylene)
3-Methyl-1-butanol (isoamyl alcohol)	Al_2O_3 . Also Al_2O_3 + additives	isoamyl ether + amylene
1-Pentanol (amyl alcohol)	Al_2O_3 . Also $AlPO_4$	dipentyl ether + pentene

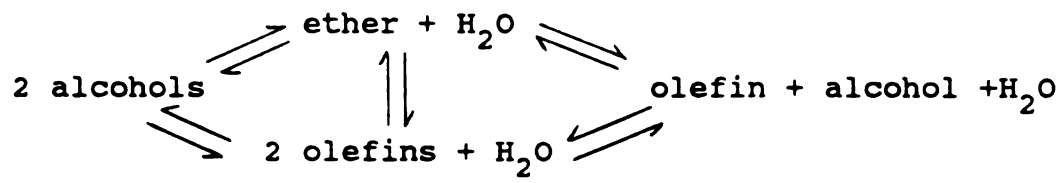

The extent to which each of these reactions paticipates depends on several factors. For example, the structure of the starting alcohol plays a major role. Alcohols which have no β-hydrogens, like methanol or benzyl alcohol, yield only ethers. The tendency for olefin formation increases with the substitution on the α-carbon; with secondary alcohols, the olefin/ether ratio is much higher than with primary and from tertiary alcohols only olefins are formed [10].

Another major factor is the selectivity of the catalyst. This factor is important because a number of solids, especially oxides, can catalyse both the dehydration and dehydrogenation of alcohols. The formation of aldehydes or ketones is then a parallel reaction to the dehydration, and the ratio of the rates depends on the nature of the catalyst [10]. This catalytic selectivity may be varied somewhat depending on the method of catalyst preparation.

For example, Szabo [11] indicated that the dehydrogenation activity increases with the ionic character of the metal-oxygen bond of the catalyst, whereas dehydration activity is enhanced by increased covalent bond character, which is illustrated by the following:

dehydrogenation <----------

CaO MgO ZnO FeO Fe_2O_3 Cr_2O_3 TiO_2 Al_2O_3 SiO_2 WO_3

----------> dehydration

In addition:

> The change in selectivity of the catalyst with gross structure and mode of preparation affords valuable insight into the mechanism of dehydration, dehydrogenation, ether formation, and alkene isomerization. Dehydrogenation is favored at the expense of dehydration in primary and secondary alcohols by methods that increase the crystal size, decrease the surface area, and reduce the catalyst porosity. For example, the dehydrating activity of alumina is decreased when it is heated to high temperatures, a process that causes healing of the irregularities in the crystal lattice. This observation suggests that dehydrogenation is a surface reaction but dehydration occurs within the pores of the catalyst [12].

As an example of this, Weisz and Frilette [13] studied the dehydration of isobutanol in the presence of 1-butanol. They found that an amorphous aluminosilicate catalyst dehydrated both alcohols at comparable rates whereas a Ca A zeolite selectively dehydrated the 1-butanol.

The above information suggests that zeolites, which are crystalline aluminosilicates, highly selective and thermally stable, would be excellent candidates for dehydration catalysts.

Rudham and Stockwell [14] investigated the dehydration of 2-propanol on HY zeolites. Using a continuous-flow reactor under a variety of temperatures, pressures, and extents of ion-exchange (the zeolites were prepared by ion-

exchanging NH_4 for Na and then deammoniating to the HY form), 2-propanol was dehydrated to both propene and di-isopropyl ether.

Ballantine et al. [15] studied the dehydration of a variety of alcohols over sheet silicates (ion-exchanged montmorillonites) under heterogeneous conditions. In contrast with homogeneous acid catalysts, where dehydration to the corresponding alkene is the primary reaction, primary alcohols were found to undergo an intermolecular dehydration reaction to the corresponding di(alk-1-yl) ether with very little formation of the corresponding alkene. Secondary and tertiary alcohols were dehydrated by the normal intramolecular process to the corresponding alkene with very little ether formation.

Chong and Curthoys [16] investigated the vapor-phase decomposition of ethylene glycol over a cation-exchanged mordenite catalyst using a constant flow microreactor system. At atmospheric pressure and using a temperature range of 230 to 500 ^{o}C, the main products of the reaction were acetaldehyde, water, and glycoaldehyde ($HOCH_2CHO$) with dioxane, ethanol, glyoxal (OHC-CHO) and ethylene as minor products.

Minachev et al. [17] used a CaY zeolite in their study of the dehydration of alcohols. Using a flow-reactor system, they found that varying the flow conditions the extent and direction of the reaction could be varied. For example, at 250 ^{o}C and a flowrate of 9.8 moles/liter * hour,

ethanol was dehydrated to an extent of 60% and diethyl ether was found among the reaction products. At a flowrate of 3.8 moles/liter * hour, however, all of the ethanol was converted to ethylene at the same temperature. Similar results were found with other primary and secondary alcohols. In a similar study using CaNaY zeolites [18], Sharf et. al. determined that 1-pentanol was dehydrated faster when the calcium content was increased.

Numerous other studies involving the dehydration of alcohols over zeolites have been conducted [19].

As mentioned previously, the hydrogenating activity of Group VIII metals such as platinum is well-represented in the literature. This catalytic activity has been found to depend on two major properties: the dispersion of the Pt metal on the catalyst and the H/Pt ratio observed during the adsorption of H_2, both of which can be affected by the mode of catalyst preparation. It was originally observed by Rabo et al. [20] that a CaY zeolite ion-exchanged with 0.5% Pt gave a H/Pt ratio of 2 which corresponded to an atomic dispersion of Pt on the zeolite surface. Several subsequent papers, however, have observed that a majority of the atomically dispersed Pt loses its ability to chemisorb hydrogen. Performing hydrogen chemisorption studies on several zeolite-supported Pt catalysts, Kubo et al. [21] observed that while for some of the catalysts the data indicated particle sizes of 1300 Å, electron microscopy data revealed most of the particles were actually 15 Å in

size. This indicated that a large portion of the Pt not detected by E. M. (scanning limit = 10 Å) had lost its ability to chemisorb hydrogen. Similar observations were made by Gallezot et al. [22] using a $PtNaNH_4Y$ zeolite pretreated in O_2 at 600°C and reduced at 300°C. A H/Pt ratio of 0.25 was found for this catalyst while X-ray methods showed that the majority of the platinum was atomically dispersed in the sodalite cages of the zeolite (see Figure 2 [23]). As with the previous paper, it was concluded that these Pt atoms were not able to chemisorb hydrogen. It was shown experimentally that as the zeolite was evacuated from 300 to 800°C, the Pt atoms migrated out of the sodalite cages and sintered into 15 to 20 Å particles while increasing the hydrogen chemisorption ratio from 0.25 to 0.65.

These data have not as yet been definitely explained, but four interpretations have been proposed [22]: 1) at least 2 Pt atoms are required to dissociate molecular hydrogen, 2) atomically dispersed platinum loses its metallic properties including chemisorption capability, 3) hydrogen chemisorption is inhibited because a partial electron transfer occurs from Pt atoms to electron acceptor sites of the support, and 4) molecular hydrogen cannot enter the sodalite cages because its kinetic diameter is 2.89 Å compared to the 2.2 Å aperture of six-membered oxygen rings.

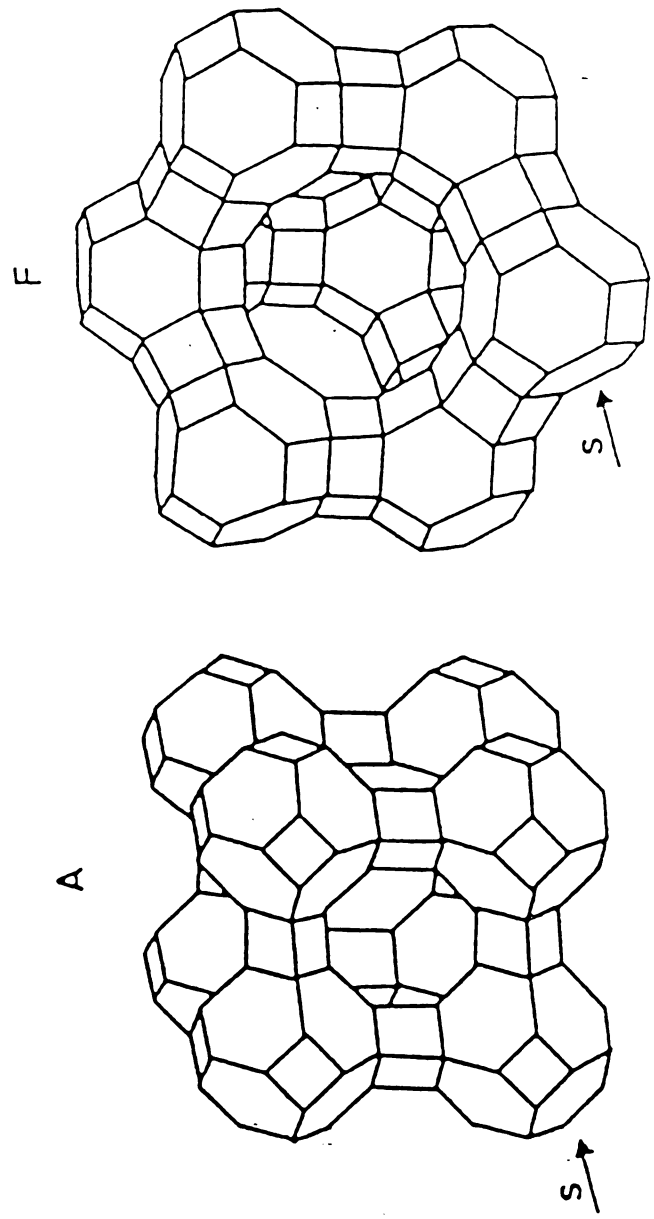

Figure 2. Location of Sodalite Cages in Type A and Type Y Zeolites [23]

Two examples of the effect of catalyst preparation on metal dispersion and catalytic activity are discussed. A two-part study on platinum particle distribution and catalytic activity of zeolite-supported Pt catalysts was done by Kubo et al. [21]. In the first part, several PtNaY and $PtNH_4Y$ catalysts were prepared by varying the calcination temperature. The Pt particle size distributions and H/Pt ratios were then measured for each of the catalysts. It was found that with increasing calcination temperature, the Pt particle size also increased: the effect was more prominent for the PtNaY catalyst. It was also shown that the H/Pt ratio increased to a maximum at 300°C and then decreased for the PtNaY while the ratio generally increased for the $PtNH_4Y$ (see Figure 3). For the catalyst calcined at 300°C, it was also shown that the majority of the Pt particles existed on the surface of the catalyst.

The second part of the report investigated the catalytic activity of these catalysts in addition to that of a PtCaY zeolite for the dehydrogenation of cyclohexane and the hydrodemethylation of toluene. The catalytic activity of these zeolites was found to correspond very closely to the H/Pt ratio previously discussed (see Figure 4).

Dalla Betta and Boudart [24] investigated the Pt dispersion and catalytic activity for PtY zeolites prepared following several different procedures. Table 2 presents the results of the Pt dispersion study and shows that

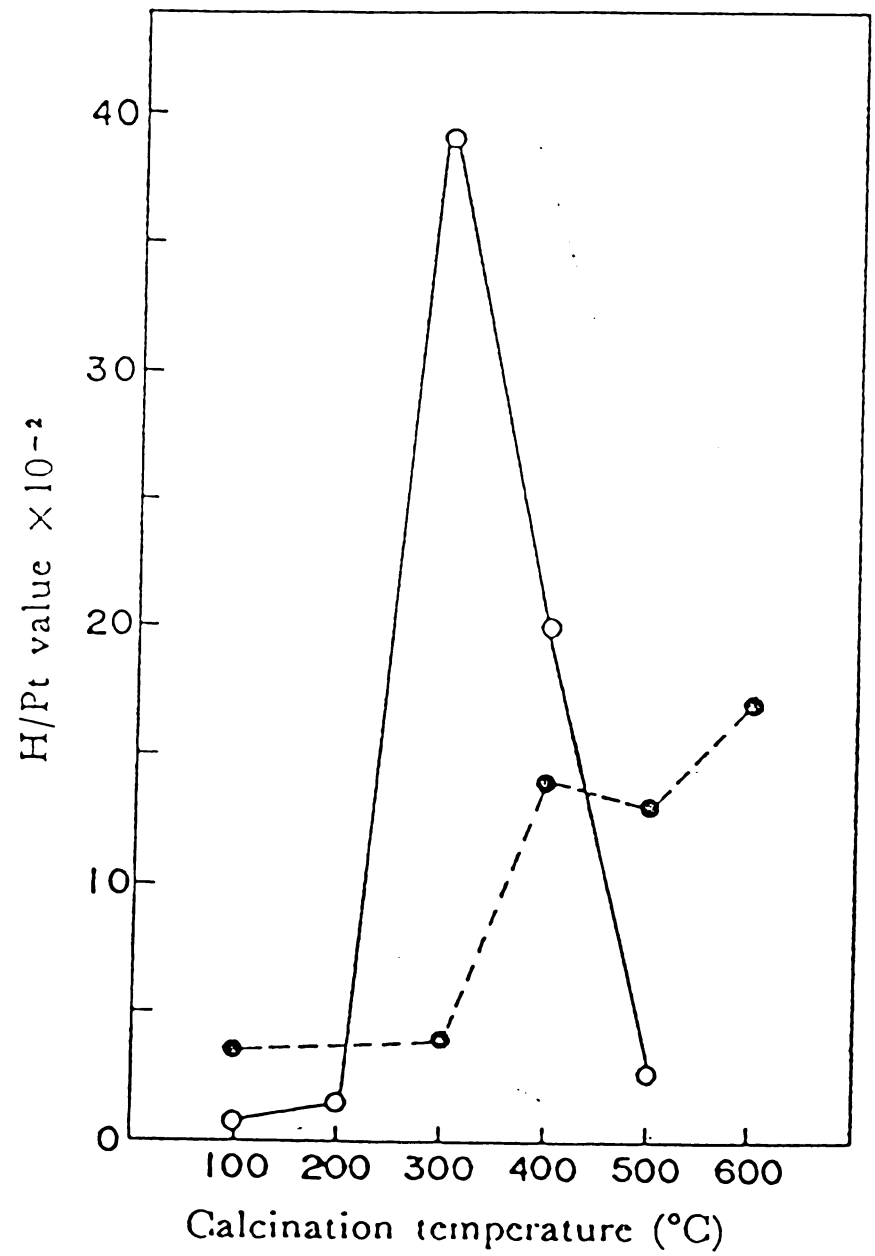

Figure 3. Plot of Atomic Ratio H/Pt vs. Calcination Temperature [21]

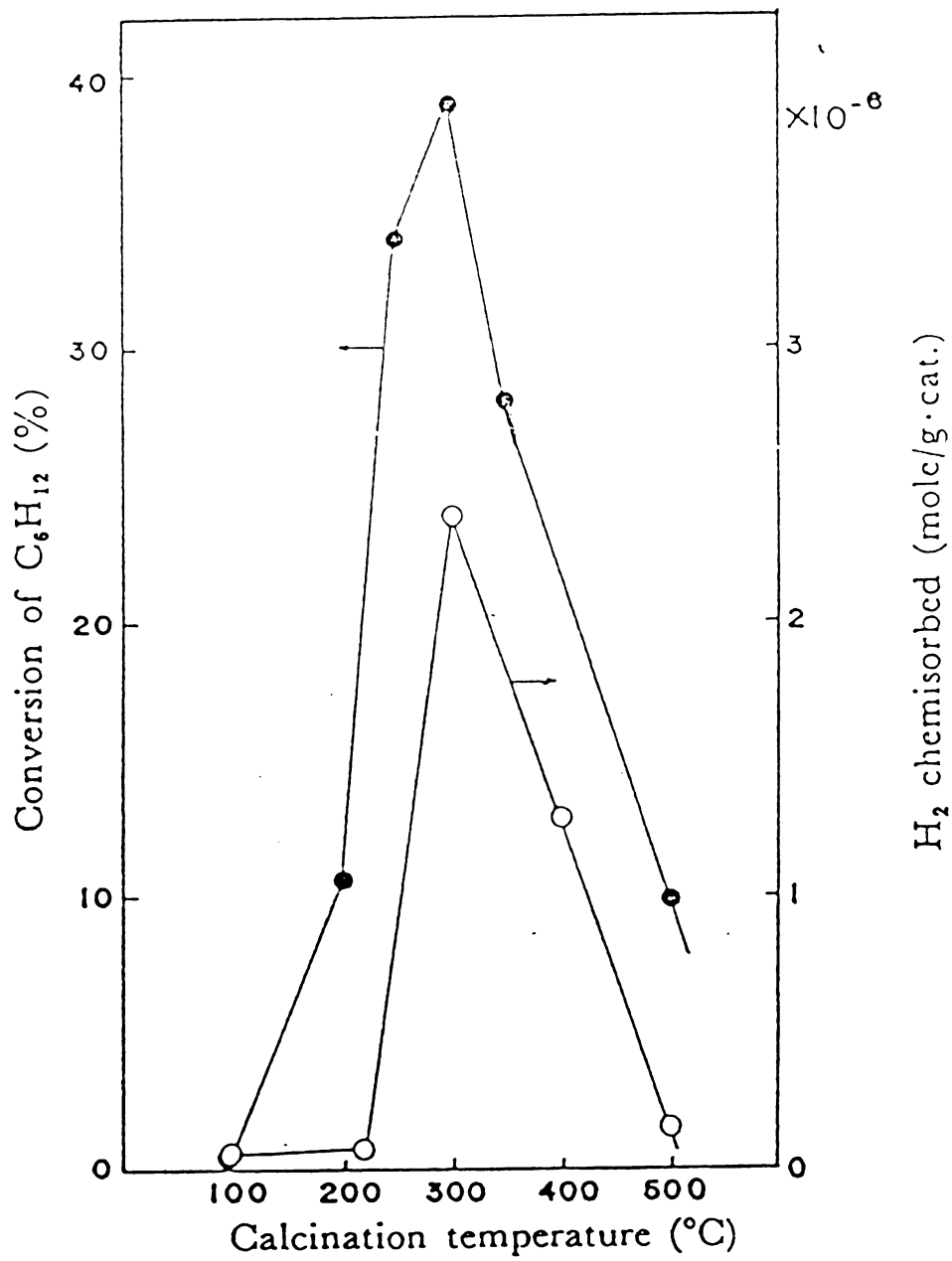

Figure 4. Plot of Cyclohexane Conversion and Hydrogen Chemisorption vs. Calcination Temperature [21]

TABLE 2

VARIATION OF PLATINUM DISPERSION WITH MODE OF PREPARATION [24]

	Preparation (degrees in °C)	Dispersion of Pt		H/Pt (total)
		ref 4)	ref 5)	
A	H_2 at 350°	0.06	0.09	0.08
B	evac. at 350°; H_2 at 400°	0.14	0.21	--
C(WD)	O_2 at 350°; H_2 at 400°	0.77	1.16	1.19
D	as above but 5g batch	0.41	0.61	0.64
E	O_2 at 350°, air + H_2O at RT; H_2 at 400°	0.63	0.95	0.99
F	O_2 at 350°; H_2 at 400°; air + H_2O at RT; H_2 at 400°	0.73	1.10	1.18

calcination in O_2 prior to H_2 reduction gives higher Pt dispersion and H/Pt ratios. The two columns under 'Dispersion of Pt' indicate the references for the methods used in this determination. Table 3 presents the catalytic results for the hydrogenation of ethylene. As can be seen from the data, the catalysts with the higher H/Pt ratio have higher catalytic activities. Also, those catalysts that have been ion-exchanged show higher activities than those that have not (PtCaY versus PtNaY).

F. CHOICE OF CATALYST AND REACTION CONDITIONS FOR CONVERSION OF D-GLUCITOL TO HYDROCARBONS

All of the papers reviewed in this chapter lead to several main factors to be considered when deciding on the catalyst to be used for the conversion of D-glucitol to hydrocarbons: 1) the catalyst must be able to carry out both dehydration and hydrogenation reactions, 2) these reactions should be carried out so as to minimize the number of products obtained, i.e. the catalyst should have some degree of selectivity, 3) the catalyst should be thermally stable to withstand both the reaction and preparation temperatures, and 4) the catalyst must be able to selectively admit reactant to the catalytic sites while inhibiting the solvent's admission. Analysis of these factors in combination with the information presented in the above papers led to the choice of a highly Ca-exchanged Y zeolite loaded with platinum as the catalyst for the

TABLE 3

TURNOVER NUMBERS N FOR HYDROGENATION OF ETHYLENE [24]

Catalyst	H/Pt (total)	N x 10^3 s^{-1}
0.54% Pt/NaY [a]	1.41	5.34
0.59% Pt/CaY [a]	1.34	25.0
0.6% Pt/MgY [b]	1.4	23.3
0.5% Pt/REY [b]	1.4	20.3
0.53% Pt/SiO_2 [a]	0.56	6.31 [c]

proposed reaction scheme.

The immediate goal of this research was to determine the applicability of the catalyst proposal. Because of this goal, identification of any reaction products was a primary objective. Batch conditions were chosen because higher conversions of sorbitol and thus higher concentrations of products could be obtained.

The choice of decahydronaphthalene as a solvent for the reaction system was based on three characteristics. First, the use of a hydrocarbon solvent as opposed to water favors dehydration due to the absence of water in the system. Second, its size inhibits its entrance to the interior catalytic sites of the zeolites, thus minimizing solvent degradation products. Finally, its use as a hydrogen transfer solvent in coal liquefaction indicates excellent H_2 solubility. This results in large amounts of H_2 being available for hydrogenation activity.

CHAPTER 2

APPARATUS

This chapter describes the equipment used in each phase of the experimental research. Sections A and B describe the equipment used in catalyst preparation, Section C describes the apparatus for the reactions, and Sections D and E describe the equipment used in analyzing and identifying the reaction products.

A. ION-EXCHANGE/METAL LOADING OF CATALYST

The equipment used for the ion-exchanging and metal loading consisted of standard laboratory equipment and included a magnetic stirrer/heater, a condenser, several Erlenmeyer flasks of various sizes with ground glass fittings, an adapter to connect the flasks to the condenser, and a vacuum filtration flask, Bűchner funnel and No. 42 filter paper for recovery and washing of the catalyst. Miscellaneous items such as a water wash bottle and tubing are used extensively in all of the experimental methods and are not listed.

B. CALCINATION/REDUCTION OF CATALYST

The reactor used for calcination and reduction procedures was designed by Treptau and Miller [25]. Figures 5 and 6 represent the reactor and process, respectively. The reactor consists of an insulated stainless steel pressure vessel equipped with a coil heater and two thermocouple probes. The gas inlet and outlet also double as entrances for the power leads and thermocouple probes, respectively.

Gas enters the reactor through the inlet in the cover of the reactor and flows down the annular space between the heater and the insulation. It then flows up the inside of the reactor tube and through the outlet in the cover. The height of the heating element is approximately three inches so that to insure uniform heating the catalyst sample must be below the top of the element. Glass wool is used above and below the catalyst to minimze material loss during operation.

For the process, two three-way valves are used downstream of the H_2, N_2 and compressed air cylinders. These three-way valves allow for easy switching between the different gases at different times during the experiment, while keeping the H_2 flow separate from the N_2 and compressed air to minimize the risk of an explosion. Each gas cylinder is equipped with a regulator and valve; H_2 was passed through a molecular sieve filter before entering the reactor. A

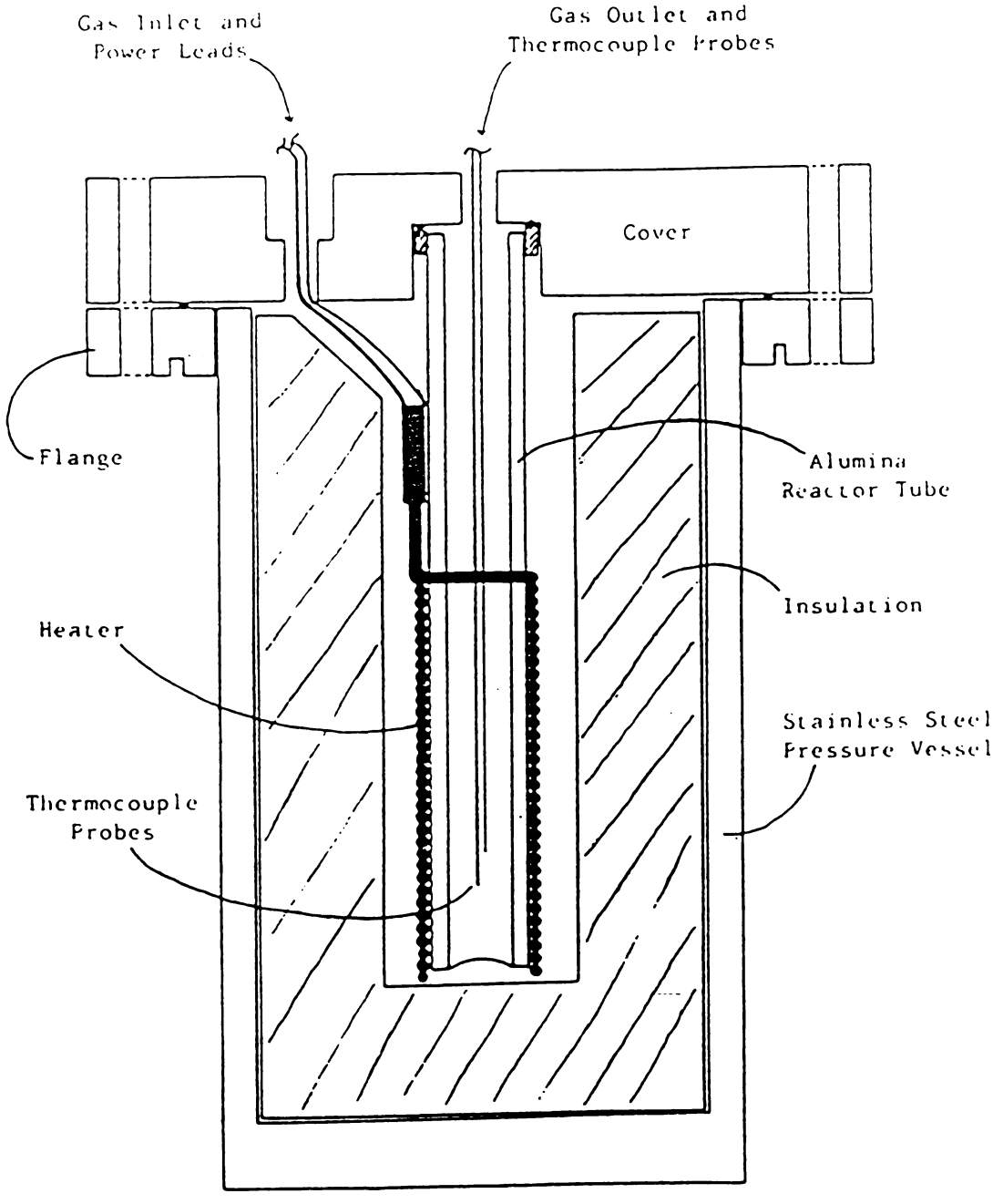

Figure 5. Sketch of Calcination/Reduction Reactor [25]

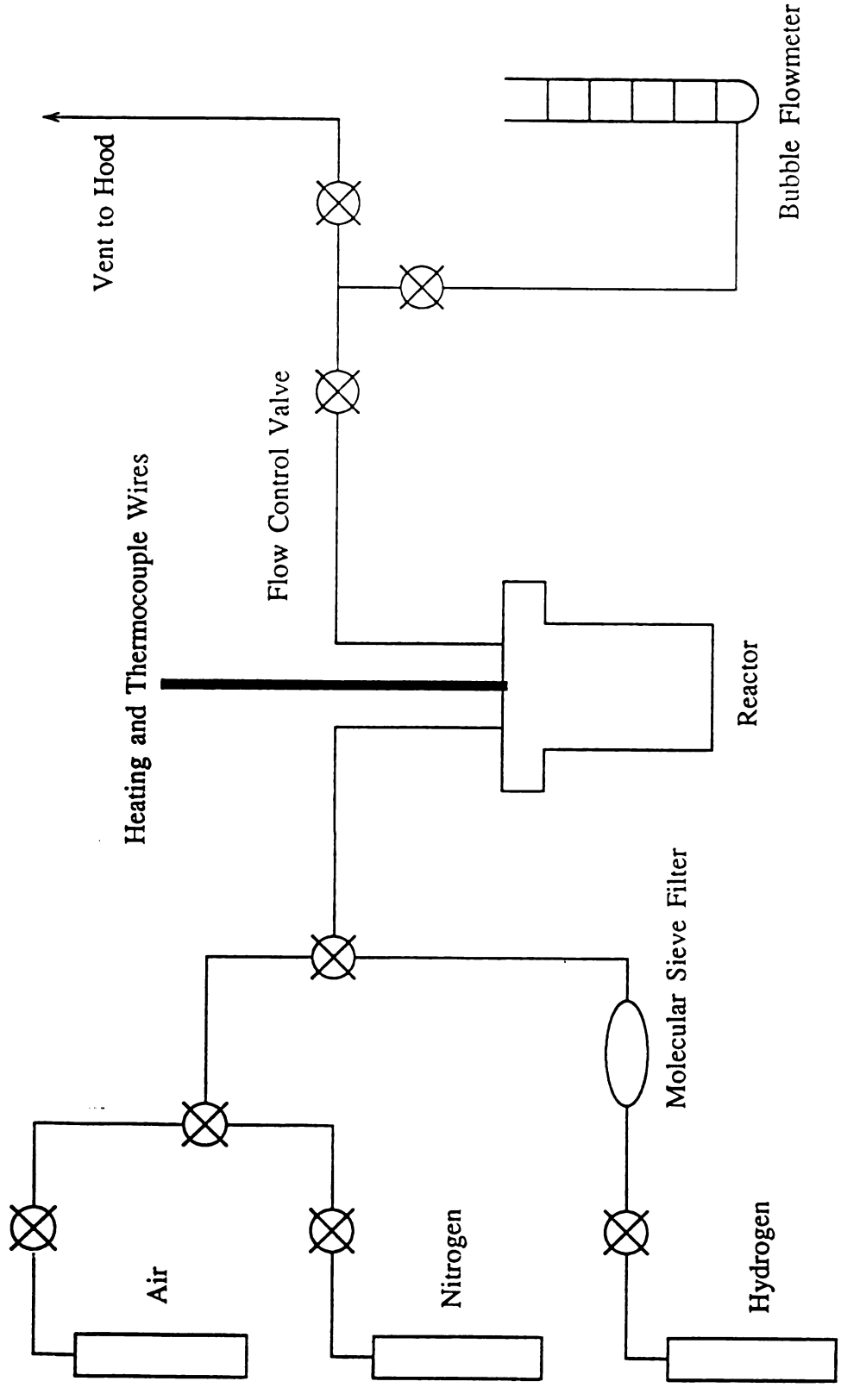

Figure 6. Sketch of Calcination/Reduction Process

needle valve is used downstream of the reactor to control the gas flow rate and two other valves are further downstream to switch the flow between the bubble flowmeter and the vent tubing. All tubing is stainless steel except for the tubing immediately before and after the reactor, which is copper.

An Omega programmable temperature controller is used for controlling themperature and heating rate and an Omega multichannel temperature indicator is used to show the temperature from the two thermocouples in the reactor.

C. BATCH REACTIONS

All of the D-glucitol conversion reactions were carried out in the reactor system illustrated in Figure 7.

The reactor used is a Parr Series 4561 300 ml High Pressure Mini reactor. The reactor is fitted with a removable glass liner which reduces its working capacity to 225 ml. The reactor is equipped with a magnetically sealed agitator drive and is rated to 3000 psig pressure at 25 ^{o} C and a maximum temperature of 350 ^{o}C. The reactor agitator speed, heating rate and temperature are controlled by a single control box which features two heating rates, continuously variable agitator speed and a maximum temperature set point of 400 ^{o}C.

All fittings on the reactor are stainless steel with the exception of the thermocouple which is a Type J

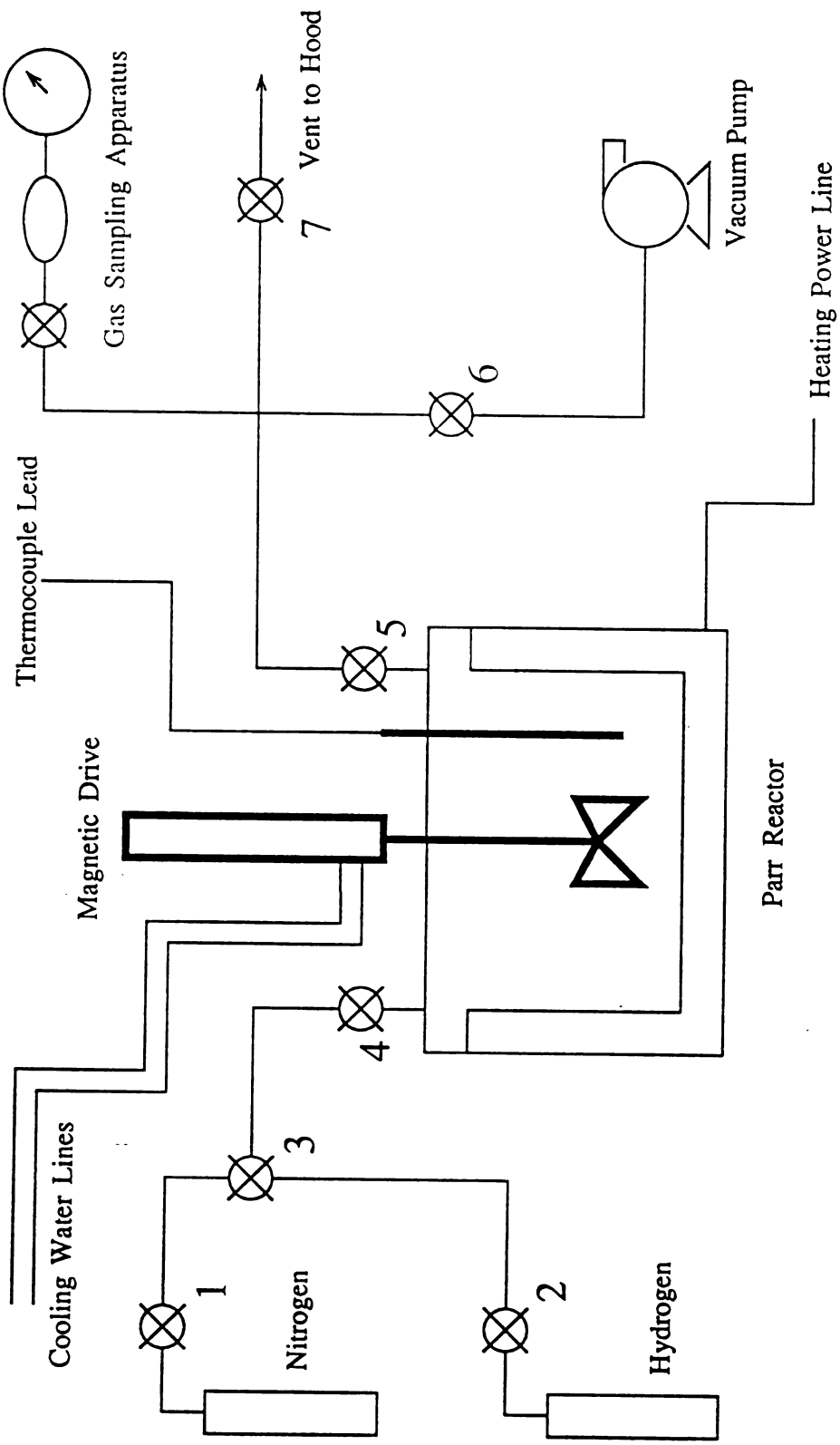

Figure 7. Sketch of Batch Reactor Process

(iron-constantan) thermocouple. External fittings include gas inlet and outlet valves, a liquid sampling valve, a rupture disc (bursting pressure of 2037 psig at 72 ^{o}F), water connections for the cooling jacket for the magnetic drive seal, and a pressure gauge with a 0-2000 psi range for working pressures up to 1400 psig. Internal fittings include a cooling coil, four-blade agitator, and sampling tube inside the reactor. The interior cooling coil was removed for the experiments since it interfered with the insertion of the glass reactor liner.

All tubing in the process is stainless steel except for the line leading to the vacuum pump which is copper attached to rubber vacuum tubing. All tubing connections are stainless steel Swagelok fittings. Regulators and valves are attached to the H_2 and N_2 cylinders. Tubing from the regulator valves leads to a three-way valve. High-pressure flexible hose supplied with the reactor runs from the three-way valve to the gas inlet valve on the reactor. Tubing from the gas outlet valve leads to a four-way connector. As can be seen in Figure 7, a gas sampling apparatus, vacuum pump, and an exhaust line are attached to the four-way connector. The gas sampling apparatus consists of a pressure gauge, a gas sampling cylinder, a septum holder for syringe sampling and a valve. This apparatus was not used in this phase of the project. A needle flow control valve used for varying the flow from the reactor is located in the exhaust line. This exhaust line

is vented directly into the fume hood exit. Similarly, a shutoff valve is used in the vacuum pump line. The vacuum pump is a Marvac model A20 rotary pump with a minimum attainable pressure of 10 microns.

A Plexiglas shield is constructed around the reactor to contain projectiles in case of a catastrophic failure of the pressure vessel. During operation, this shield and the Plexiglas fume hood door were both closed. Also, the fume hood was operating during all phases of the experimental procedure. Other safety precautions included the rupture disc previously mentioned and the operating procedure of purging the reactor with N_2 for 5 minutes to minimize H_2 and O_2 contact which could result in an explosion.

D. PRODUCT ANALYSIS VIA GAS CHROMATOGRAPHY AND HIGH PERFORMANCE LIQUID CHROMATOGRAPHY

The gas chromatograph used is a Varian Model 3700 outfitted with a 6 foot x 1/8 inch stainless steel 3% OV-101 packed column. All gas chromatography results, unless otherwise indicated, were obtained on this column. A Flame Ionization Detector (FID) on the GC is used for data generation. Carrier gas (He), H_2, and air flow rates for the FID were 30 cc/minute, 30 cc/minute, and 300 cc/minute, respectively. The results were recorded using a Hewlett-Packard 3390A Integrator.

The HPLC (High Performance Liquid Chromatograph) is a Waters Model 600 Multisolvent Delivery System Chromato-

graph equipped with an Aminex Ion Exclusion HPX-87H Organic Acid Analysis Column and 2 guard columns. The detector used is a Waters Model 410 Differential Refractometer. Data was collected by an IBM XT Personal Computer and analyzed using the WIRC data acquisition package supplied by Waters. The solvent used for the analysis was 0.01N sulfuric acid. The system was operated isochratically with a 336 psig back pressure and a flow rate of 0.5 ml/minute.

E. PRODUCT ANALYSIS VIA GAS CHROMATOGRAPHY-MASS SPECTROMETRY

Three mass spectrometers located in other laboratories were used in analyzing the reaction products.

A Hewlett-Packard 5985 Quadrupole Gas Chromatograph-Mass Spectrometer located in the Biochemistry Mass Spectrometry Department was used for the hexanol and 1,2-hexanediol experiments. This gas chromatograph was equipped with a 21 meter DB-5 Megabore capillary column. A temperature program of 40-140 ^{o}C at a rate of 5 ^{o}C/minute was used for the hexanol and 1,2-hexanediol analyses. This machine was also used for analysis of Experiment Eight but was equipped with a 6 foot 3% OV-1 packed column. For Experiment Eight, a temperature program of 55-225 ^{o}C at a rate of 5 ^{o}C/minute was used.

A Finnegan 2000 Gas Chromatograph-Mass Spectrometer located in the Chemistry Mass Spectrometry Department was also used in the analysis for Experiment Eight. This gas

chromatograph was equipped with a 6 foot 3% OV-101 packed column. The same temperature program used for Experiment Eight on the Hewlett-Packard instrument was used for this machine, however a 3 minute initial hold was added.

For Experiment Six, a JEOL JMS HX110 Double-Focusing Gas Chromatograph-Mass Spectrometer located in the Biochemistry Mass Spectrometry Department was used. This gas chromatograph was equipped with a 50 meter ULTRA-2 DB-5 capillary column. The same temperature program used on the Hewlett-Packard was used on this machine for Experiment Six.

CHAPTER 3

EXPERIMENTAL CONDITIONS AND PROCEDURES

This chapter discusses the experimental procedures used in preparing the Pt/Ca Y zeolites, running the reactions, and removing the products from the reactor in preparation for analysis.

A. CATALYST PREPARATION

Two forms of Y zeolite, approximately 100 grams each of Y-62 and Y-82, were obtained from Union Carbide Corporation. The Y-62 form of the zeolite is a NH_4-exchanged form of their primary Y zeolite, Y-52 which is a Na-Y zeolite. The Y-82 of the zeolite is a NH_4-exchanged form of their steam-stabilized zeolite, Y-72. The advantage of using this zeolite is its increased thermal stability resulting from steam treating. Because the expected reaction temperatures were well below the decomposition temperature of the zeolite and because of the higher cation content (12.3 wt. % for the Y-62 vs. 4.2 wt. % for the Y-82) which results in a higher Ca-exchange and Pt-loading potential, the Y-62 form of the zeolite was chosen for the

experiments. As can be seen from Table 4 several different Pt/Ca Y zeolite catalysts were prepared.

A.1. ION-EXCHANGE/METAL LOADING

When received from Union Carbide Corporation, the Y zeolite was in the NH_4 form and thus had to be modified through two ion-exchange processes in order to achieve the desired Pt/Ca Y form. The first of these processes involved contacting the zeolite in a calcium nitrate solution. During this contacting, a majority of the NH_4 ions present in the zeolite structure were exchanged with the Ca ions from the solution. Several contacts with fresh solution were used to achieve as complete an exchange as possible.

The second of these processes involved loading the Ca Y zeolite with Pt to achieve the final catalyst. This loading was achieved by contacting the zeolite with a solution of tetraamineplatinum (II) chloride (Alfa Products, 55.69 % Pt) under the same conditions as the Ca ion-exchange. In this case, however, only one contact was needed since the Pt loading was essentially quantitative.

The ion-exchange/metal loading procedure used was as follows:

The following procedure is for 10 g of Y-62 zeolite. Dissolve 135.04 g of calcium nitrate (Baker Chemicals, 99%

TABLE 4

CATALYSTS PREPARED

Catalyst	% Pt	Amount	Calcination/ Reduction Temp.	Calcination/ Reduction Time
Ca Y-62	5.0	5.0 g	300/500 °C	4 hrs./4 hrs.
Ca Y-62	0.5	5.0 g	300/500 °C	4 hrs./4 hrs.
Ca Y-62	0.0	5.0 g	300/500 °C	4 hrs./4 hrs.
Ca Y-62	0.0	5.0 g	not calcined/reduced	
Ca Y-82	5.0	5.0 g	300/500 °C	4 hrs./4 hrs.
Ca Y-82	0.5	5.0 g	not calcined/reduced	

purity) in 500 ml of deionized water. The amount of calcium nitrate and water is based on five zeolite/solution contacts and a 500% excess of calcium nitrate. Place 10 g of zeolite and 100 ml of deionized water in an Erlenmeyer flask. Place the flask on a heater/stirrer and heat under reflux for one hour to degas the zeolite. Slowly add 100 ml of the calcium nitrate solution (over a period of two hours) to the zeolite slurry to ensure uniform distribution. Continue heating under reflux for 2 hours. Filter the mixture while hot and wash with 500 ml of deionized water. Dry the zeolite at 120 ^{o}C for two hours then repeat contacting and drying procedure four times to maximize Ca loading.

For the metal loading, place the zeolite in twice its weight of deionized water. To produce a 5 wt. % zeolite catalyst, dissolve 0.9155 g of the tetraamineplatinum (II) chloride mentioned earlier in 300 ml of deionized water. Add all of the salt solution and heat under reflux using the same procedure as for the ion-exchanging. Filter, wash and dry the catalyst as before.

When loading Pt, only one contacting with the Pt solution is needed.

A.2. CALCINATION/REDUCTION

To obtain the final catalyst, the zeolite was calcined and then reduced so that the catalyst would remain stable

at elevated temperatures. The calcination step was run at an elevated temperature under air to drive off ammonia and adsorbed water. The reduction step was run at an elevated temperature under hydrogen to reduce Pt to its zero-valent state. All calcination/reduction procedures were performed in the reactor designed by Treptau and Miller [25].

The calcination/reduction procedure used was as follows:

Place plug of glass wool in bottom of inner ceramic reactor tube (0.75 in. O.D. and 0.5 in. I.D.) and load with catalyst to a depth of three inches (the height of the heating element). This depth corresponds to approximately five grams of catalyst. This is done to ensure even heating of the catalyst during the reactions. Place another plug of glass wool in top of tube and secure to reactor head, making sure thermocouples are properly inserted into the catalyst (thermocouples should not be touching). Seal the reactor and attach all tubing, thermocouple and power supply wires. Turn on controller and temperature indicator. While controller is warming up, establish an air flow rate of 30-40 cc/minute by calibrating with the bubble flowmeter. Once controller has stabilized, heat reactor to calcination temperature of 300 ^{o}C and hold for four hours.

After four hours have elapsed, stop the air flow and purge reactor with N_2 for 15 minutes at the same flowrate. Purging is done to minimize contact of H_2 and O_2 which

could result in an explosion. Upon completion of the N_2 purge, establish a 30-40 cc/minute H_2 flowrate. Set the controller to the reduction temperature of 500 ^{o}C and run for another four hours. Turn off power to the heater, then turn off the H_2 flow and purge the reactor with N_2 again for 15 minutes. Let cool to room temperature. Remove catalyst from reactor and store in sealed sample bottles. The calcination and reduction conditions used in these experiments were reported by Kubo et al. [21] as giving both the most uniform Pt dispersion and highest catalytic activity.

B. DEHYDRATION/HYDROGENATION REACTIONS

All D-glucitol conversion reactions were carried out under batch conditions in the Parr microreactor system previously described. During the entire procedure the fume hood was operating.

The reaction procedure used was as follows:

Weigh out 2.00 grams of reactant and 1.00 grams of catalyst into glass reactor liner. Add 125 ml of Decalin (decahydronaphthalene; Alfa Products, 99% purity), place liner in reactor and seal. Connect the gas and cooling water tubing and the thermocouple wire. Set N_2 regulator to approximately 20 psi. Referring to Figure 7 in Chapter 2, open valves 1 and 3, and slowly open valve 4 to bring

reactor to the regulated pressure. Open valve 5 and slowly open valve 7 until a small amount of bubbling is heard inside of the reactor. Do not open the valve too far because excessive gas flow will result in reactant mixture overflowing into the space between the liner and reactor wall. Purge the reactor for five minutes. Close valve on N_2 cylinder and then close valves 1, 3, and 4. When reactor reaches atmospheric pressure, close valves 5 and 7.

To evacuate the reactor, turn on the vacuum pump and open valve 6. Slowly open valve 5 and evacuate the reactor for five minutes (pressure gauge on reactor will deflect slightly in the negative direction). Close valves 5 and 6 and turn off vacuum pump.

Set H_2 regulator to approximately 80 psi and open valves 2 and 3. Very slowly open valve 4 to bring reactor up to 80 psi (this step must be done with care because of the large pressure difference between the reactor and the gas inlet line which can result in overflowing as before). Once reactor is pressurized, open valves 5 and 7 in same manner as when purging reactor with N_2. Let H_2 flow continue for five minutes then close valves 7 and 5 in order. Next, pressurize reactor to the desired starting H_2 pressure using the reactor gauge reading. Finally, close valves 4, 3, and 2 in order.

Raise the heating mantle around reactor, start the cooling water flow to stirrer drive seals, and turn on the power to controller box. Close the inside Plexiglas door.

Turn on the stirrer motor then set speed by turning knob clockwise to the second setting. Set controller to desired reaction temperature. Turn heater on HIGH until temperature is 40 ^{o}C below desired temperature then switch heater to LOW and close hood door. Once the reactor reaches set temperature, run batch reaction for desired time.

After reaction has been allowed to progress for the desired time, turn the heater to OFF, lower the heating mantle, and let the reactor cool to room temperature (the stirrer should be left on until temperature is 100 ^{o}C and the cooling water left running until temperature is around 70 ^{o}C). Once the reactor has cooled, open valves 5 and 7 and vent the reactor through the hood until atmospheric pressure is reached.

C. PRODUCT REMOVAL

Once the reactor was vented, the reaction products were ready to be removed. Deionized H_2O was used to rinse out the reactor, wash the catalyst, and remove any water-soluble products from the reaction mixture. Rubber gloves were worn during this step to minimize contact with the reaction mixture. This step was also carried out under the hood to minimize inhaling any potentially harmful vapors.

The product removal procedure used was as follows:

Fill a one liter volumetric flask with deionized H_2O. Place approximately one-half of the water in a wash bottle. Remove the glass liner from the reactor and pour the reaction mixture into a two liter beaker. Holding the reactor head over the beaker, rinse stirrer, liquid sampling tube, and thermocouple until clean. Next rinse the glass liner, using a spatula to dislodge solid particles from liner walls. The beaker should now contain the organic phase and approximately one-half liter of an aqueous phase.

Using a piece of Tygon tubing as a siphon, remove almost all of the aqueous phase and catalyst (lower phase) to a second beaker. This is done to facilitate filtering and washing of the catalyst, since the organic phase does not pass through the filter paper very well. Decant organic phase into a third beaker and pour remaining organic/aqueous mixture and any remaining catalyst into a graduated cylinder. By using a graduated cylinder almost all of the organic phase may be removed and thus minimize the amount having to be filtered.

Using a vacuum filtration flask, filter the aqueous phase to recover the catalyst, making sure to wash the sides of the beaker and graduated cylinder holding the aqueous phase into the filter funnel. Wash the catalyst with the remaining deionized H_2O. Pour the aqueous and organic phases back into the two liter beaker, place on a magnetic stirrer, and mix rapidly for 10 minutes to thoroughly contact the organic phase with the aqueous phase

This will extract any water-soluble products. After mixing, remove the beaker from the magnetic stirrer, let phases separate and take samples of each. While the phases are separating, thoroughly wash catalyst with acetone to remove residual organic phase and dry at 120 ^{o}C overnight.

D. PRODUCT ANALYSIS

Since the water-soluble products are essentially non-volatile, trimethylsilyl derivatization was used to volatilize these compounds for both GC and GC-MS analysis.

The derivatization procedure used was as follows [26]:

Place 10 ml of the aqueous phase in a small (25 ml) Erlenmeyer flask. Attach a needle to one end of a piece of Tygon tubing and the other end to a N_2 regulator fitted with a tubing adapter. Place the tubing in a clamp on a ring stand so that the end of the needle is approximately one-quarter inch above the surface of the sample.

Using a regulator pressure of 8-10 psi, establish a flowrate such that a small depression is formed in the surface of the aqueous sample by the N_2. Dry overnight until all the water is evaporated. Using a stirrer/heater on the lowest heat setting in combination with the N_2 flow will expedite drying.

Once dry add 1-2 ml of pyridine to the Erlenmeyer flask to act as a solvent. When residue is dissolved, place

solution in a small, screw-top sample bottle. Add 150 ul of BSTFA (N, O-bis(Trimethylsilyl)trifluoroacetamide, Pierce Chemical) directly to the solution. Let sample stand for 15 minutes, swirling occasionally. Sample is now ready for GC or GC-MS analysis. Typical injection size for GC and GC-MS is 0.7 Ìl. To prevent degradation of derivatized products, samples should be stored in a refrigerator.

CHAPTER 4

RESULTS AND DISCUSSION

This chapter consists of the results and discussion of the experiments performed and the analysis of the products obtained.

A. PRELIMINARY EXPERIMENTS

A.1. BLANK RUNS

A series of blank runs were conducted to initially investigate the performance and response of the proposed reaction system. All of the blank runs were performed using the procedures outlined in Chapter 3. The conditions used for the blank runs are summarized in Table 5.

The first of these, Run One, was performed in order to observe the pressure response of the reactor when loaded with decalin. This was done to determine if any unusual pressure changes, which could result in catastrophic failure of the reactor, occurred when the reactor was being heated.

The reactor was loaded with 125 ml of decalin,

TABLE 5

SUMMARY OF BLANK RUNS, HEXANOL AND HEXANEDIOL EXPERIMENTS

BLANK RUN SUMMARY

Run	Material(s)	Hydrogen Pressure	Heating Program
One	decalin	160 psig	20 °C every 5 minutes, 100 °C-260 °C. Hold 10 minutes.
Two	decalin, catalyst	160 psig	same as One
Three	decalin, sorbitol	160 psig	same as One

HEXANOL AND 1,2-HEXANEDIOL EXPERIMENTS SUMMARY

Reactant	Catalyst Used	Run Temp.	Hydrogen Pressure	Run Time
Hexanol	5% Pt/Ca Y-62	220 °C	160 psig	1 hour
Hexanediol	5% Pt/Ca Y-62	220 °C	160 psig	1 hour

pressurized to 160 psig with H_2 and heated. After reaching a temperature of 100 ^{o}C, the reactor was held at that temperature for 5 minutes to allow the reactor to stabilize. The pressure of the system was recorded; the temperature was then increased 20 ^{o}C and the process repeated until a temperature of 260 ^{o}C was reached and held for 10 minutes. The reactor was then cooled to room temperature, unloaded, and cleaned.

During the entire run, an essentially linear pressure increase was observed for the system, with a maximum pressure of approximately 280 psig occurring at 260 ^{o}C.

Run Two was performed to determine whether the catalyst would have any effect on the decalin. This was done to both check the applicability of decalin as the solvent and to mark any decalin degradation products for comparison with the products formed during the experimental reactions.

The reactor was loaded with 125 ml of decalin and 1.00 grams of the 5% Pt/Ca Y-62 catalyst, pressurized with H_2 to 160 psig, and heated according to the procedure used in Run One. After reaching 260 ^{o}C, the reactor was again held at that temperature for 10 minutes before being cooled to room temperature. The reactor was then unloaded, the catalyst recovered using a filter funnel and vacuum filtration flask and the decalin analyzed via gas chromatography to determine if any catalytic degradation had occurred.

Gas Chromatography analysis of the decalin revealed no observable degradation; the only peak observed was that of

tetralin (tetrahydronaphthalene), the major impurity in decalin.

Run Three was performed to determine if any thermal decomposition of sorbitol occurred in the absence of catalyst. This was done so that any products formed could be compared with those formed via the catalyzed reactions. This comparison would show which products were formed via thermal decomposition, which were formed catalytically, and which were formed by both reactions.

The reactor was loaded with 1.00 grams of sorbitol and 125 ml of decalin, pressurized with H_2 to 160 psig, and operated according to the same procedure as Runs One and Two. After opening the reactor, the mixture was separated and the sorbitol and any products recovered using the same procedure as outlined in Chapter 3. The aqueous phase was analyzed using High Performance Liquid Chromatography to determine if any thermal decomposition of sorbitol had occurred.

Results from the HPLC analysis revealed that no thermal decomposition occurred.

A.2. HEXANOL AND HEXANEDIOL EXPERIMENTS

After the blank runs were completed, the catalytic activity of the Pt/Ca-Y zeolite was tested using 1-hexanol (Alfa Products, 99+% purity) and 1,2-hexanediol (Aldrich Chemical, 98+% purity) as model compounds. This was

required in order to determine if the catalyst had significant dehydration and/or hydrogenation activity. For these reasons, two reaction runs were performed using the batch reaction procedure outlined in Chapter 3: one with hexanol and one with 1,2-hexanediol. The conditions and catalysts used for the hexanol and 1,2-hexanediol experiments are summarized in Table 5.

The hexanol dehydration experiment was performed primarily to determine if the catalyst had dehydrating and hydrogenating activity for alcohols, and if these activities would take place simultaneously. This experiment was performed first because it represents the "easiest" dehydration reaction: a reaction involving a primary hydroxyl group.

The 1,2-hexanediol experiment was performed to determine whether or not the catalyst had the capability to perform dehydration and hydrogenation on polyhydroxyl compounds.

B. EXPERIMENTAL RESULTS

B.1. RESULTS OF HEXANOL DEHYDRATION EXPERIMENT

The primary product of the hexanol experiment was hexane with a small amount of hexene as a secondary product.

Figure 8, from top to bottom, presents the gas

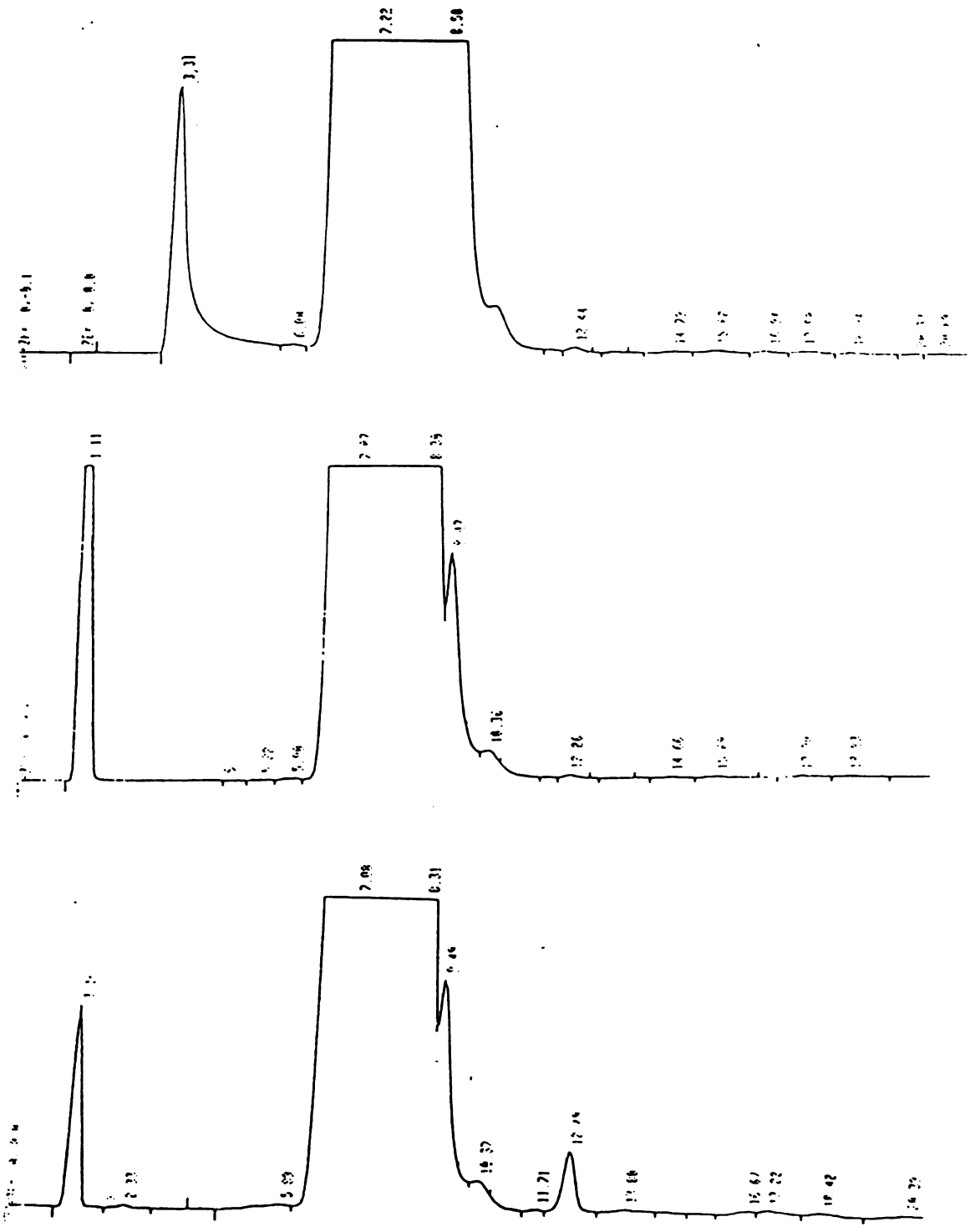

Figure 8. Gas Chromatography Traces for Hexanol Dehydration Experiment

chromatography traces of a 1% hexanol/decalin standard, a 1% hexanes/decalin standard, and the reaction mixture from the hexanol experiment. Comparison of the reaction trace with those of the standards indicates the presence of both hexanol and hexane. The absence of a hexanol peak in the reaction GC trace would suggest complete conversion of the hexanol. However, some residual hexanol may remain in the catalyst after being washed, and thus not be recovered.

To confirm this observation, a sample of the reaction mixture was sent to the Mass Spectrometry Facility in the Biochemistry Department, where mass spectra were taken of each of the standards and the reaction mixture.

Figures A-1 through A-3 represent the mass spectrum of hexane, the mass spectrum of hexene and the mass spectrum of hexanol, respectively. All of these were obtained from the EPA/NIH Mass Spectral Data Base and were used for comparison with the mass spectra obtained from the reaction mixture. Figure B-1 includes the TIC (Total Ion Count) of the reaction mixture taken at the Mass Spectometry Facility and Figures A-4, A-5, and A-6 represent the mass spectra of the major peaks in Figure B-1. Comparison of these spectra with those from the Mass Spectral Data Base indicate that the products of the hexanol dehydration experiment are predominantly hexane and some hexene. Based on the specific ion traces given in Figure B-1 for hexane (m/z 86.2) and hexene (m/z 84.2), the peak areas give approximate concentrations of 88% hexane and 12% hexene.

B.2. RESULTS OF 1,2-HEXANEDIOL EXPERIMENT

Two main products, hexane and hexanol, and one secondary product, hexene, are produced in the 1,2-hexanediol experiment. No gas chromotography trace is given for the 1,2-hexanediol standard since the hexanediol peak is covered by the decalin peak.

Figure 9 is the gas chromatography trace of the reaction mixture. When compared with the GC traces of the hexane and hexanol standards given in Figure 8, the reaction mixture trace indicates the presence of hexanol and hexane. As with the hexanol experiment, a sample of the 1,2-hexanediol reaction mixture was submitted for to the Biochemistry Mass Spectrometry Department for analysis.

Figure B-2 includes the TIC trace from the Mass Spectrometry Department and Figures A-7, A-8, and A-9 are the mass spectra of the major peaks in Figure B-2. Comparison of these mass spectra with those from the Mass Spectral Data Base indicate that the products of the 1,2-hexanediol experiment are predominantly hexane and hexanol and a small amount of hexene. Because the specific ion traces in Figure B-2 do not include the m/z 31 trace for hexanol, the peak areas cannot be used to determine concentrations. These peak areas, however, do give relative concentrations for the hexane (94%) and hexene (6%) peaks. Comparison of the areas for the hexane/hexene and hexanol peaks in

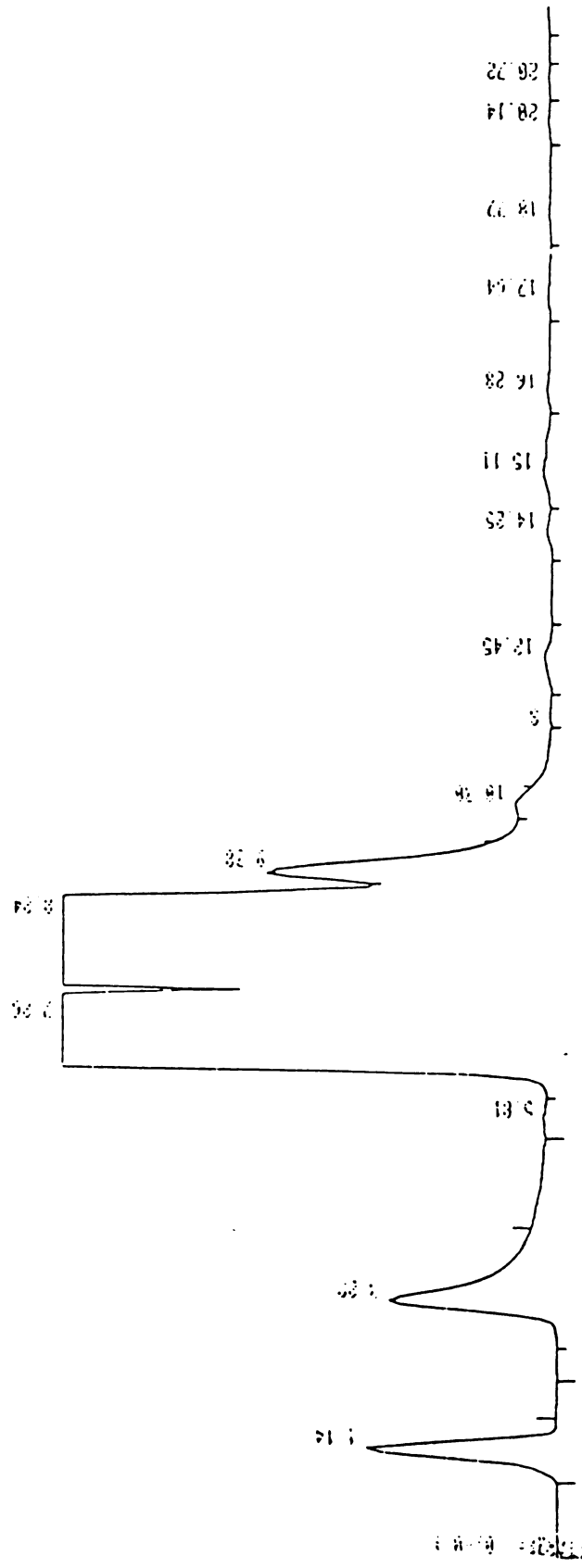

Figure 9. Gas Chromatography Trace for 1,2-Hexanediol Experiment

Figure 9 gives approximate concentrations of 41% hexane/hexene and 59% hexanol. Combining these results gives approximate individual concentrations of 59% hexanol, 38% hexane, and 3% hexene.

B.3. RESULTS OF SORBITOL EXPERIMENTS

Having determined that the catalyst had at least some desired catalytic activity, the major set of reactions, with sorbitol (Aldrich Chemical, 99+% purity) as the reactant, were performed. These were performed with different catalysts at a variety of temperatures, pressures, and time duration to determine the effect of these parameters on the conversion of sorbitol and the types and concentrations of products formed from the reactions.

The conditions and catalysts used and the conversion for all of the sorbitol experiments are summarized in Table 6.

Determination of the types of products formed in the sorbitol experiments was not nearly as straightforward as with the previous two experiments. First, both water-soluble and organically-soluble products were formed. The formation of water-soluble products is shown in the next section. The formation of organically-soluble products was shown by both a yellow color and "caramel" aroma present in the organic phase. Second, upon analysis of the organic phase by gas chromatography, the only peak observed was for

TABLE 6

SUMMARY OF SORBITOL EXPERIMENTS

Expt.	Catalyst	Temp.	Charge Pressure	Time	Sorbitol Conv.
One	CaY-62 5% Pt	180 °C	160 psig	1 hr.	0
Two	CaY-62 5% Pt	200 °C	160 psig	1 hr.	0
Three	CaY-62 5% Pt	220 °C	160 psig	1 hr.	6%
Four	CaY-62 5% Pt	240 °C	160 psig	1 hr.	34%
Five	CaY-82 5% Pt	180 °C	160 psig	1 hr.	10%
Six	CaY-62 5% Pt	260 °C	160 psig	1 hr.	87%
Seven	CaY-62 5% Pt	240 °C	300 psig	1 hr.	21%
Eight	CaY-62 0% Pt	240 °C	160 psig	1 hr.	92%
Nine	CaY-62 5% Pt	240 °C	900 psig	1 hr.	43%
Ten	CaY-62 5% Pt	260 °C	160 psig	4 hrs.	91%
Eleven	CaY-62 5% Pt	260 °C	300 psig	1 hr.	80%

Temperature, °C	180	200	220	240	260
% Increase in Pressure	37	38	50	55	75

decalin, indicating that the organic products were non-volatile.

This led to the decision to first investigate the water-soluble products, which was done using both HPLC and GC-MS.

B.3.1. ANALYSIS BY HIGH PERFORMANCE LIQUID CHROMATOGRAPHY

High Performance Liquid Chromatography was used as a preliminary method of determining how many different products were formed and the relative amounts of each product. The chromatogram obtained from the HPLC analysis was also used to determine the sorbitol conversion in each experiment.

As can be seen from the HPLC results in Figures 10-12, there is little difference in the types of products formed in the various reactions; the only difference is in the relative amounts of the products, which arises from the use of different catalysts. Figures 10 and 11 represent the chromatograms for Experiments Six and Ten, respectively, and show similar concentrations of the products. Figure 12, the chromatogram for Experiment Eight, shows a much greater concentration for the compound labeled P6D1 and a smaller concentration for the compound labeled P5D1, when compared with Experiments Six and Ten. For this reason Experiment Six, performed with the Pt Ca-Y catalyst and Experiment Eight, performed with the Ca-Y catalyst, were

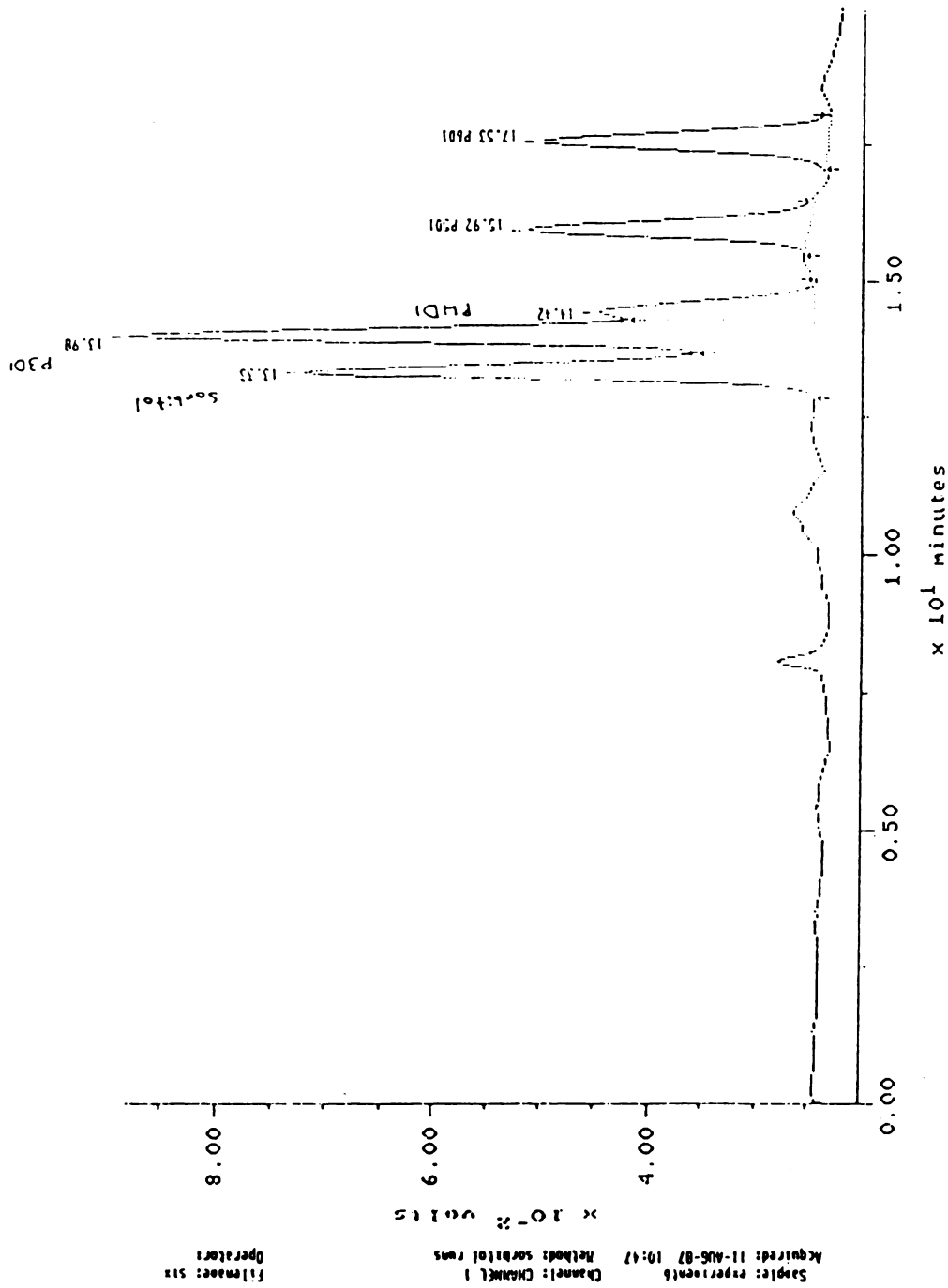

Figure 10. High Performance Liquid Chromatography Trace for Experiment Six

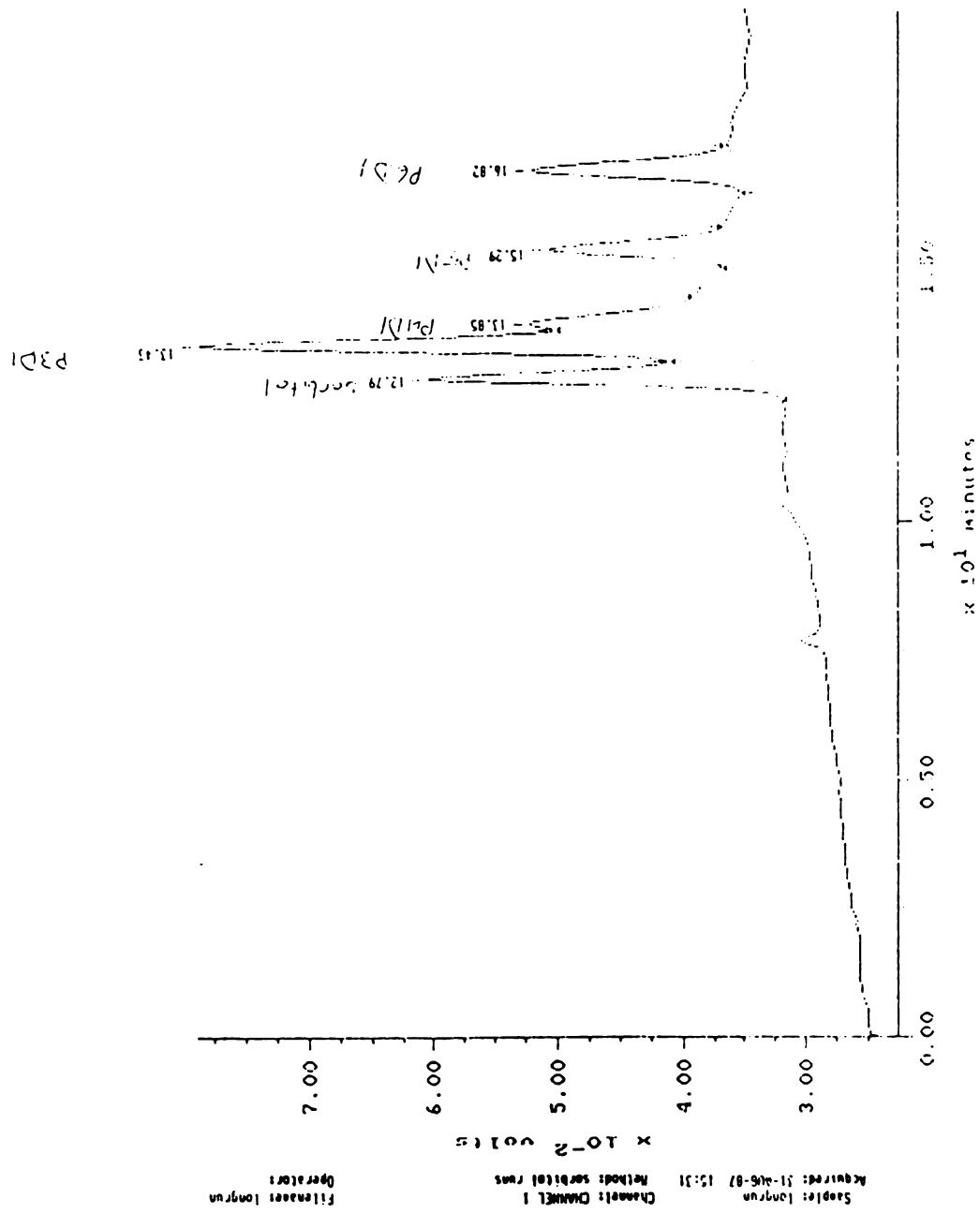

Figure 11. High Performance Liquid Chromatography Trace for Experiment Ten

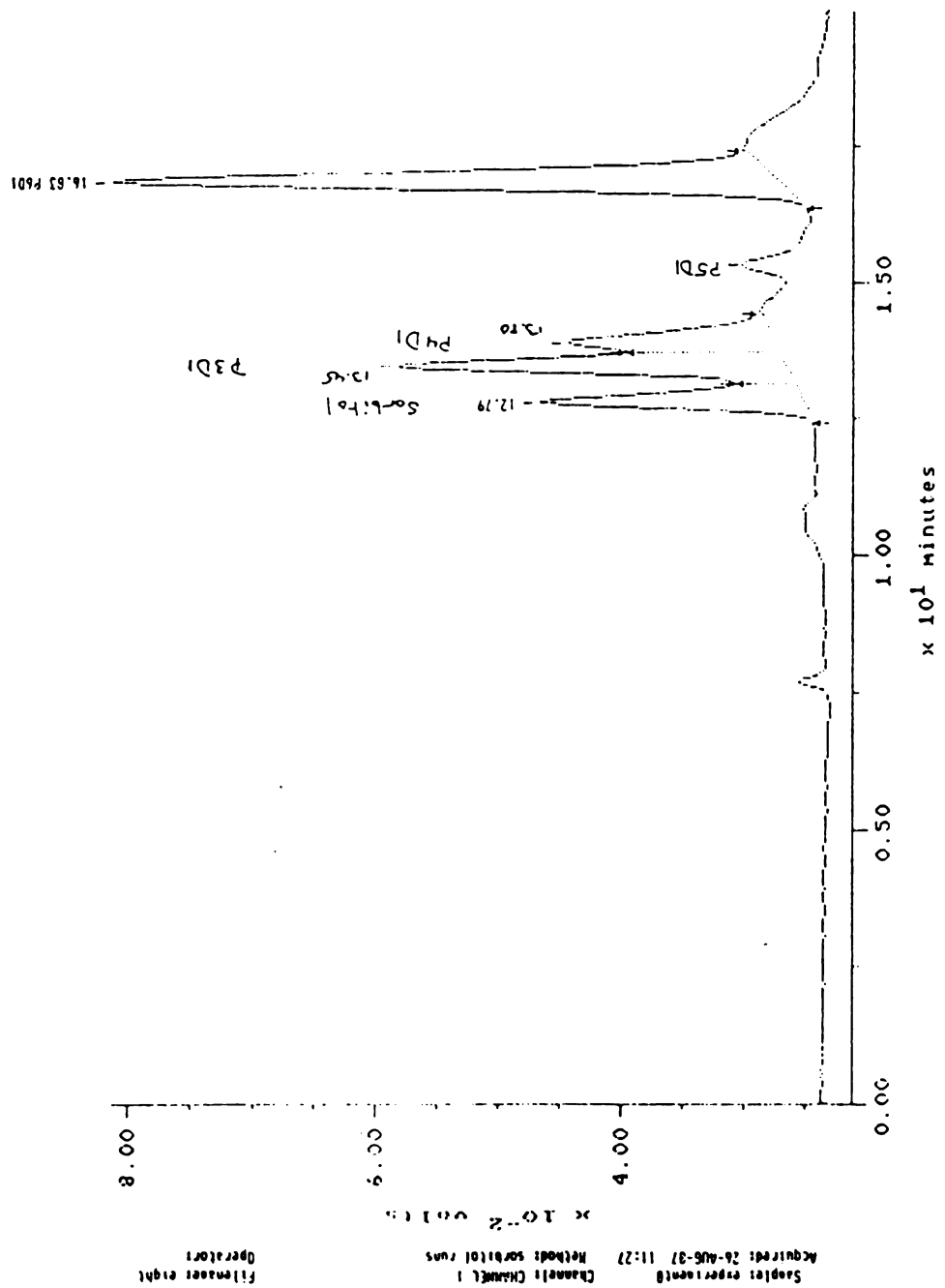

Figure 12. High Performance Liquid Chromatography Trace for Experiment Eight

chosen as representative examples for product identification.

Experiment Eight was run for one hour at a temperature of 240 ^{o}C and an initial H_2 charging pressure of 160 psig. One gram of the Ca-exchanged Y-62 zeolite (0% Pt) was used as the catalyst. According to Minachev et al. [17], this Ca Y zeolite is a dehydration catalyst.

Experiment Six was run for one hour at a temperature of 260 ^{o}C and an initial H_2 charging pressure of 160 psig. One gram of the Pt/Ca-exchanged Y-62 zeolite (5% Pt) was used as the catalyst. As mentioned in Chapter 1, this catalyst was expected to have both dehydration and hydrogenation activity.

B.3.2. ANALYSIS BY GAS CHROMATOGRAPHY-MASS SPECTROMETRY

Gas Chromatography-Mass Spectrometry was used as the primary method for determining the types of products formed. Since the water-soluble products are non-volatile, the TMS derivatization procedure described previously [26] was used to facilitate GC-MS characterization. This derivatization technique replaces the hydroxyl groups on a compound with a trimethylsilyl group:

$$R\text{----}OH + (CH_3)_3Si\text{----}NCH_3COCF_3 \text{ -------}>$$

$$R\text{--}O\text{--}Si(CH_3)_3 + CF_3CONCH_3OH$$

This reaction yields stable, volatile products which can be separated by gas chromatography. These TMS ethers have similar fragmentation pathways to those of methyl ethers. In addition, derivatization facilitates improved GC separation; mass spectrometry of TMS carbohydrates is a major analytical technique for compound characterization.

The major ions obtained in the mass spectra of TMS compounds result from two major fragmentation pathways: 1) the cleavage of a C-C bond in the carbohydrate chain and 2) the loss of trimethylsilanol. A general fragmentation scheme is given in Figure 13.

Cleavage of the carbon chain results in ions of mass M - (103 + n x 102) where M is the mass of the parent compound and n the number of secondary carbons in a straight chain with a hydroxyl group. The strongest of these is the (M-205) ion. The ion corresponding to M-103 represents the loss of a terminal carbon with a primary hydroxyl group. Loss of a methyl group from the TMS substituent may also be classified as a cleavage loss and generates an M-15 ion.

Loss of trimethylsilanol ($(CH_3)_3SiOH$) results in ions of mass M - m x 90 where m is the number of trimethylsilanol molecules that are lost. As can be seen in Figure 13, these losses can be combined in a variety of ways.

The two pathways listed above result in ions whose structure can be directly traced back to that of the parent compound. Other major ions, however, cannot be immediately

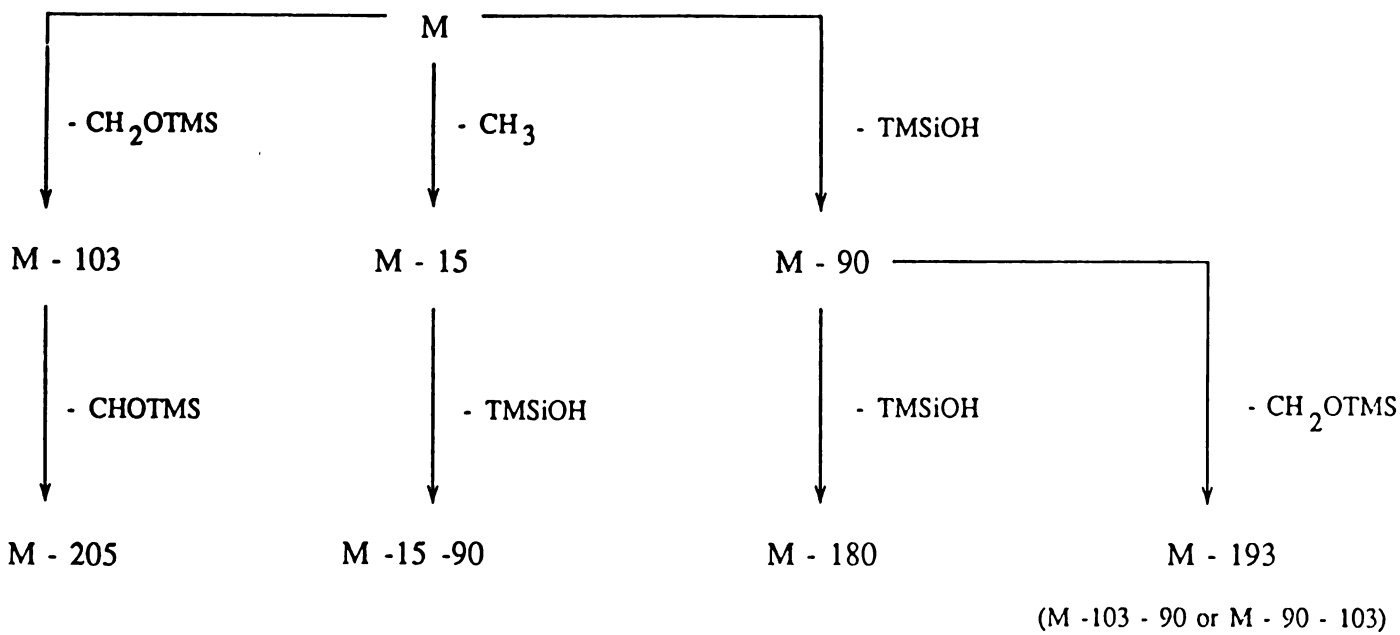

- CH_3: loss from TMS group

- CH_2OTMS: indicates primary -OH group

- CHOTMS: indicates secondary -OH group

Figure 13. General Fragmentation Scheme for TMS Carbohydrate Ethers

connected to the parent compound and result from structural rearrangement, common to TMS compounds [27]. Some of these ions and their proposed structures [27] are given in Figure 14. Ions m/z 73, m/z 217, and m/z 204 are all common to TMS ethers of carbohydrates. Ion m/z 147 is also common to TMS carbohydrate ethers and is characteristic for most compounds with more than one trimethylsiloxyl group [28].

Since most of the rearrangement ions listed above and in Figure 14 are common to TMS carbohydrate ethers, structural determination must usually be done using the higher mass ions obtained from the chain cleavage and trimethylsilanol loss pathways [28].

Another problem in determining structures arises when isomers are present. In almost all cases, the mass spectra of diastereoisomers differ only in the relative intensity of particular ions [29-31]. Thus, for example, it is virtually impossible to differentiate between the TMS mass spectra of D-glucitol and D-mannitol.

Molecular formulas, however may be determined from the mass spectral data. If a molecular ion is not present, as is often the case with higher mass TMS compounds [29-31], molecular weight determinations may be made based on the presence of the M-15 (M - CH_3) and M-90 (M - $Si(CH_3)_3$) ions. After the molecular weight is determined, a simple procedure may be used to determine plausible molecular formulas:

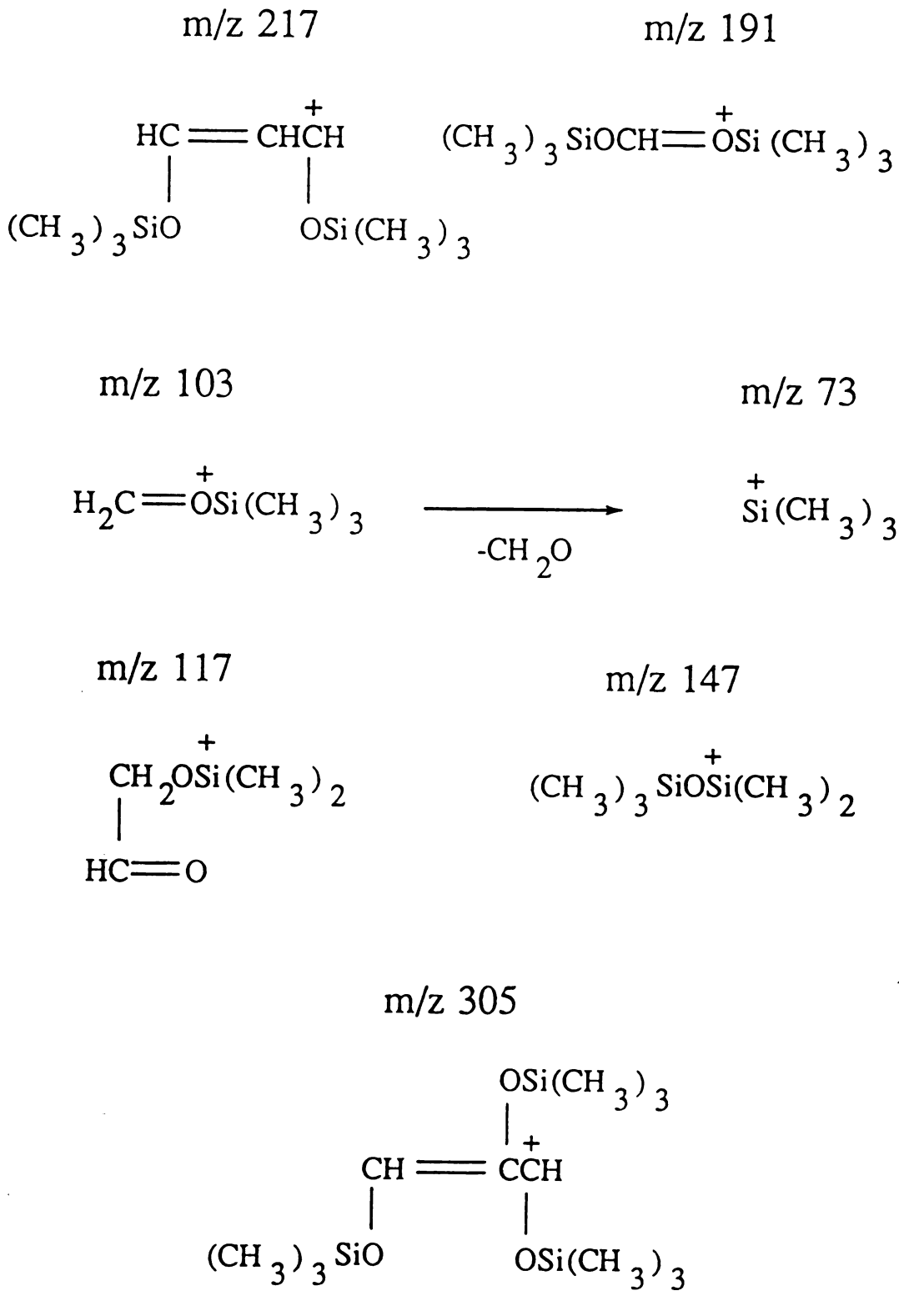

Figure 14. Rearrangement Ions of TMS Carbohydrate Ethers [27]

1. Subtract the molecular weight of the carbon chain from the total molecular weight e.g. 6 carbon atoms yields M - 72,

2. Subtract 89 for each TMSiO group assumed to be present in the compound,

3. Subtract 16 for each oxygen atom assumed to be present and not part of a TMSiO group,

4. Use the 2n + 2 formula to determine the number of hydrogens for a saturated hydrocarbon of the chain length assumed in step 1,

5. Subtract 1 for each TMSiO group from the number obtained in step 4,

6. Subtract the number obtained in step 5 from the number in step 3 and divide by 2. This will give the number of double bonds and/or rings present in the compound.

If the number obtained in step 6 before dividing is negative, too many carbon atoms, TMSiO groups, or oxygen atoms were assumed and vice versa if the number obtained is larger than the mass of an oxygen atom. Having a preliminary idea of the type of reaction going on (i.e. no chain cracking of reactant) greatly reduces the number of permutations since one of the above values (i.e. chain length) can be assumed as constant.

C. MASS SPECTROSCOPIC ANALYSIS OF EXPERIMETS SIX AND EIGHT

C.1. MASS SPECTROSCOPIC ANALYSIS OF EXPERIMENT EIGHT

Mass spectra for Experiment Eight were taken at the Mass Spectrometry Facility in the Biochemistry Department using the Hewlett-Packard 5985 GC-MS described in

Chapter 2. Mass spectra were also taken in the Chemistry Department using the Finnegan 2000 GC-MS described in Chapter 2. As mentioned in Chapter 2, the Hewlett-Packard was equipped with a 6 foot 3% OV-1 packed column and the Finnegan with a 6 foot 3% OV-101 packed column. The results from both runs were comparable. Because the mass spectrometers used for the analysis are both quadrupole-type mass spectrometers, higher mass ion sensitivity is not as great as that for a double-focusing type such as the JEOL machine used for Experiment Six. Subsequently, small, low-intensity peaks such as 701 and 733 do not exhibit enough high mass ions to give an accurate description of the compound. Thus, only peaks 558, 756, and 870 will be discussed in detail.

The gas chromatogram from the Finnegan 2000 GC-MS for Experiment Eight is given in Figure 15 and shows three major peaks. Each of the individual peaks can be identified by either scan numbers or retention time, both of which are plotted along the bottom of the graph. In this discussion, the peaks will be identified by scan number.

C.1.1. Peak 558

Peak 558 represented a compound with a molecular weight of 290. This was determined from both the ion at 275 (M-15) and from the more extensive analysis of Experiment Six. The mass spectrum of peak 558 is given in Figure A-10. Applying the procedure outlined previously, it

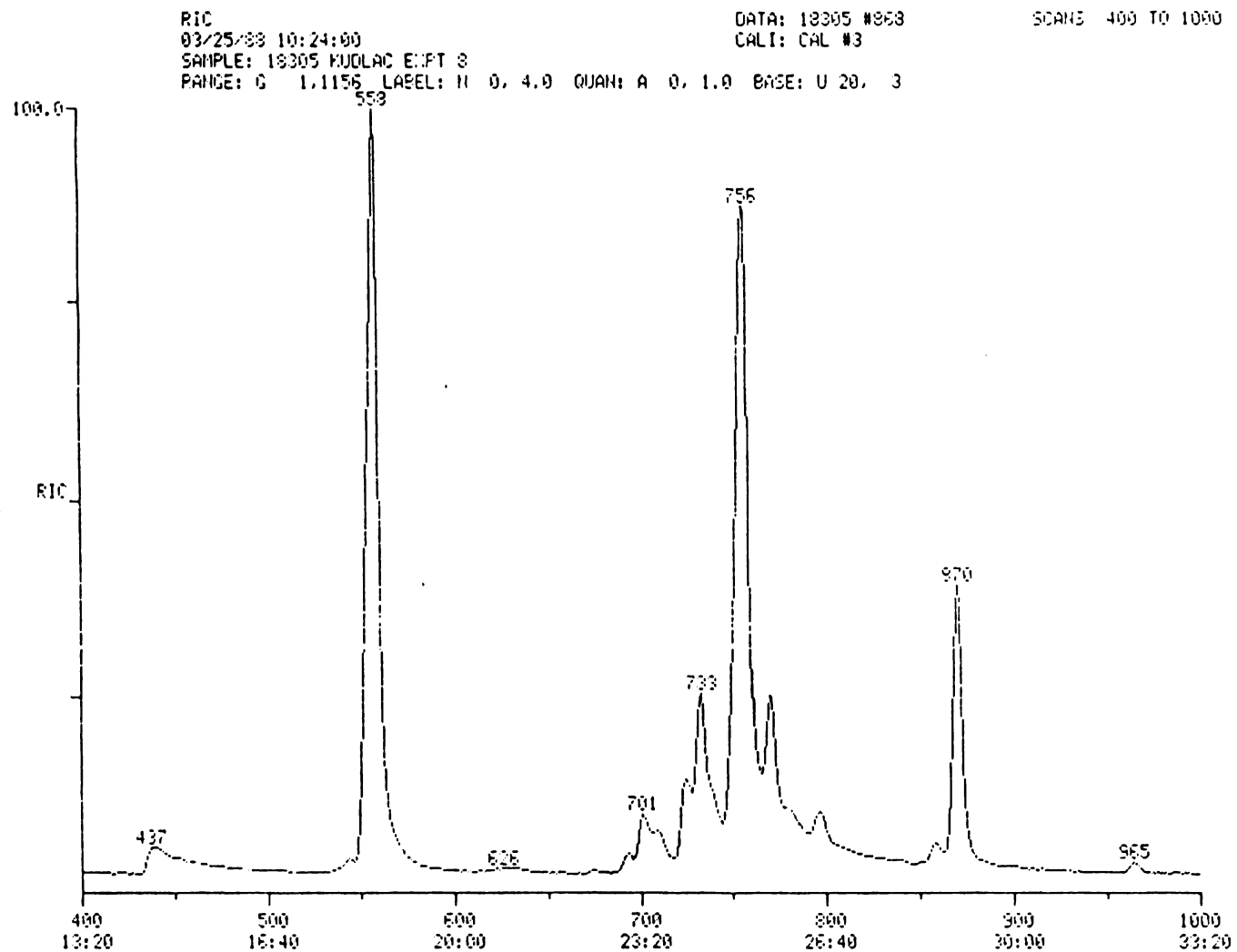

Figure 15. Gas Chromatography Trace for Experiment Eight

was determined that the compound had the molecular formula $C_6H_8O_2(TMSiO)_2$ with 2 double bonds or rings.

An M-90 peak is present at m/z 200 and an M-15-90 peak is present at m/z 185. No peak is present at M-103 indicating that the TMSiO groups are not on a primary carbon. A small ion at m/z 247 could be an M-43 (M - $COCH_3$) fragmentation indicating a pinacol-type dehydration, however this would imply that the two TMSiO groups would be adjacent leading to a much larger m/z 147 than is present. The m/z 147 is present at a low intensity, indicating that there is more than one trimethylsiloxyl group present, but m/z 147 is too small to indicate adjacency. The total number of oxygens present suggests that two dehydrations have taken place. According to several studies [32,33], the preferential product for dehydration of D-glucitol in acids is 1,4:3,6-dianhydro-D-glucitol (isosorbide). This compound matches the observed mass spectra by having no adjacent hydroxyl groups and no primary carbons with hydroxyl groups, and is thus tentatively assigned as peak 558.

The mass spectrum of isosorbide dimethyl ether was taken as a check and is given in Figure A-11. As mentioned previously, methyl ethers have some similar fragmentation pathways as TMS ethers (but with less rearrangement) so that the data obtained should provide some similar ions but exhibiting a mass difference of 58 due to the different substituents. The ion at m/z 174 corresponds to the m/z 290

ion of the TMS compound. The ion at m/z 133 results from a M-CH_3O loss, which is comparable to the M-90 loss (m/z 200). The following comparisons can also be made (dimethyl ether ions are listed first): the group between m/z 111 and m/z 116 to the small m/z 169-174 group; the m/z 99-101 group to the m/z 157-159 group; the m/z 85-88 and the m/z 143-146 groups; the m/z 71-75 and m/z 129-133 groups; the m/z 41-45 and m/z 99-103 groups; the m/z 69 and m/z 185 and the m/z 58-59 and m/z 116-117 ions.

C.1.2. Peak 756

Peak 756, whose mass spectrum is given in Figure A-12, exhibited a highest mass ion of m/z 362; however, upon comparison with the data from the Hewlett-Packard 5985 on the same peak, an ion at m/z 437 was seen to be present. This ion, in combination with the m/z 362 (M-90) and m/z 349 (M-103) ions, suggest a compound with a molecular weight of 452. This molecular weight gives a molecular formula of $C_6H_8O(TMSiO)_4$ with one double bond or ring. Comparing the mass spectral data from both runs with the general fragmentation scheme given in Figure 13 yields all of the high mass ions expected from a compound with mass 452. Also, no ion is found at the M-103-204 site, indicating that there is a primary carbon and one secondary carbon with hydroxyl groups. A stronger 147 ion than that for peak 558 indicates adjacent hydroxyl groups. Ion m/z 157 comes from the decomposition of the M-205 ion, m/z 247, which loses a

trimethylsilanol group. In addition, an ion at m/z 335 is a result of a rearrangement and gives evidence for a 5-membered anhydro ring and is shown in the partial fragmentation scheme given in Figure 16 [34]. From the molecular formula already determined, the compound is the product of a single dehydration reaction. The preferential compound formed from the dehydration of D-glucitol is 1,4-anhydro-D-glucitol [32,33]. This compound fits well with the mass spectral data, having adjacent hydroxyl groups to give the m/z 147 ion, a primary and secondary carbon with hydroxyl groups to give the M-103 and M-205 ions, and a 5-membered anhydro ring to give the m/z 335 ion. Thus it is tentatively assigned as peak 756.

C.1.3. Peak 870

The mass spectra of the final peak, 870, is given in Figure A-13. Comparing the data from both spectrometers with the mass spectrum found in [28] shows that this compound is the starting material, D-glucitol.

C.2. MASS SPECTROSCOPIC ANALYSIS OF EXPERIMENT SIX

Mass spectral for Experiment Six were taken at the Biochemistry Mass Spectroscopy Department using the JEOL JMS HX110 gas chromatograph-mass spectrometer described in Chapter 2. The gas chromatogram for Experiment Six is given in Figure 17. As with Experiment Eight, the

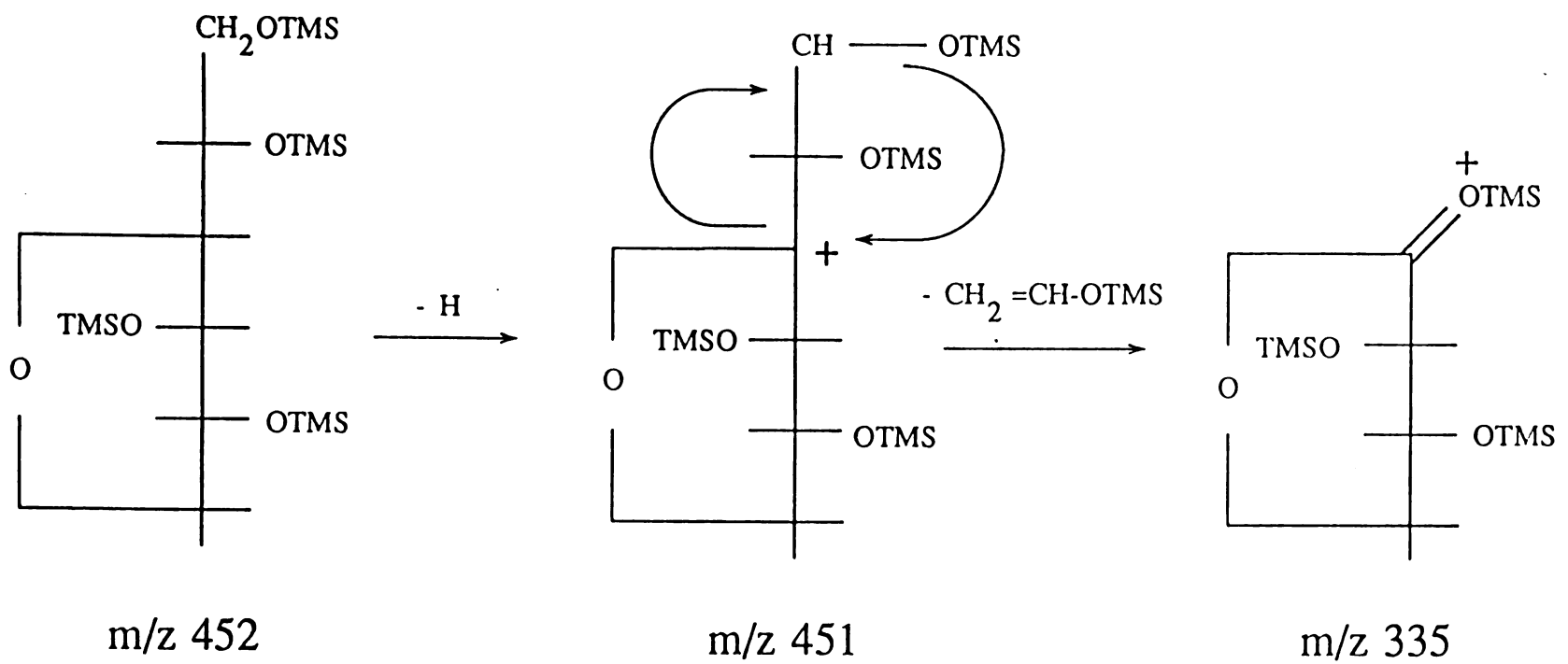

Figure 16. Partial Fragmentation Scheme for 1,4-Anhydro-D-Glucitol [34]

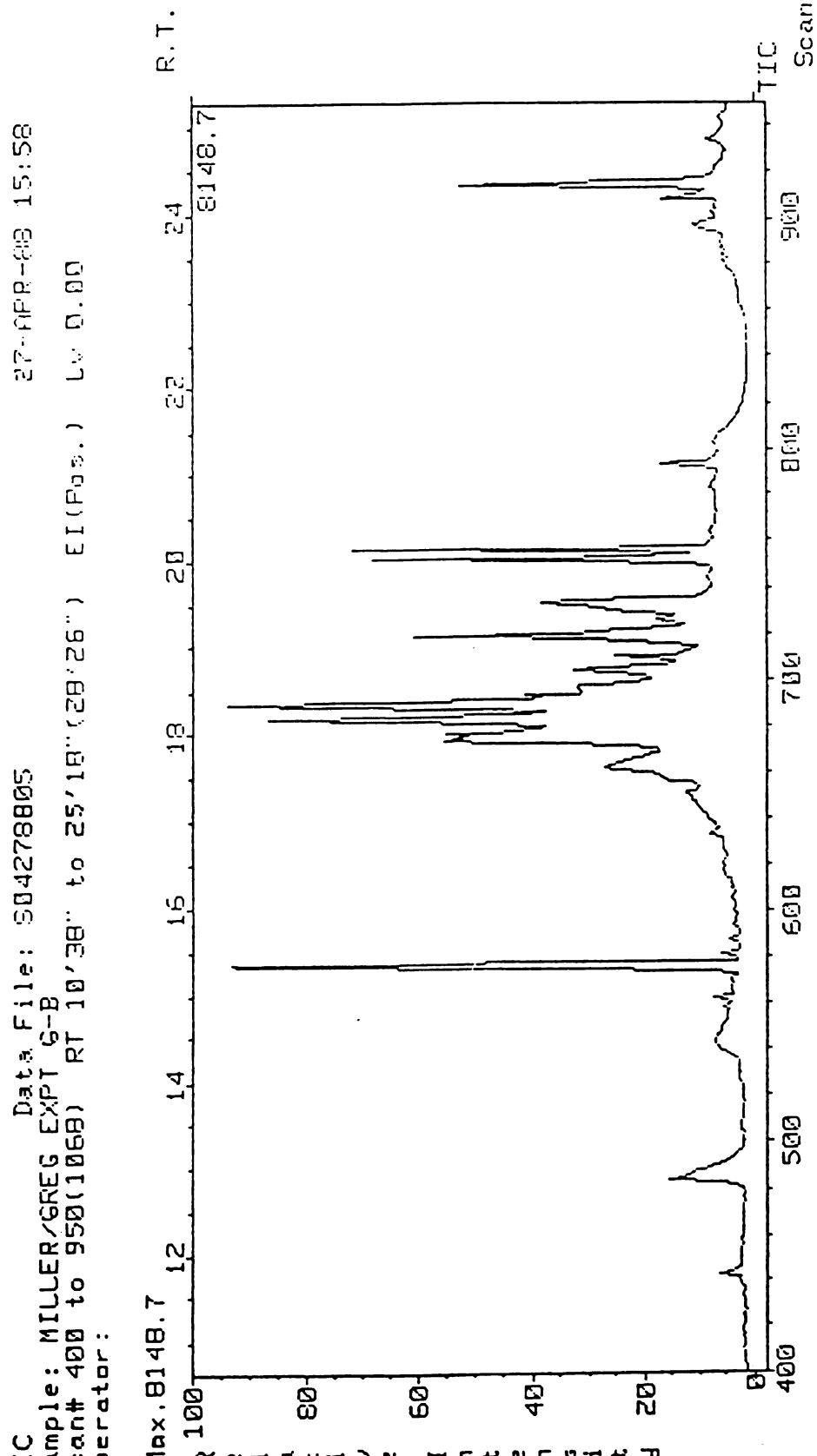

Figure 17. Gas Chromatography Trace for Experiment Six

individual peaks can be identified by either scan number or retention time. Because of the extensive manipulation performed on the raw data to obtain usable spectra, the peaks are identified here by retention time. Depending on how the background subtraction is done, the scan numbers for each peak can change.

C.2.1. Peak 20:07

Peak 20:07, whose mass spectrum is given in Figure A-14, exhibits a molecular ion at m/z 452. Applying the molecular formula procedure, a molecular formula of $C_6H_8O(TMSiO)_4$ with one double bond or ring was determined for this compound. This is supported by the the higher mass ions found in the fragmentation scheme: m/z 437 (M-15), m/z 362 (M-90), m/z 349 (M-103), m/z 347 (M-105), m/z 272 (M-90-90), m/z 259 (M-103-90), and m/z 247 (M-205). The absence of a significant ion at m/z 145 indicates that the fragmentation pathway M - (103 + n x 102) stops at one secondary carbon. The ion found at m/z 231 has been reported for TMS sugar derivatives and has $C_9H_{19}Si_2O_3$ as its probable formula [27,28]. The ion found at m/z 244 may be the product of a M-103-90-15 fragmentation pathway. As mentioned previously, the ions at m/z 305 and m/z 319 are common to TMS carbohydrate derivatives. In addition, an ion at m/z 335 suggests the presence of a 5-membered anhydro ring [34]. Furthermore, the data for this peak is comparable to that of peak 756 from Experiment Eight, so

that 1,4- or 3,6-anhydro-D-glucitol is a likely compound for this peak.

C.2.2. Peak 20:01

The mass spectrum for peak 20:01 is given in Figure A-15. This compound exhibits a molecular ion at m/z 380. This is supported by the presence of the higher mass ions for the fragmentation scheme given in Figure 13: m/z 365 (M-15), m/z 290 (M-90), m/z 277 (M-103), m/z 275 (M-105), m/z 200 (M-90-90), m/z 187 (M-103-90), and m/z 175 (M-205). Even though m/z 73 is a possiblity for an M-205-102 ion, indicating one primary and two secondary carbon atoms with hydroxyl groups, the fact that m/z 73 is a common TMS ion tends to preclude this conclusion. Due to the close proximity to peak 20:07, the presence of ions m/z 259 and m/z 362 are suspected to be carryovers, since they do not fit the major fragmentation pathways for a compound with mass 380.

A mass of 380 yields a molecular formula of $C_6H_9O_2(TMSiO)_3$ with one double bond or ring. This formula is similar to that of the previous peak, except that there is one less TMSiO group, one more oxygen atom, and one more hydrogen atom. However, this compound only has one double bond or ring, suggesting that one of the oxygen atoms is not present in a ring or double bond and thus singly bound to a carbon atom. Furthermore, the mass difference between this compound and the previous one is 72, which can be

represented by a TMSi group minus a hydrogen, $(CH_3)_3Si$ - H. In other words, one of the hydroxyl groups on the compound was not derivatized; a hydrogen atom is lost during the derivatizing reaction and the mass of the TMSi group is 73 (i.e. the difference in mass between a -OH substituent and a -OTMSi substituent is 72).

Possibile compounds to exhibit this effect include 3,6-anhydro-D-glucitol and 1,4-anhydro-D-mannitol. As shown in Figure 18, 3,6-anhydro-D-glucitol, 1,4-anhydro-D-mannitol being similar, has hydroxyl groups in a cis configuration within the ring while 1,4-anhydro-D-glucitol exhibits a trans configuration for the hydroxyl groups within the ring. This cis configuration may result in one of the hydroxyl groups being derivatized and hindering the derivatization of the second. Primary OH groups are derivatized more readily than secondary or tertiary OH groups [35]. Another possibility is that of inadequate derivatizing agent although this is doubtful, as large excess is present. As will be seen, this phenomenon is not isolated to this particular peak.

Another factor which supports the idea that one of the ring hydroxyl groups is hindered is the absence of the m/z 335 ion which is present when the compound contains a 5-membered fully-derivatized anhydro ring. It is probable that if one of the ring hydroxyl groups is hindered the structure that gives the m/z 335 ion should give a m/z 263 ion (335 - 72 = 263). This ion is not present, however,

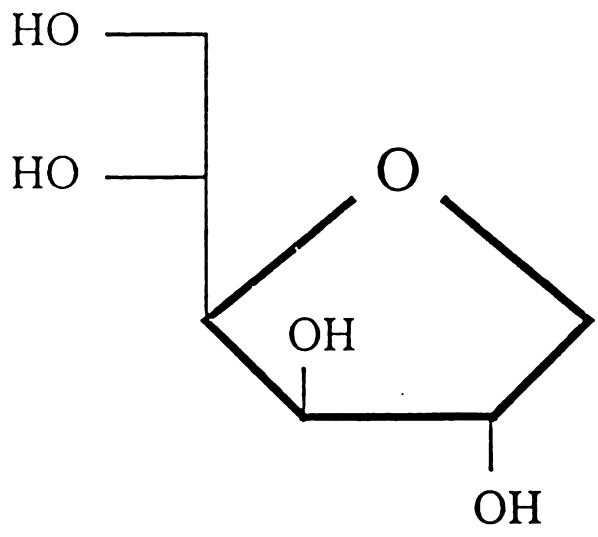

1,4-Anhydro-D-glucitol

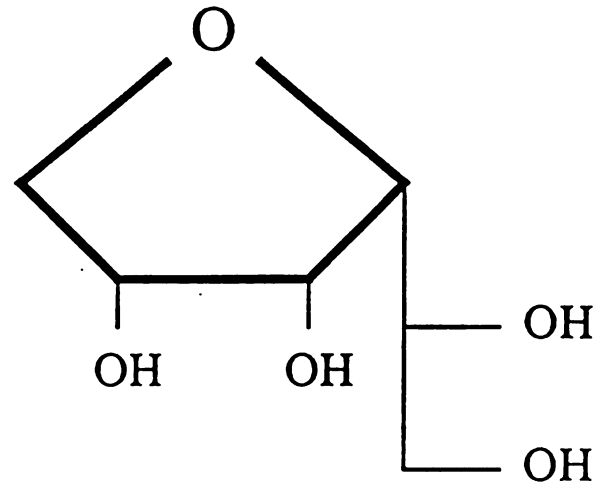

3,6-Anhydro-D-glucitol

Figure 18. Cis and Trans Hydroxyl Group Configuration for 1,4 and 3,6-Anhydro-D-Glucitol

and ions m/z 175 and m/z 205 are very small, suggesting that this compound contains a 6-membered anhydro ring, such as 1,5-anhydro-D-mannitol. Finally, most of the mass spectra which suggest a hindered hydroxyl group also exhibit a m/z 158 or m/z 159 ion, which is not seen in most TMS carbohydrates. The origin of this ion is as yet unexplained. An ion at m/z 157, however, is commonly seen for TMS carbohydrates and is not present for the hindered hydroxyl compounds.

C.2.3. Peak 19:27

Peak 19:27 contains two compounds, one having a molecular ion of m/z 452 and the other having a molecular ion of m/z 380. The mass spectra are given in Figures A-16 and A-17, respectively. The separate mass spectra were obtained by first determining where the m/z 452 and m/z 380 ions were at highest intensity. This was done by using the specific ion traces given in Figures B-3 and B-4, respectively. From these traces it was determined that the maximum for the m/z 452 ion occurred at the front of the peak and the maximum for the m/z 380 ion at the back. Using this information, mass spectra scans were taken at the appropriate positions to give Figures A-16 and A-17.

Even though the mass spectra given in Figure A-16 shows a highest mass ion of m/z 362, the specific ion traces in Figure B-3 both m/z 452 and m/z 437 ions at 19:27 which were evidently subtracted when Figure A-16 was

generated. As with the compound corresponding to peak 20:07, this compound shows a fragmentation scheme consistent with that from a molecular ion of m/z 452: m/z 437 (M-15), m/z 362 (M-90), m/z 349 (M-103), m/z 347 (M-105), m/z 272 (M-90-90), m/z 259 (M-103-90), and m/z 247 (M-205). An ion at m/z 169 results from the loss of a trimethylsilanol group from the m/z 259 ion. As with the spectrum for the 20:07 peak, no ion is found at m/z 145 and the m/z 244 and m/z 231 ions are present. Also, the m/z 335 ion is present and indicates a 5-membered anhydro ring. The absence of the m/z 145 ion suggests that the compound has one primary and one secondary hydroxyl-containing carbons attached to the ring (see Figure 16). The m/z 231 and m/z 244 are also present and have been previously discussed (peak 20:07). Due to the similarity between the fragmentation pathways for this peak and the 20:07 peak, it can be assumed that this peak at 19:27 is a single dehydration product, where the dehydration has formed a 5-membered anhydro ring and does not contain a hindered hydroxyl group.

As with the compound in peak 20:01, the mass spectrum presented in Figure A-17, the second compound at 19:27, exhibits a molecular ion of m/z 380. Due to the significant overlap of the two compounds at 19:27, m/z 349, m/z 305, and m/z 247 are thought to come from the m/z 452 compound. Also, these ions do not fit the major fragmentation pathways given earlier for the generation of higher mass ions from a compound with a molecular ion of m/z 380. The other

ions present, however, do fit the fragmentation scheme and are the same as those found in peak 20:01. In addition, the ion at m/z 263 shows a difference of 72 from the m/z 335 ion which is indicative of a 5-membered anhydro ring. Thus, this ion could result from the anhydro ring of a hindered hydroxyl compound. The loss of $C_2H_2O_2$TMS (mass 131) via a rearrangement fragmentation of the anhydro ring is a possible source for the ion at m/z 249. Finally, this compound exhibits the m/z 158-159 peak which appears with the hindered hydroxyl compounds. This compound also shows some isomeric tendency with that of peak 20:01 because of the similarity in ions. Because of the m/z 263 ion, however, this compound is a more likely candidate to be 1,4-anhydro-D-mannitol or 3,6-anhydro-D-glucitol, which both have hindrance potential.

C.2.4. Peak 19:07

The peak at 19:07 also contains two compounds. The original mass spectrum taken for this peak exhibited ions indicative of a fragmentation pattern for both m/z 452 and m/z 380. This spectrum is given in Figure A-18. Using the ion traces given in Figures B-3 and B-4 it was determined that the m/z 380 maximum occurred at the front of the peak and the m/z 452 at the back of the peak. The mass spectra for these compounds are given in Figures A-19 and A-20, respectively. Because of the overlap, several ions show up for both compounds. These include m/z 247, m/z 259,

m/z 349, and m/z 362 carrying over from the m/z 452 compound onto the spectrum for the m/z 380 compound.

As with the other m/z 380 peaks, this compound exhibits the m/z 365 (M-15), m/z 290 (M-90), m/z 277 (M-103), m/z 275 (M-105), m/z 200 (M-90-90), m/z 187 (M-103-90), and m/z 175 (M-205) ions. As stated previously, the M-205 ion indicates one primary and one secondary carbon with a hydroxyl group coming from the carbon-chain fragmentation. The m/z 158-159 ion is also present, showing this compound to be of the hindered-hydroxyl type. Once again, this data is comparable to that for the other m/z 380 compounds, varying primarily in ion intensity, so that this compound is also likely to be a 5-membered anhydro ring compound that has hindrance potential.

The m/z 452 component of this peak exhibits the same fragmentation scheme as that of the other m/z 452 peaks. As can be seen in Figure A-20 two ions, m/z 404 and m/z 479, are also present. These ions are thought to be "junk" ions since they do not yield any feasible fragmentation paths that give the other major ions present in the scan. As with the other m/z 452 compounds, the m/z 437 (M-15), m/z 362 (M-90), m/z 349 (M-103), m/z 347 (M-105), m/z 272 (M-90-90), and m/z 259 (M-103-90) ions are present. The M-205 ion, m/z 247 is not shown in Figure A-20, but is present in both Figure A-18, the original mass spectra for the peak and Figure B-5, the specific ion scan for m/z 247, suggesting that the m/z 247 ion was subtracted during the

scan generation. The m/z 169 (M-103-90-90) and a small m/z 335 (5-membered ring rearrangement) ions are also present. Thus, this compound seems to be yet another isomer of the single dehydration compounds discussed earlier.

C.2.5. Peak 18:54

Figure A-21 shows the mass spectrum for the peak at 18:54. The molecular ion for this compound is m/z 452 which is apparent from the ions present (same fragmentation as previous m/z 452 compounds). Also, the specific ion traces given in Figure B-3 show the presence of both the m/z 452 and m/z 437 ions. This compound, however, generates no m/z 247 (M-205) ion, indicating that the compound only loses the primary carbon from the carbon chain and not the adjacent secondary carbon. Furthermore, there is no m/z 335 ion to suggest the presence of a 5-membered ring; the m/z 205 ion intensity is also very small. This suggests the formation of a 6-membered anhydro ring rather than a 5-membered ring.

C.2.6. Peak 18:44

The mass spectrum in Figure A-22 corresponds to the peak at 18:44. Even though no ion is present at m/z 380, this compound exhibits other high mass ions such as m/z 365 (M-15), m/z 290 (M-90), m/z 277 (M-103), m/z 275 (M-105), and m/z 200 (M-90-90) to support m/z 380 as the molecular

ion. Even though this compound exhibits almost no m/z 175, suggesting that a M-205 pathway is not present, the strength of the m/z 205 ion precludes this conclusion. The ion at m/z 187 is formed by the decomposition of the m/z 277 ion (m/z 277-90). Because the m/z 349 ion is not present for this compound, as shown in Figure B-6, it is probable that the m/z 259 (349-90) and m/z 169 (259-90) ions are not from this compound. From this information this peak seems to be a 5-membered anhydro ring compound with a hindered hydroxyl group even though this is the only compound that does not show the m/z 158-159 ion.

C.2.7. Peak 18:20

The next and largest peak occurs at 18:20 and also contains two compounds. One of these compounds exhibits a molecular ion at m/z 362 while the other at m/z 380. The mass spectra for these two compounds are given in Figures A-23 and A-24, respectively.

Because of the absence of a m/z 452 or m/z 437 ion in both Figures A-23 and B-3, the m/z 362 ion is the molecular ion of this compound. The M-15 ion, m/z 347, is not present on the mass spectrum given in Figure A-23 but does show up in the specific ion trace given in Figure B-6. The m/z 272 (M-90) and m/z 257 (M-105) ions are present in small amounts but show up more in Figure A-24 due to the overlap of the two compounds. Also present is the m/z 259 (M-103) ion. The m/z 290, m/z 277, and m/z 290 ions are

all carryovers from the m/z 380 compound.

This compound exhibits two major differences from the others that have been discussed. The first is the presence of the m/z 319 ion. As mentioned before, this is a common rearrangement ion for TMS carbohydrates. To form this ion, the compound loses a fragment of mass 43 which corresponds to a formula of C_2H_3O or H_3CCO. A common dehydration reaction for polyols is the pinacol rearrangement shown in Figure 19 for a glycol. As can be seen in the figure, the pinacol rearrangement reaction results in a portion of the molecule whose mass is 43. In addition, the presence of a methyl group in the molecule inhibits the cleavage of the C_1-C_2 bond and promotes the cleavage of the C_2-C_3 bond which is also shown in Figure 19. This fragmentation results in the formation of an M-43 ion.

Another major difference for this compound arises when the molecular formula is obtained. Using the procedure outlined previously, this compound gives a molecular formula of $C_6H_7O(TMSiO)_3$ with two double bonds or rings. Because there is only one oxygen atom, however, the other double bond must be between two carbon atoms. This leads to the possible reaction scheme shown in Figure 20. The proposed location of the C-C double bond in Figure 20 is a result of the presence of the m/z 205 ion, requiring the compound to have a primary and an adjacent secondary carbon with a derivatized hydroxyl group. Based on the structure in Figure 20, the m/z 362 is tentatively identified as

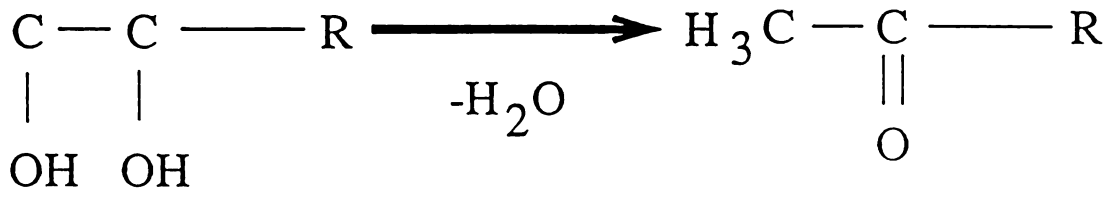

Pinacol Formation

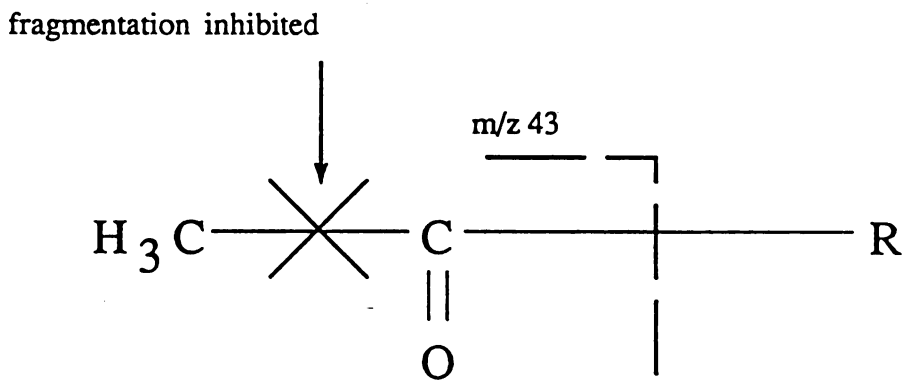

Pinacol Fragmentation

Figure 19. Pinacol Rearrangement Reaction and Fragmentation

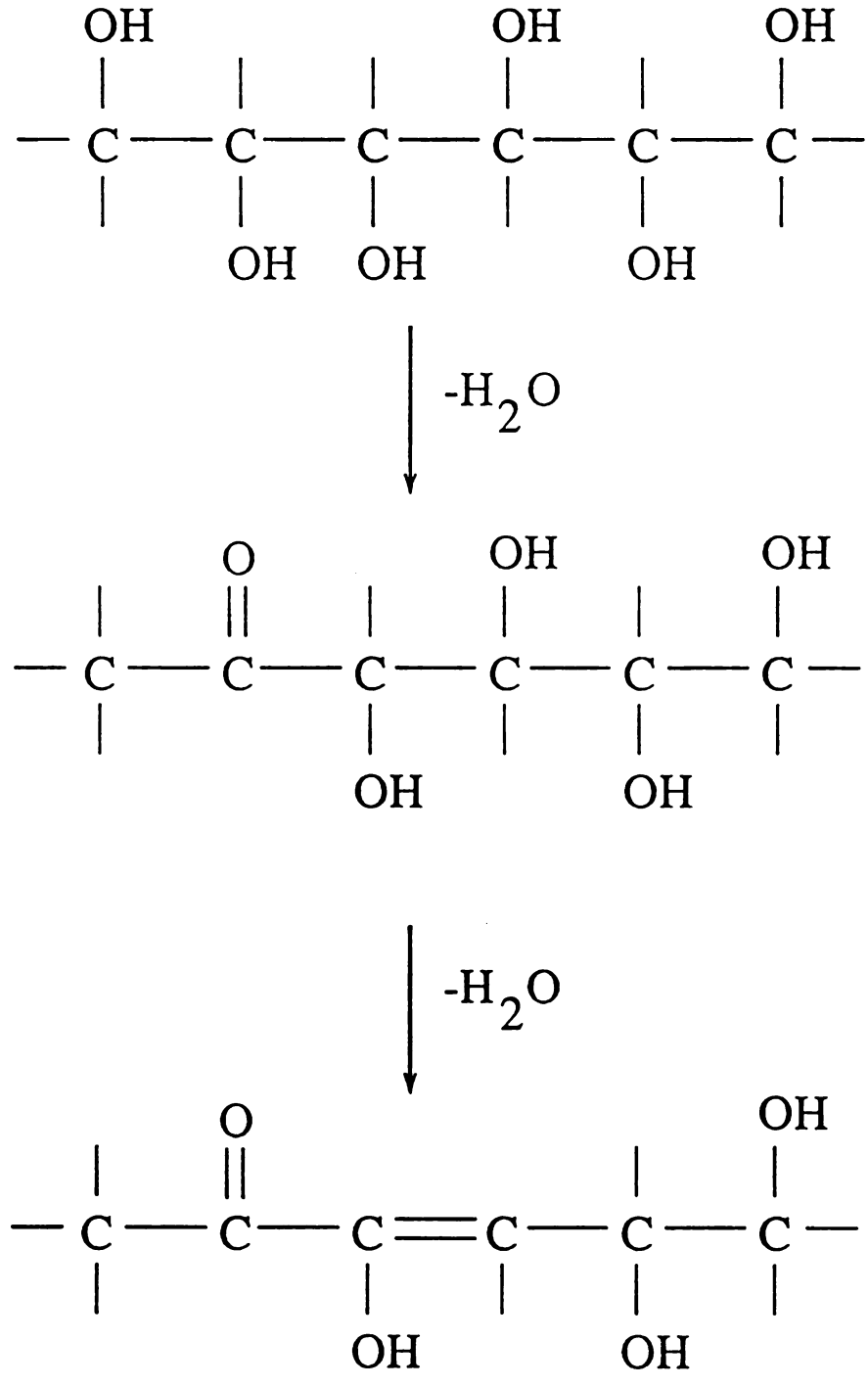

MW 362 in TMS ether form

Figure 20. Reaction Scheme for 3,5,6-Trihydroxy-3-Hexen-2-one Formation

3,5,6-trihydroxy-3-hexen-2-one.

The m/z 380 portion of this peak also exhibits an M-43 ion. The m/z 337 ion is not present in Figure A-24 but is present in Figure A-23 and the original mass spectrum (Figure A-25) and was probably subtracted out during the scan generation. This compound gives the M-15, M-90, M-103, M-105 (small), and M-205 ions which is consistent with the earlier fragmentation descriptions of the m/z 380 compounds. The m/z 205 and m/z 200 (M-90-90) ions are present in Figure A-25 and were likely subtracted out due to the close choices for background scan numbers (the scan was taken at 687 and the background was subtracted at 686 and 691). Since this compound has a mass of 380 the molecular formula obtained for it is the same as that for the other m/z 380 compounds: $C_6H_9O_2(TMSiO)_3$ with one ring or double bond. In this case, however, it is probable that the dehydration resulted in the formation of a pinacol rearrangement product rather than an anhydro ring, due to the presence of the M-43 ion.

C.2.8. Peak 18:09

The peak at 18:09 also consists of two compounds, one with a molecular ion of m/z 290 and the other m/z 308. The mass spectra are given in Figures A-26 and A-27, respectively. As can be seen from Figure B-7, however, the intensity of the m/z 290 compound is 20 times greater than that of the m/z 308 compound. Therefore, the discussion of

the m/z 308 compound will be limited to saying that it is some sort of dehydration compound with at least one pinacol rearrangement because of the m/z 265 (M-43) ion. Applying the molecular formula procedure yields the following formula: $C_6H_{10}O_3(TMSiO)_2$ with one ring or double bond.

The m/z 290 compound gives the same molecular formula as isosorbide, $C_6H_8O_2(TMSiO)_2$ with two rings or double bonds. This compound, however, exhibits both an M-43 (m/z 247), indicating a pinacol fragment, and the m/z 205 ion, indicating the one primary, one secondary carbon pathway. Because of the presence of both the M-43 and the m/z 205 ions, the presence of a ring in this compound is very unlikely. This is because both of these ions require both a primary and an adjacent secondary carbon in order to occur. Because the general formula indicates two dehydrations, the second must occur between the C_3 and C_4 carbons. Thus this compound is a dianhydro compound with at least one pinacol dehydration present.

C.2.9. Peak 15:20

Comparison of the mass spectrum for the 15:20 peak (shown in Figure A-28) with that of peak 558 from Experiment Eight show both to be isosorbide.

C.2.10. Peaks 24:20, 24:12 and 23:53

Peak 24:20 is shown in Figure A-29. The highest mass ion is at m/z 452, however the presence of the m/z 307, m/z

409, and m/z 421 ions identify this compound as sorbitol. These ions, respectively, represent the (M-205-102), (M-105-90) and (M-103-90) ions for sorbitol. The peaks at 24:12 and 23:53 (Figures A-30 and A-31) also exhibit the m/z 307 which has been shown to be a marker for sorbitol [28]. Because of the size of the peaks, it is not possible to accurately determine whether the other high mass ion peaks for sorbitol are present, although the 23:53 peak has the m/z 409 and m/z 419 ions (the mass spectrum in [28] shows a m/z 419 ion in the m/z 421 ion group). The m/z 512 ion present in Figures A-29 and A-31 is a "junk" ion, as shown in Figure B-8.

D. DISCUSSION

Inspection of the results presented in Table 6 reveals several characteristics of the effect of the catalyst and reaction conditions on D-glucitol conversion.

First, temperature had the strongest effect on sorbitol conversion, with little reaction at 180 ^{o}C and nearly complete conversion at 260 ^{o}C.

Second, Experiments Four, Seven, and Nine, performed at 240 ^{o}C but with varying pressures, show that 1) the conversion for Experiment Seven deviates from the conversion for the other two experiments, and 2) that increasing the pressure does not substantially affect the conversion of sorbitol. The conversion deviation for Experiment Seven

is probably due to data scatter caused by a loss of water during product recovery. During this step some water was spilled, the amount of which could not be determined.

Increasing the pressure 800 psi at 240 ^{o}C increases the conversion only 9%; a 20 ^{o}C increase from 240 ^{o}C to 260 ^{o}C results in a 53% increase in conversion.

Third, Experiments Six and Ten, performed under identical conditions but with different run times, show little difference in the amount of sorbitol conversion and product distribution. The small difference in sorbitol conversion is most likely a result of the small amount of sorbitol remaining being unavailable to the catalyst. The sorbitol may be adhered to the glass liner wall or to the reactor head attachments.

Finally, Experiments Four and Eight, performed under identical conditions but with different catalysts, show a large difference in sorbitol conversion. This is the result of exchanging some of the Ca ions with Pt and thus losing some dehydration activity. On a molar basis alone, 5 wt. % Pt will replace approximately 8% of the Ca ions present. However, approximately 50% of the Ca ions are situated at site 1 in Figure 21 and the rest at site 2 [20,37]. The Pt ions are too large to enter the site 1 positions and will only replace the Ca ions located at site 2. This results in the Pt replacing approximately 15% of the Ca ions and reducing the dehydration activity of the catalyst.

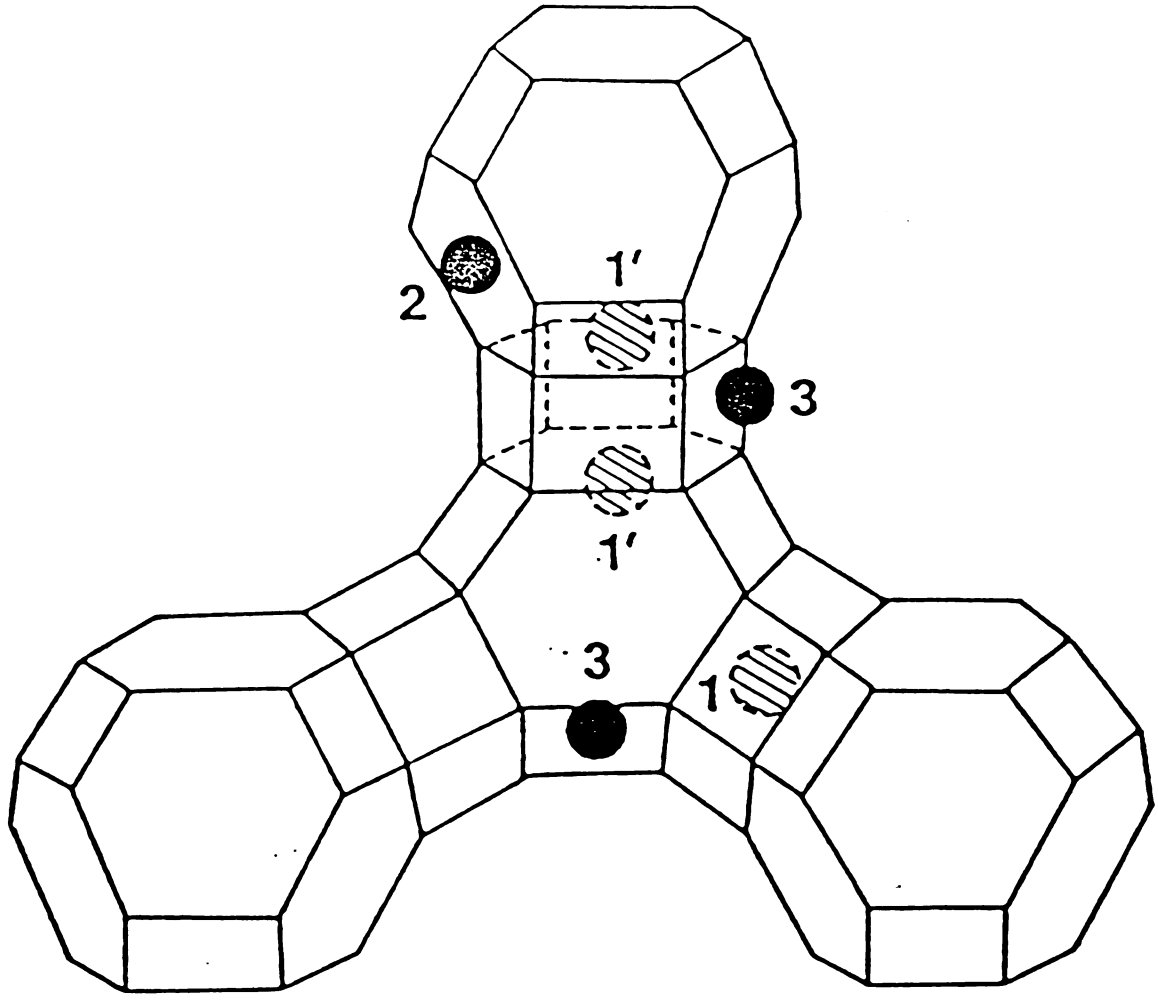

Figure 21. Location of Ca Ions in Type Y Zeolite Structure [37]

A summary of HPLC and GC retention times, approximate product yields, and probable product names is given in Table 7. The term "Alditans" refers to the family of compounds possessing a single anhydro ring. The term "Pinacolones" refers to the family of compounds formed via the pinacol dehydration reaction. The names given to some of these compounds are not 100% certain due to the difficulty in identifying isomers via mass spectrometry of TMS carbohydrate ethers; rather, they represent the types of compounds which exhibit the observed spectra.

The combination of the mass spectrscopic analysis and the retention characteristics of the GC and HPLC columns allowed for the calculation of the product yields for each compound or class of compounds.

Analysis of the mass spectral data for Experiment Six was much more involved than for Experiment Eight. This was due primarily to the fact that most of the peaks displayed on the gas chromatogram actually represented two (or possibly more) compounds and that cyclic compounds give more than one peak upon derivatization. This resulted in data that did not initially reflect plausible fragmentation schemes.

In Experiment Eight, the major products formed were 1,4-anhydro-D-glucitol and 1,4:3,6-dianhydro-D-glucitol. As mentioned in Section C.1., these are the preferential dehydration products of D-glucitol in acids. This was not unexpected since it was shown by Minachev et al. [17] that

TABLE 7

SUMMARY OF WATER-SOLUBLE PRODUCTS

Experiment Six

Product	TMS MW	GC-MS Retention Time	HPLC Retention Time	Approximate Yield
Isosorbide	290	15:20	17.53	10.5%
Alditans			13.98/14.42	29%
1,4-anhydro-D-glucitol	452	20:07		
1,5-anhydro-D-mannitol	380	20:01		
1,4-anhydro-D-mannitol	380/452	19:29		
3,6-anhydro-D-glucitol	380/452	19:07		
1,5-anhydro-D-glucitol	452	18:54		
5-membered ring unknown	380	18:44		
Pinacolones			15.92	9.5%
3,5,6-trihydroxy-3-hexen-2-one	362	18:17		
noncyclic monoanhdyro unknown	380			
noncyclic dianhydrol unknown	290	18:09		
Sorbitol	614	24:20	13.2	13%
L-iditol	614	23:53		
D-mannitol	614	24:12		

TABLE 7 cont.

SUMMARY OF WATER-SOLUBLE PRODUCTS

Experiment Eight

Product	TMS MW	GC-MS Retention Time	HPLC Retention Time	Approximate Yield
Isosorbide	290	18:21	16.83	21%
Alditans			13.45/13.80	17%
1,4-anhydro-D-glucitol	452	25:10		
Pinacolones	362	24:00	15.2	trace
Sorbitol	614	29:00	12.79	8%

a Ca Y zeolite is an effective alcohol dehydration catalyst.

A variety of products were formed in Experiment Six. These included 1,4-anhydro-D-glucitol, 1,4:3,6-dianhydro-D-glucitol, 3,6-anhydro-D-glucitol, and 3,5,6-trihydroxy-3-hexen-2-one (shown in Figure 20). A number of other alditans and pinacolones were formed and are listed in Table 7. As mentioned before, the positive identification of these compounds is not possible.

Two major differences occur between this experiment and Experiment Eight. First, the number of products is much larger. This can be attributed to the presence of the Pt. The isomerization characteristics of Pt acid zeolite catalysts is well-documented. In addition, it is reported that the high-pressure hydrogenation of D-glucitol in the presence of Pt results in an equilibrium between D-glucitol, D-mannitol, and L-iditol [32]. This leads to the possibility of forming dehydration products from all three of these compounds. For the compounds shown in Figures A-29 through A-31, the major difference is in the relative intensities of the major ions. This similarity in spectra lends credibility to the occurence of isomerization. Due to the size of the peaks, however, the positive identification of the 24:12 and 23:53 peaks as D-mannitol and L-iditol is not possible.

The second difference is the presence of pinacol dehydration products. This can also be attributed to the

presence of the Pt. Because Pt is both an excellent hydrogenation/dehydrogenation catalyst and an excellent hydrogen adsorber, it facilitates the hydrogen abstraction necessary for the pinacol dehydration to occur and offers adsorption sites for the H^+ ions generated from the reaction.

In addition to the pinacol reaction, another dehydration reaction was observed. As can be seen in Figure 20, a C-C double bond is formed via a dehydration reaction. Because the compound formed from this reaction does not occur in Experiment Eight, this reaction can also be attributed to the presence of the Pt. This reaction occurs after the formation of a pinacolone compound and involves the β-hydroxyl group [36]. Because of the keto group, the dehydration of the β-hydroxyl group is greatly enhanced and the α-hydroxyl dehydration is greatly inhibited. Because this reaction also involves hydrogen abstraction, the catalytic property of Pt mentioned in the previous paragraph is also applicable here.

From the above discussion, it is apparent that the Pt exhibits no significant hydrogenation activity, even at H_2 pressures above 1300 psig. Instead, the catalytic activity of the Pt is primarily dehydrogenation, with isomerization as a secondary activity.

CHAPTER 6

CONCLUSIONS

A summary of the conclusions obtained from the research is given below.

First, the catalytic activity of the catalysts used was primarily dehydration and dehydrogenation, with some isomerization activity. The dehydration activity was higher for the Ca Y catalyst than the Pt/Ca Y catalyst which is due to the replacement of some of the Ca ions with Pt ions during the metal loading. This dehydration activity resulted in the formation of anhydro ring compounds, primarily 1,4-anhydro-D-glucitol.

The dehydrogenation and isomerization activities were present only for the Pt/Ca Y catalyst. The presence of the Pt resulted in pinacol rearrangement and β-hydroxyl dehydration reactions in addition to the anhydro ring formation. The Pt activity resulted in the formation of pinacolone compounds, specifically 3,5,6-trihydroxy-3-hexen-2-one.

Second, high conversions of sorbitol were obtained under relatively mild conditions. Between 87% and 92%

conversion was observed at 240-260 ^{o}C and 160 psig. This high conversion of sorbitol was much more sensitive to changes in temperature as opposed to changes in pressure.

Finally, shape selectivity was apparent for the catalysts used due to the small number of water-soluble products obtained. This shape selectivity resulted in good yields of isosorbide, especially in Experiment Eight. Because it is relatively volatile, the gas phase conversion of isosorbide to hydrocarbons should be considered as a possibility for further investigation.

LIST OF REFERENCES

LIST OF REFERENCES

[1] Boyles, D. T., Bio-energy: Technology, Thermodynamics, and Costs, Ellis Howard Limited, 1984 pp. 46-60.

[2] Dubeck, M. and Knapp, G. G., United States Patent 4,430,253, 1984.

[3] Arena, B. J., United States Patent 4,401,823, 1984.

[4] Chen, N. Y. and Koenig, L. R., United States Patent 4,503,278, 1985.

[5] Arena, B. J., United States Patent 4,380,679, 1983.

[6] Ibid., United States Patent 4,380,680, 1983.

[7] Ibid., United States Patent 4,382,150, 1983.

[8] Ibid., United States Patent 4,413,512, 1983.

[9] Winfield, M. E., Emmett, P. H. ed., Catalysis, Volume VII, Reinhold Publishing Corporation, 1960

[10] Baunford, C. H. and Tipper, C. F. H., eds., Comprehensive Chemical Kinetics, Volume 20, Elsevier Scientific Publishing Company, 1978 pg. 281.

[11] Szabo, Z. G., J. Catalysis, 6, 458 (1966).

[12] Saunders, W. H., Jr. and Cockerill, A. F., Mechanisms of Elimination Reactions, John Wiley and Sons, 1973 pg. 256.

[13] Weisz, P. B. and Frilette, V. J., J. Phys. Chem., 64, 382 (1960).

[14] Rudham, R. and Stockwell, A., Imelik, B. et al., eds., Catalysis by Zeolites, Elsevier Scientific Publishing Company, 1980 pp. 113-119.

[15] Ballantine, J. A., Davies, M., Patel, I., Purnell, J. H., Rayanakorn, M., Williams, K. J., and Thomas, J. M., J. Mol. Catal., 26, 37 (1984).

[16] Chong, P. J. and Curthoys, G., Zeolites, 1, 41 (1966).

[17] Minachev, Kh. M., Garanin, V. I., and Isakov, Ya. I., Izv. Akad. Nauk SSSR, Ser. Khim., 1635 (1964).

[18] Sharf, V. Z., Piontkovskaya, M. A., Freidlin, L. Kh., Neimark, I. E., Rastorgueva, M. N., and Shameka, G. S., Izv. Akad. Nauk. SSSR. Ser. Khim., 2196 (1971).

[19] Jacobs, P. A., Carboniogenic Activity of Zeolites, Elsevier Scientific Publishing Company, 1977 pg. 101.

[20] Rabo, J. A., Schomaker, V., and Pickert, P. E., Proc. 3rd Int. Congress on Catalysis, 1964, North Holland Publishing Company, 2, 1264 (1965).

[21] Kubo, T., Arai, H., Tominaga, H., and Kunugi, T., Bull. Chem. Soc. of Japan, 45, 607 (1972).

[22] Gallezot, P., Alarcon-Diaz, A., Dalmon, J-A., Renouprez, A. J., and Imelik, B., J. Catalysis, 39, 334 (1975).

[23] Reference 19, pg. 3.

[24] Dalla Betta, R. A. and Boudart, M., Catalysis, 1, pg. 1329, North-Holland Publishing, 1973

[25] Treptau, M. H. and Miller, D. J., Ind. Eng. Chem., Res., 26, No. 10, 2007 (1987).

[26] Pierce Chemical Company Catalog, 1987, pg. 186.

[27] DeJongh, D. C., Radford, T., Hribar, J. D., Hanessian, S., Bieber, M., Dawson, G., and Sweeley, C. C., J. Am. Chem. Soc., 91, 1728 (1969).

[28] Petersson, G., Tetrahedron, 25, 4437 (1969).

[29] Kochetkov, N. K. and Chizhov, O. S., Methods Carb. Chem., 6, 540 (1972).

[30] Ibid., Adv. Carb. Chem. Biochem., 21, 39 (1966).

[31] Lönngren, J. and Svensson, S., Adv. Carb. Chem. Biochem., 29, 42 (1974).

[32] Stanek, J., The Monosaccharides, Chapter 26, New York Academic Press, 1963 pp. 636-639.

[33] Bock, K., Pedersen, C., and Thogersen, H., Acta Chem. Scan. B., 35, 441 (1981).

[34] Chizhov, O. S., Zolotarev, B. M., Usov, A. I., Rechter, M. A., and Kochetkov, N. K., Carbohyd. Res., 16, 29 (1971).

[35] Knapp, D. R., Handbook of Analytical Derivatization Reactions, John Wiley and Sons, 1979 pg. 8.

[36] Streitweiser, A., Jr. and Heathcock, C. H., Introduction to Organic Chemistry, MacMillan Publishing Company, Incorporated, 1976 pp. 678-679.

[37] Vaughan, D. E. W., Chem. Eng. Prog., February 1988, pg. 25.

APPENDIX A

86
Hexane

C_6H_{14}

110-54-3

$Me(CH_2)_4Me$

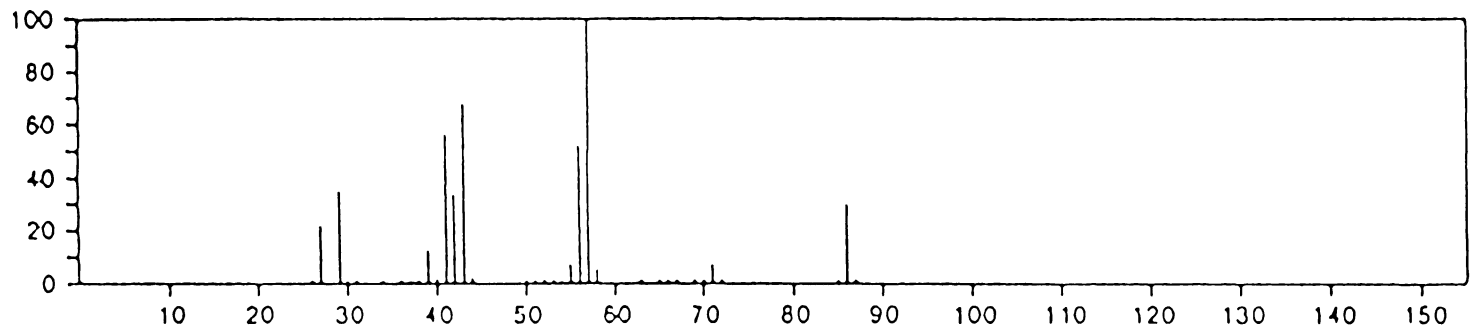

Figure A-1. Mass Spectrum of Hexane from EPA/NIH Mass Spectral Data Base

84 C_6H_{12} 592-41-6

1-Hexene

$H_2C:CH(CH_2)_3Me$

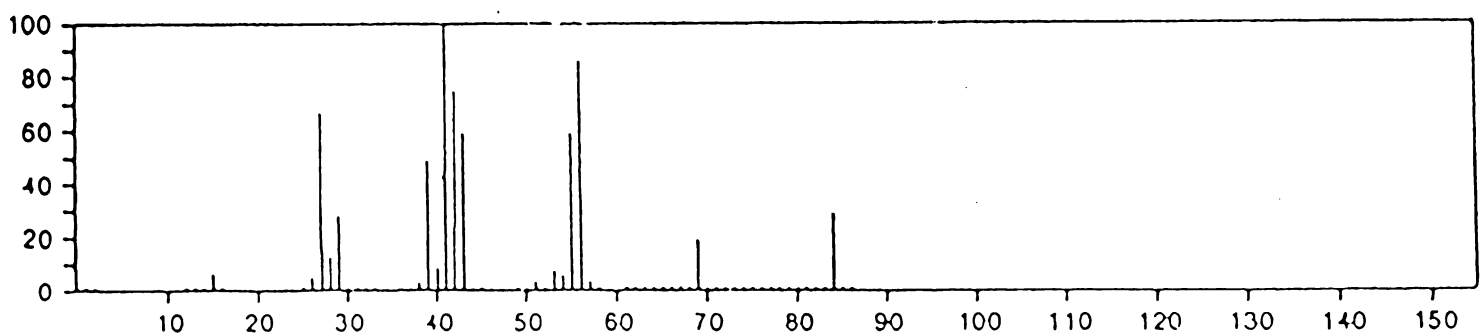

Figure A-2. Mass Spectrum of 1-Hexene from EPA/NIH Mass Spectral Data Base

102
1-Hexanol

$C_6H_{14}O$

111-27-3

Me (CH_2) 5 OH

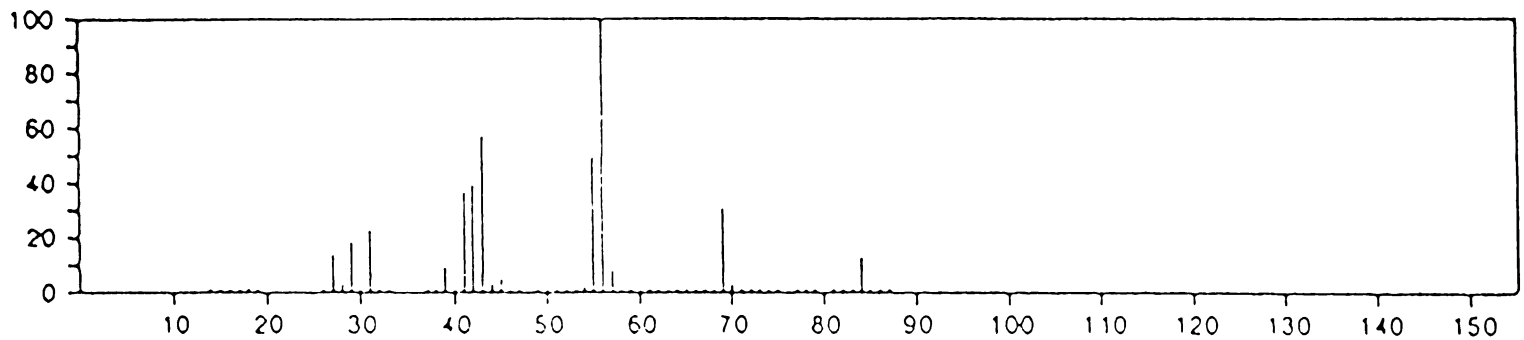

Figure A-3. Mass Spectrum of 1-Hexanol from EPA/NIH Mass Spectral Data Base

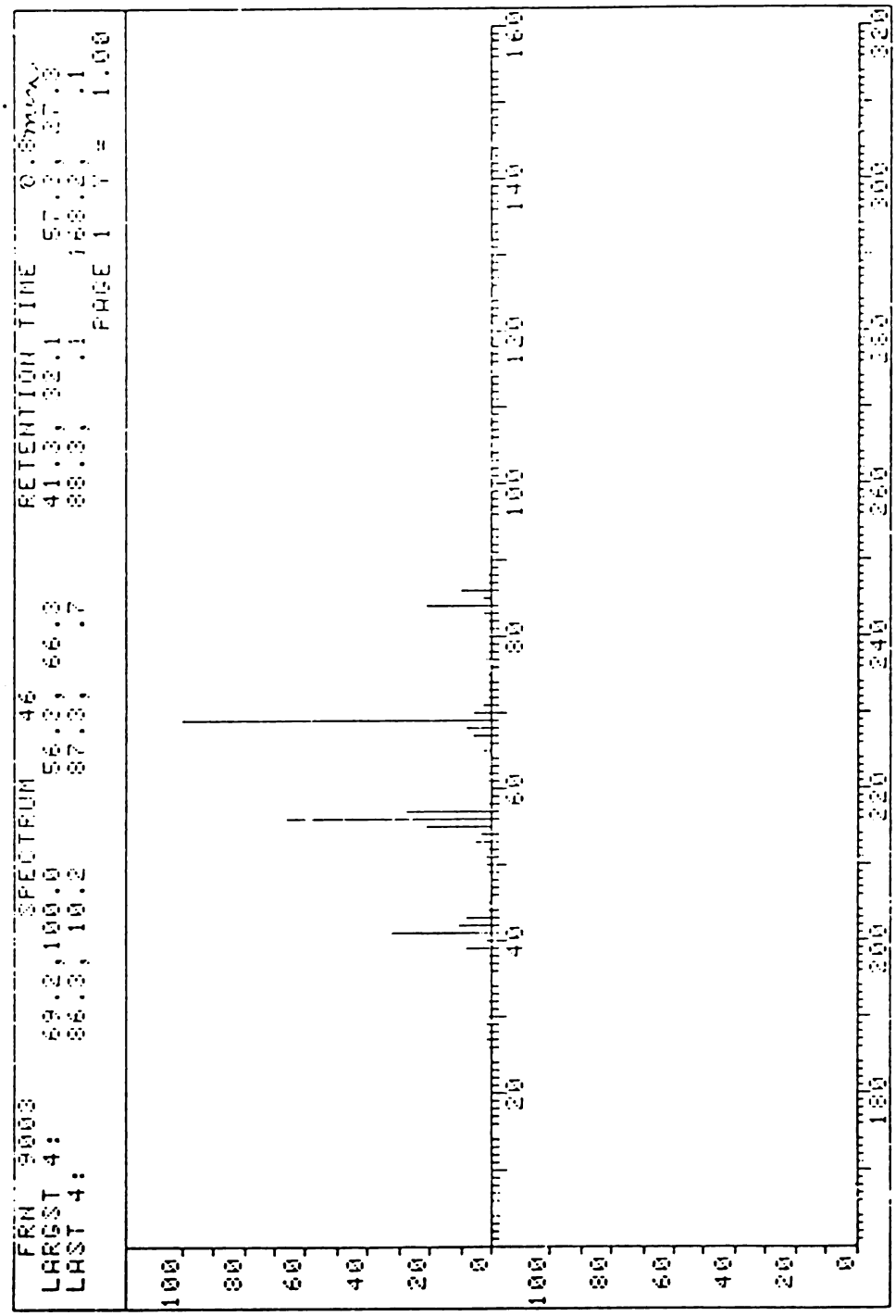

Figure A-4. Mass Spectrum of Hexene from Hexanol Experiment

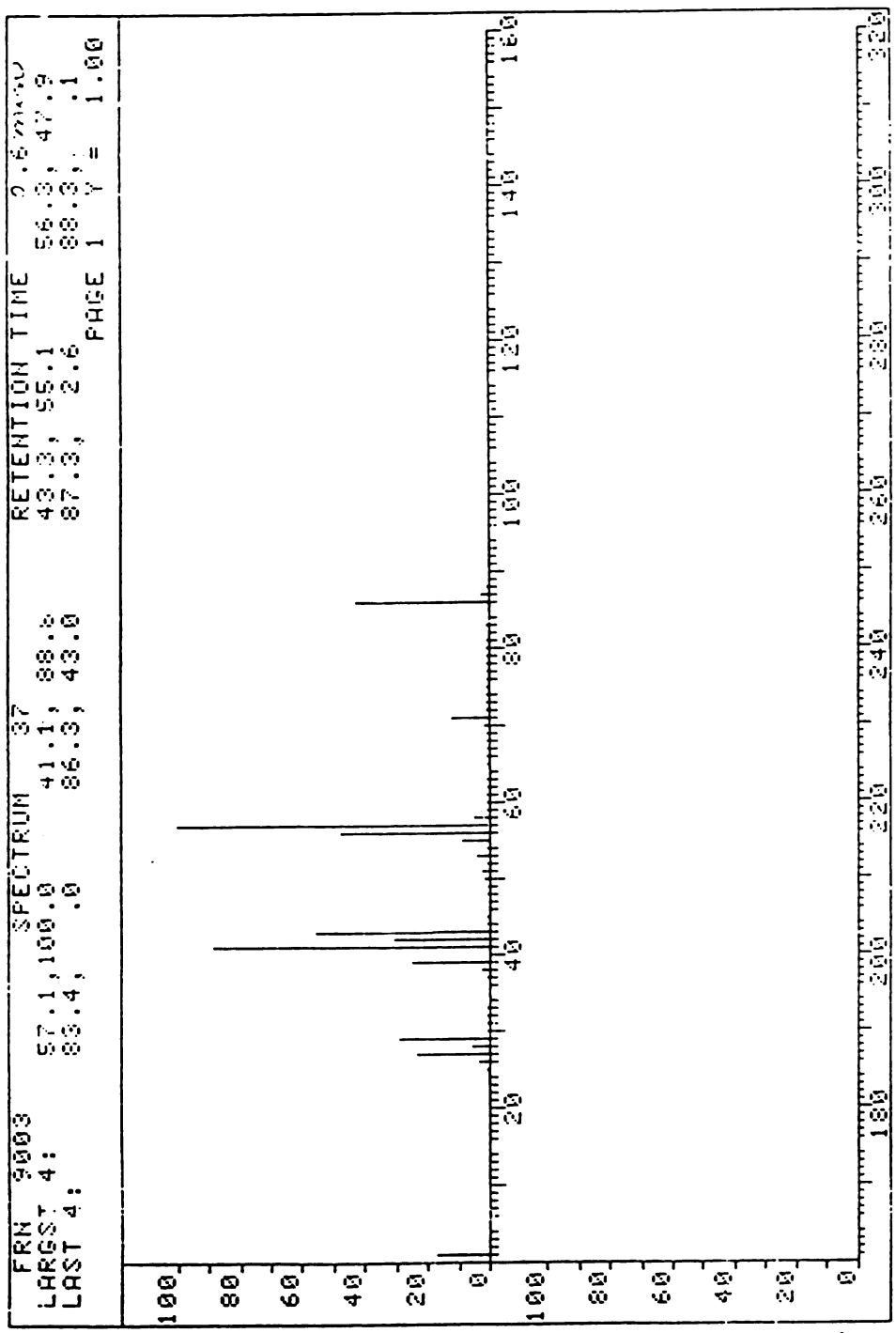

Figure A-5. Mass Spectrum of Hexane from Hexanol Experiment

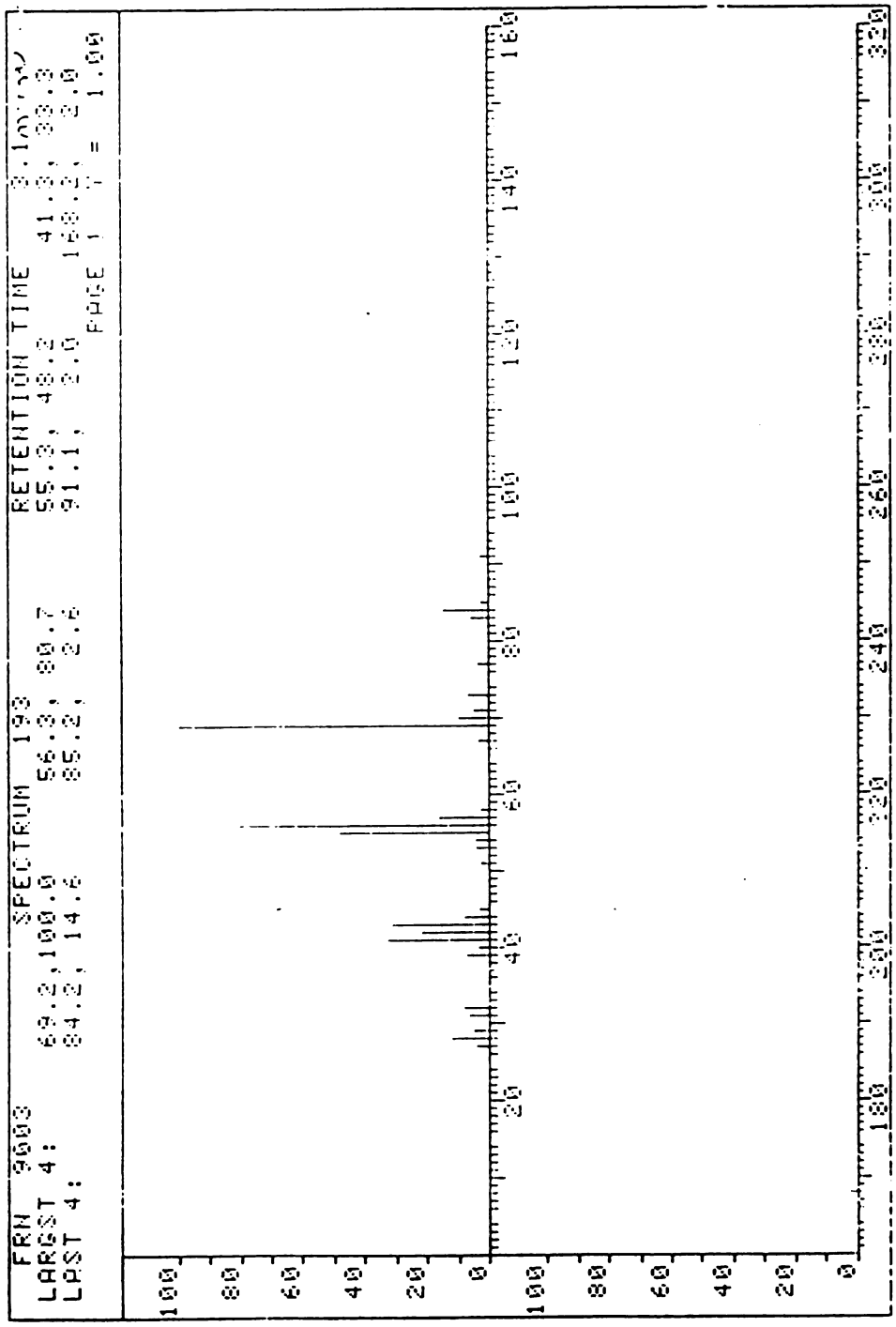

Figure A-6. Mass Spectrum of Hexanol from Hexanol Experiment

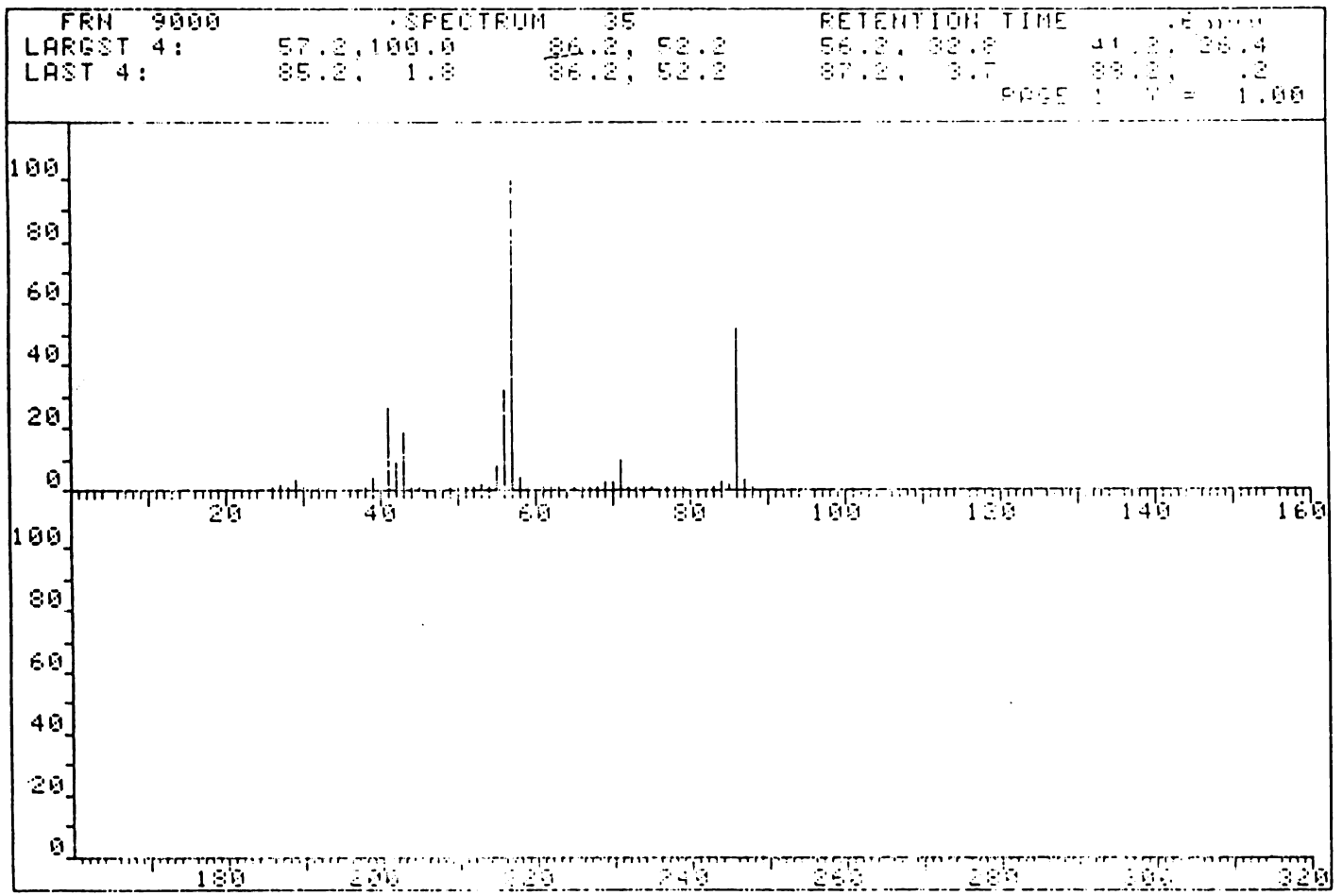

Figure A-7. Mass Spectrum of Hexane from 1,2-Hexanediol Experiment

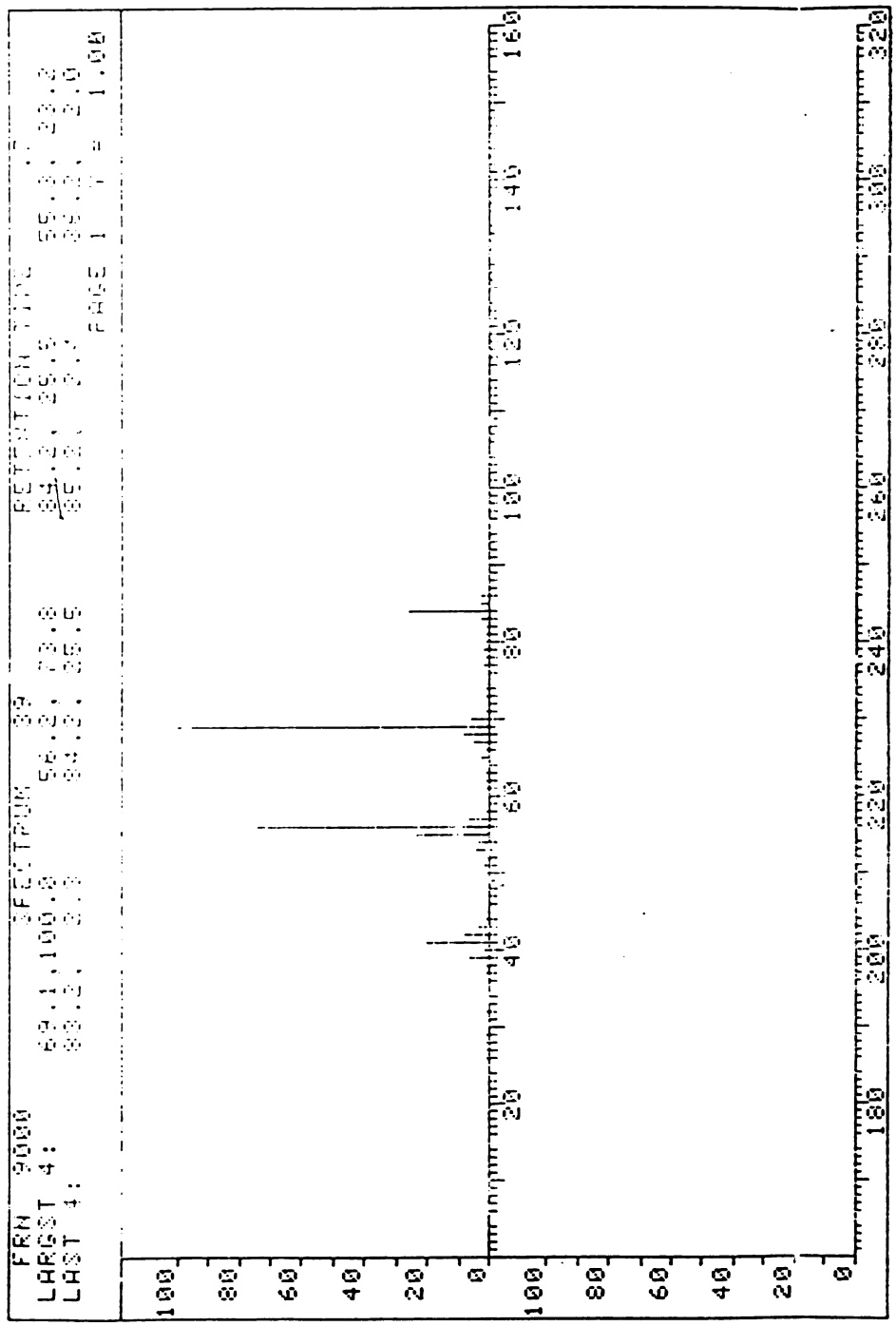

Figure A-8. Mass Spectrum of Hexene from 1,2-Hexanediol Experiment

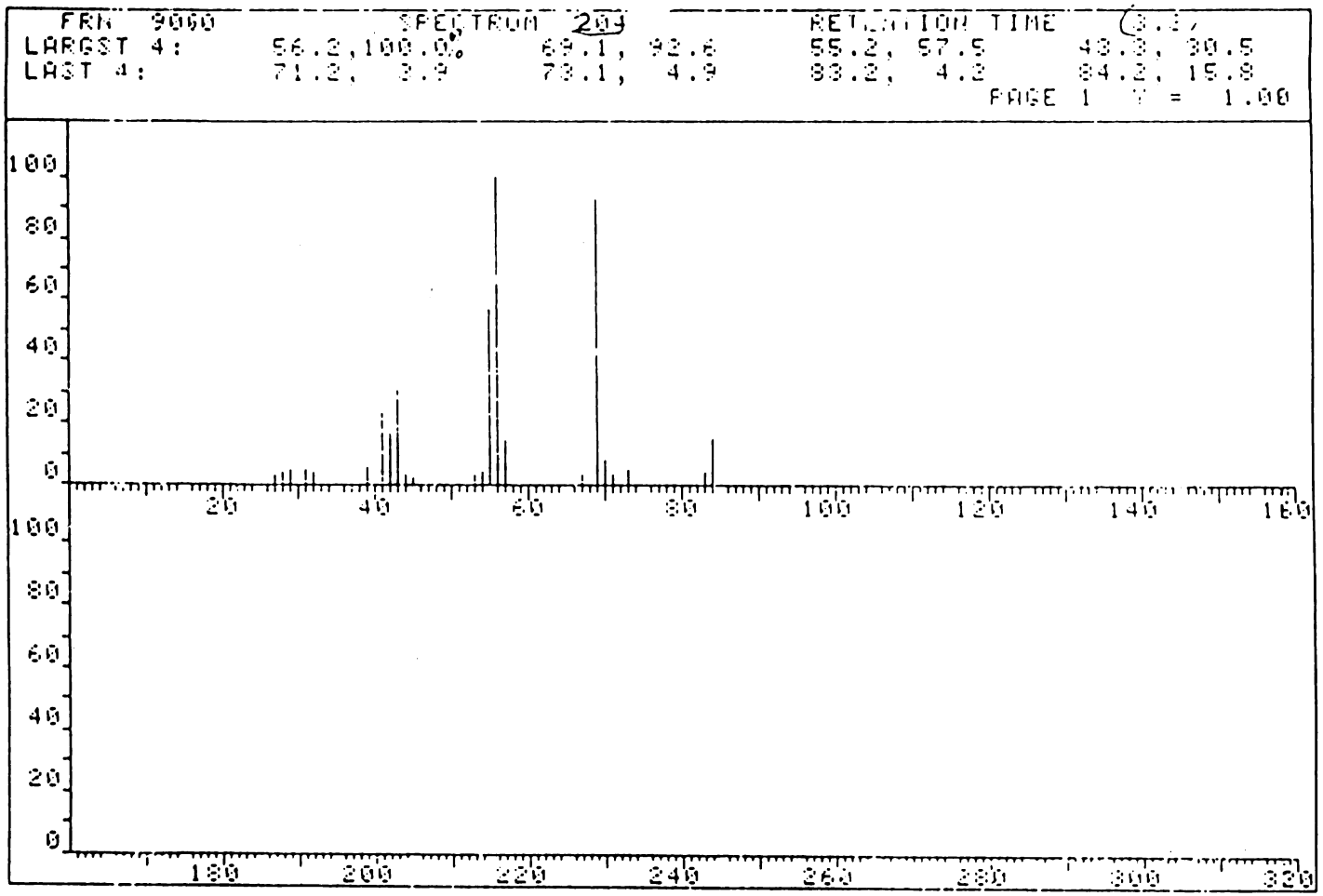

Figure A-9. Mass Spectrum of Hexanol from 1,2-Hexanediol Experiment

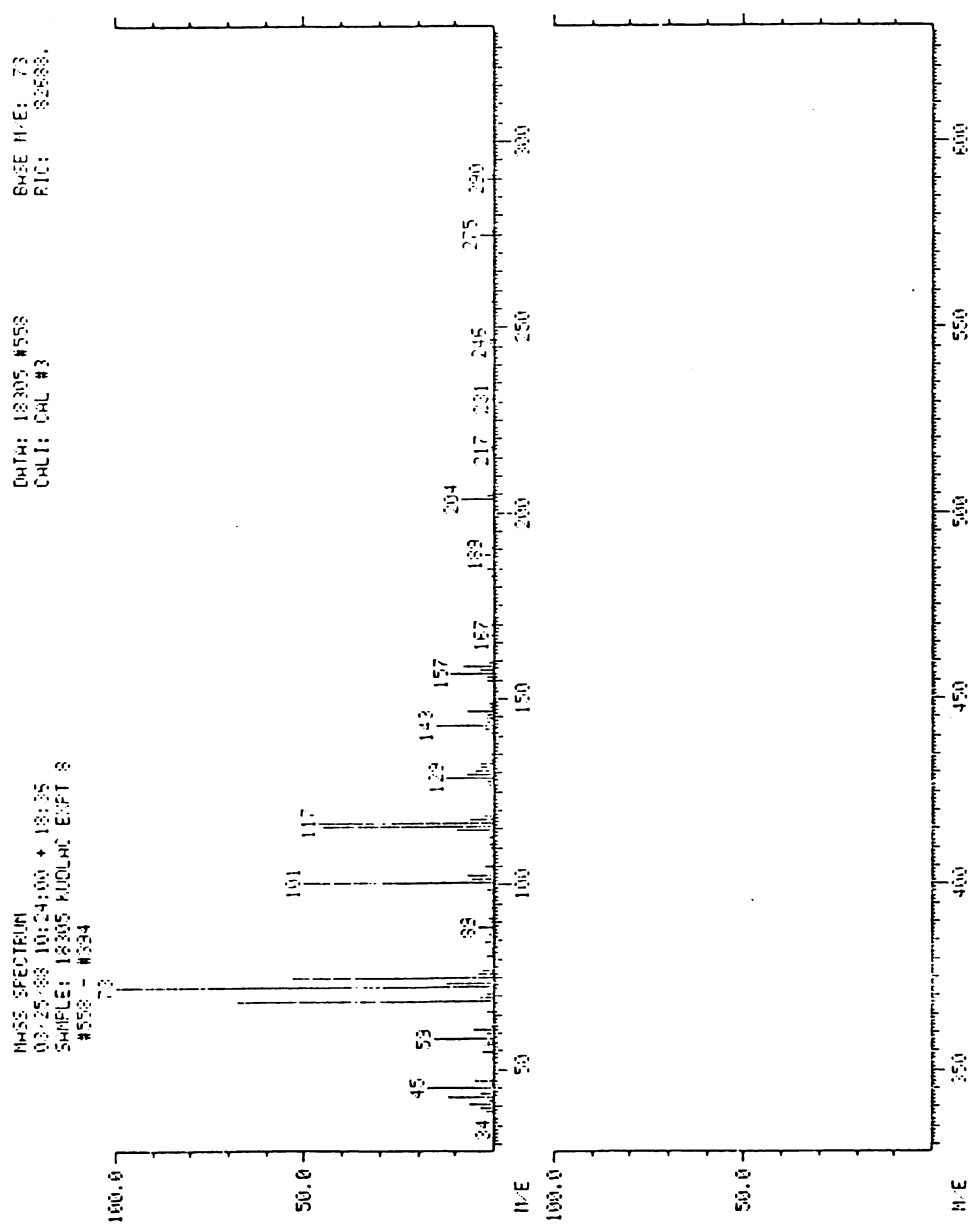

Figure A-10. Mass Spectrum of Peak 558

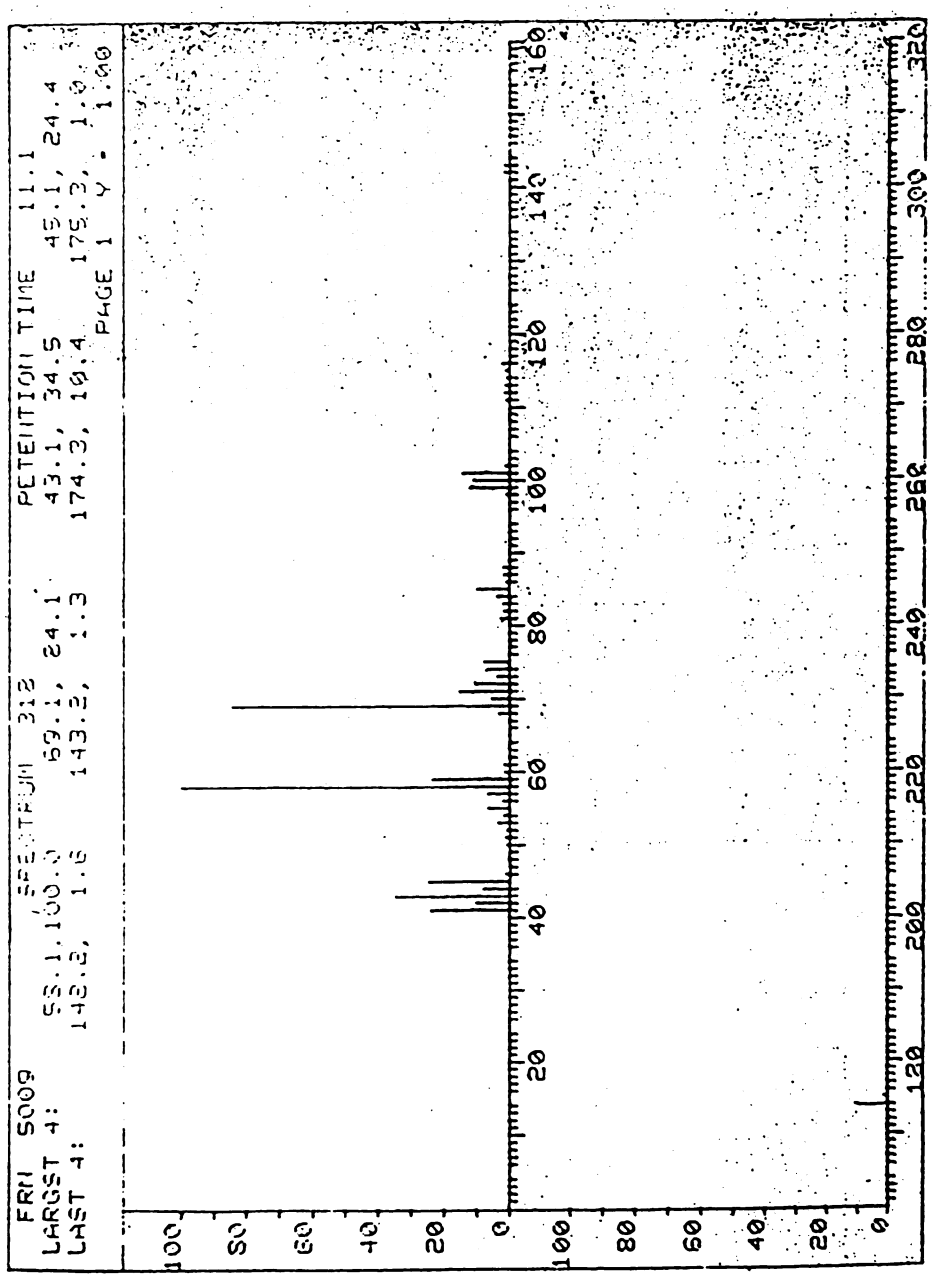

Figure A-11. Mass Spectrum of Isosorbide Dimethyl Ether

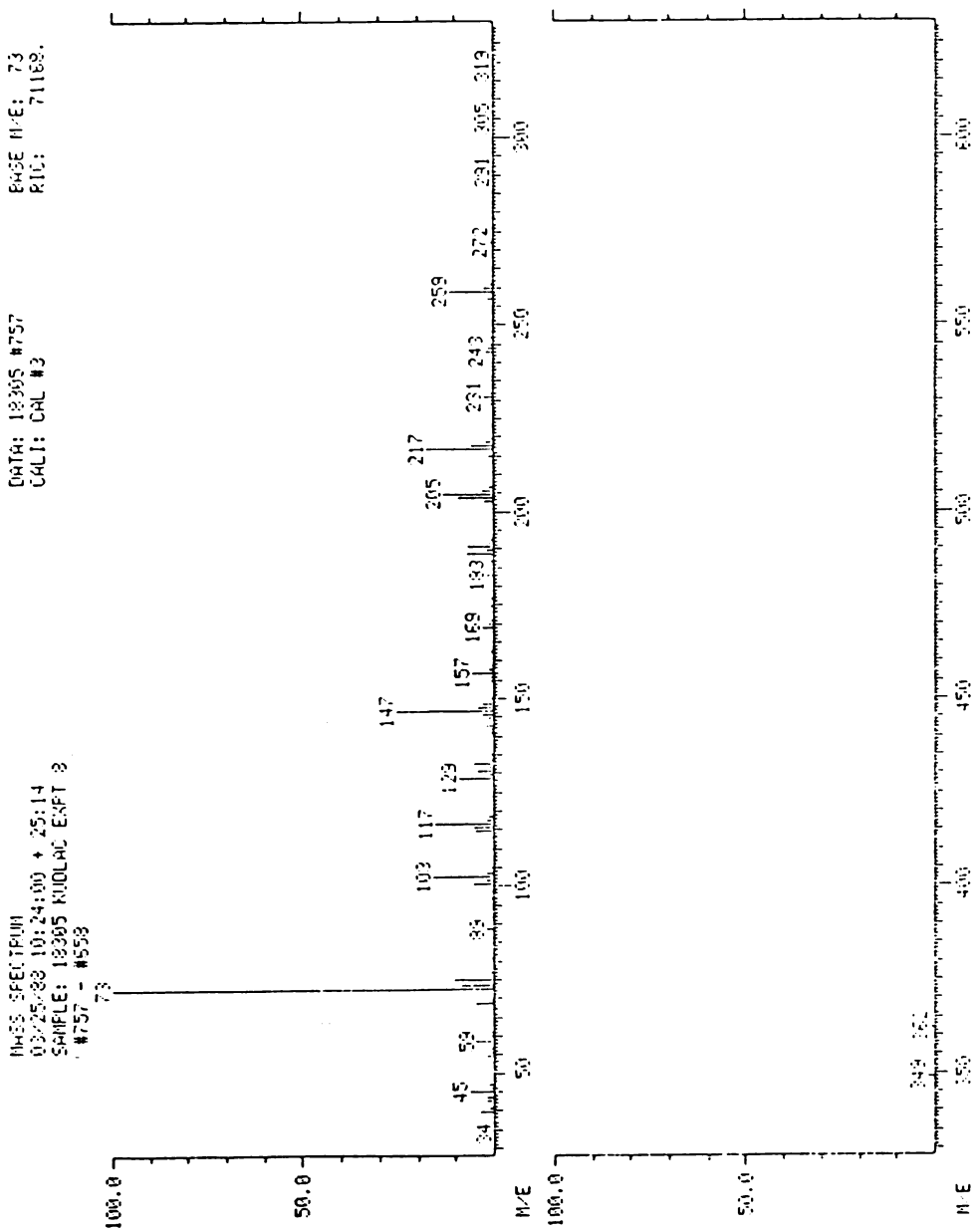

Figure A-12. Mass Spectrum of Peak 756

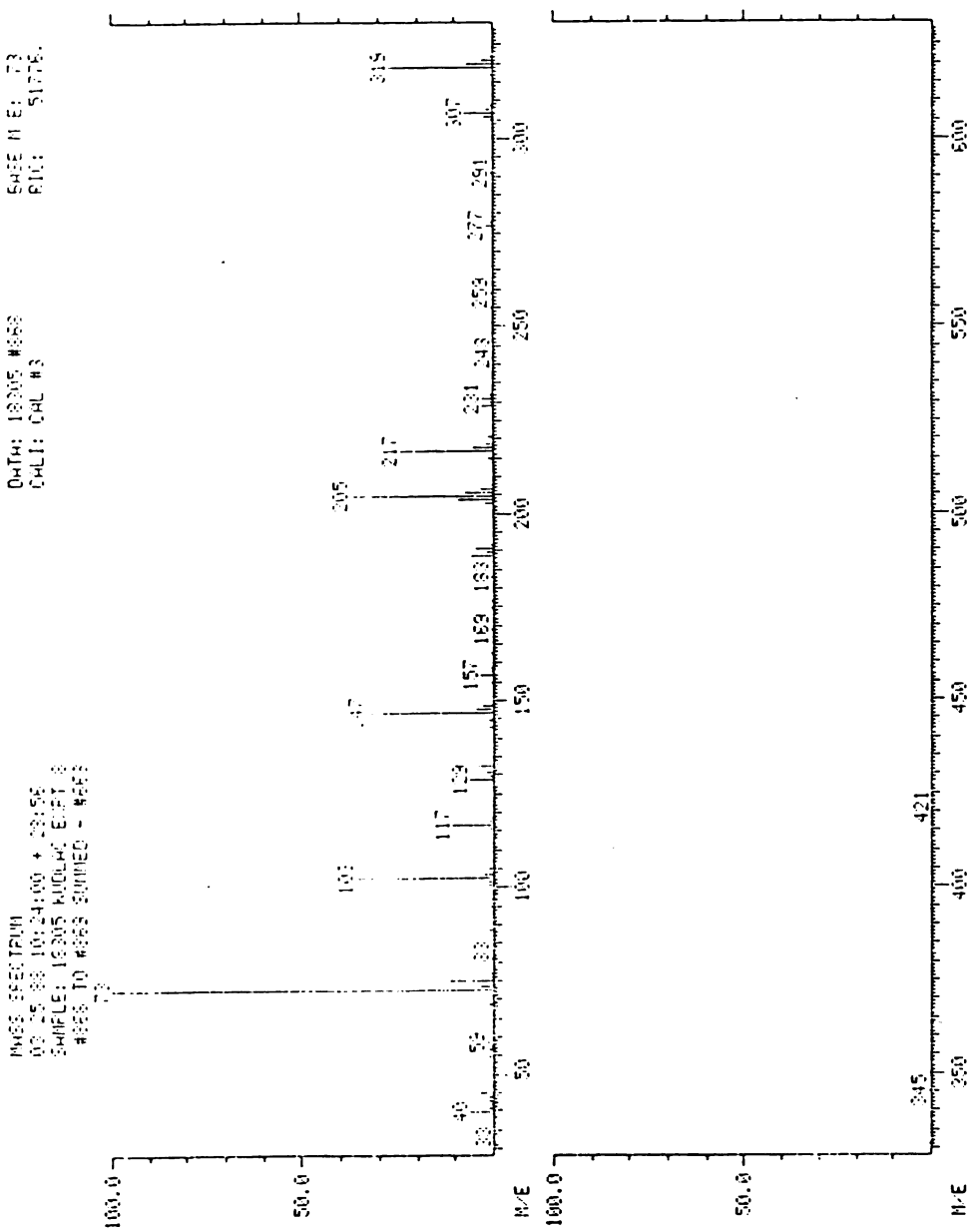

Figure A-13. Mass Spectrum of Peak 870

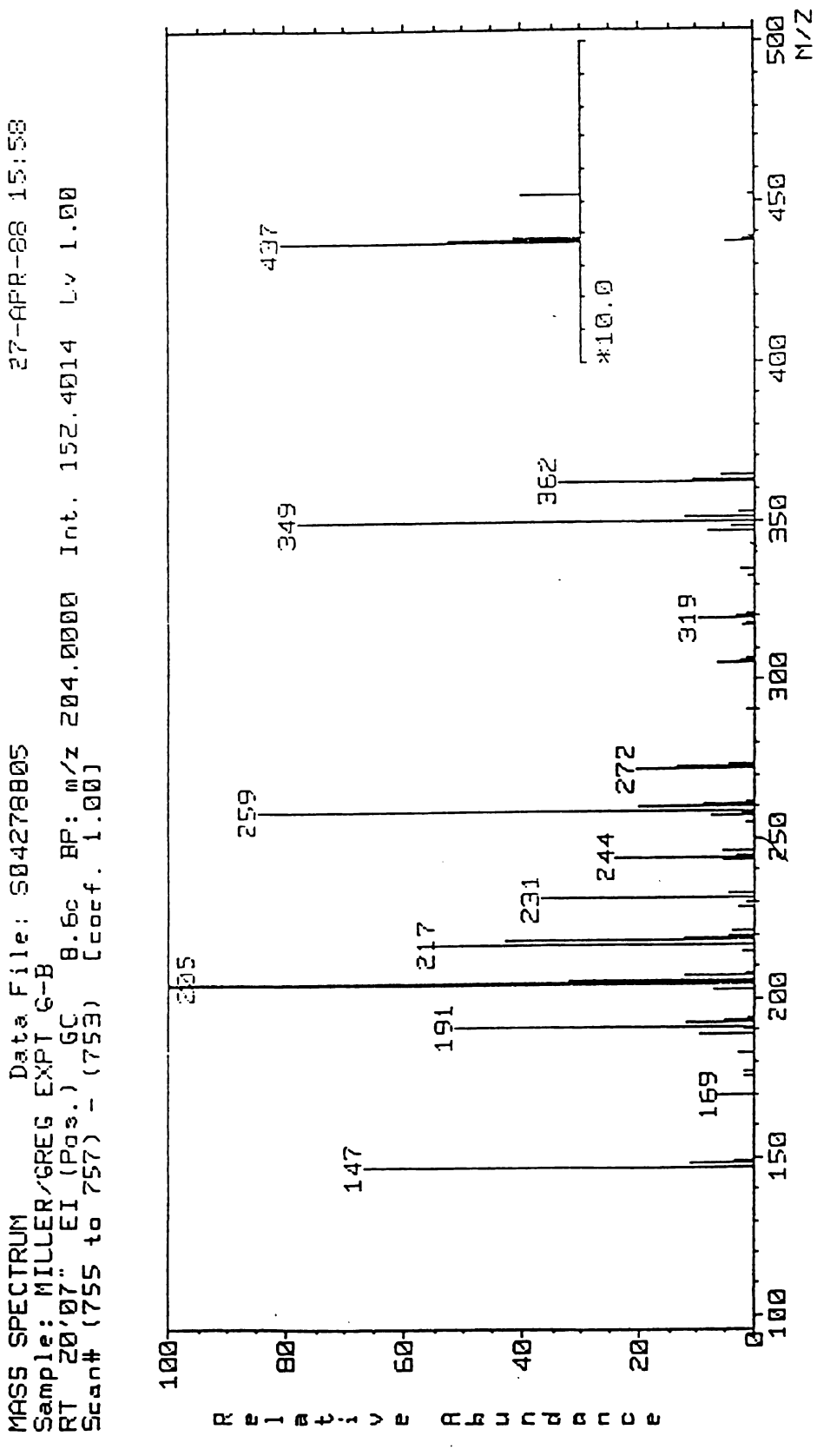

Figure A-14. Mass Spectrum of Peak 20:07

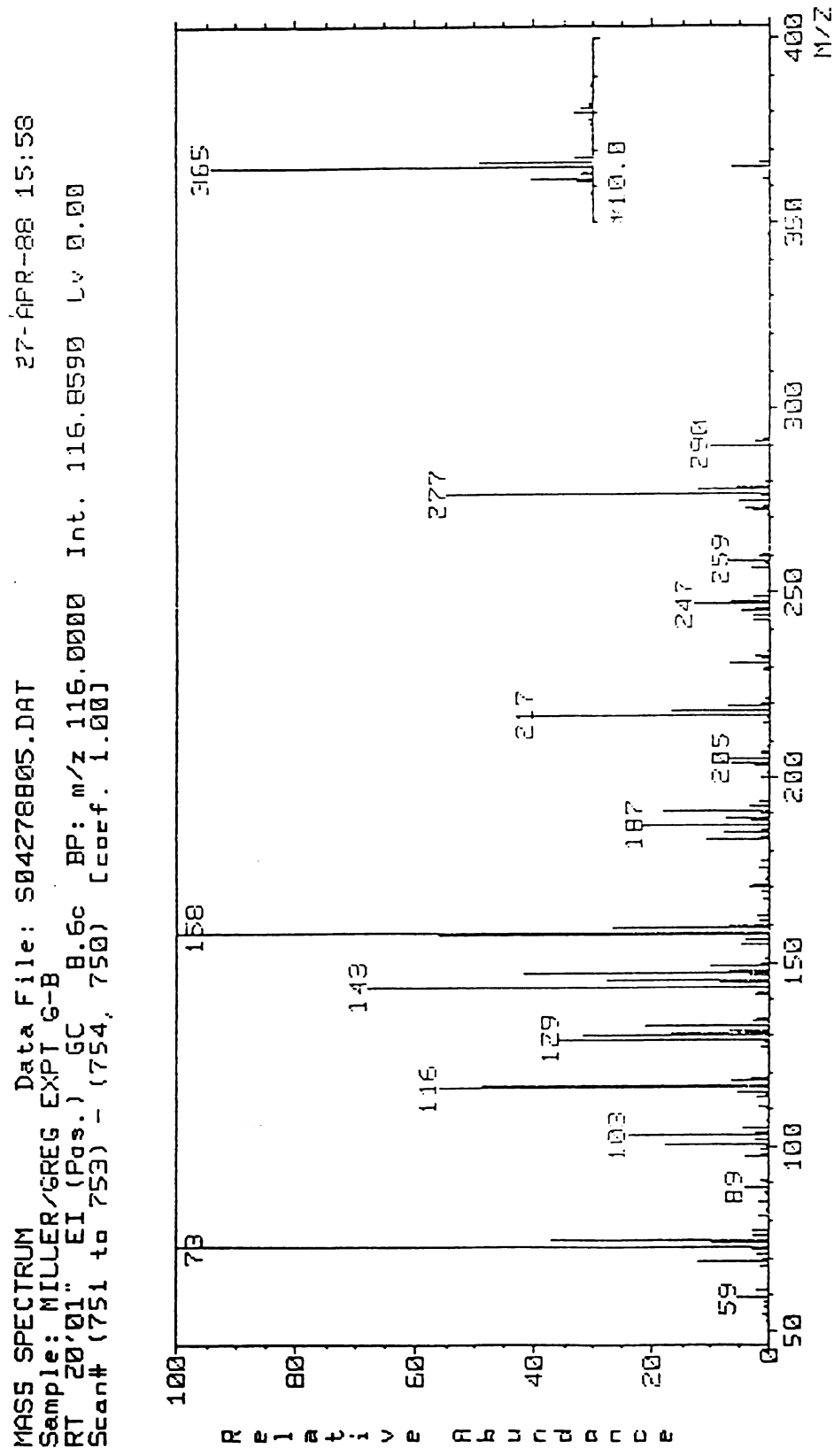

Figure A-15. Mass Spectrum of Peak 20:01

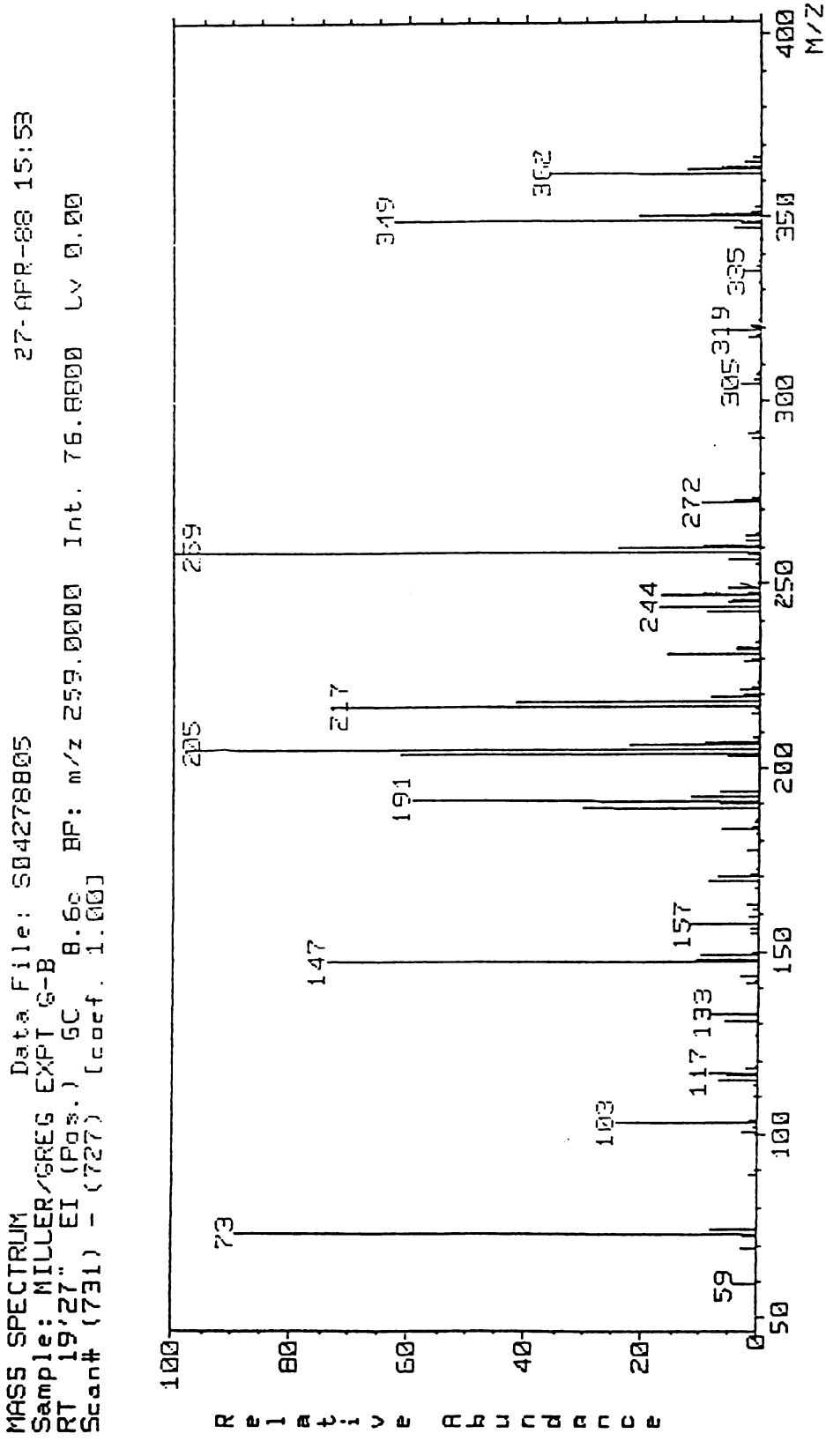

Figure A-16. Mass Spectrum of Peak 19:27, m/z 452

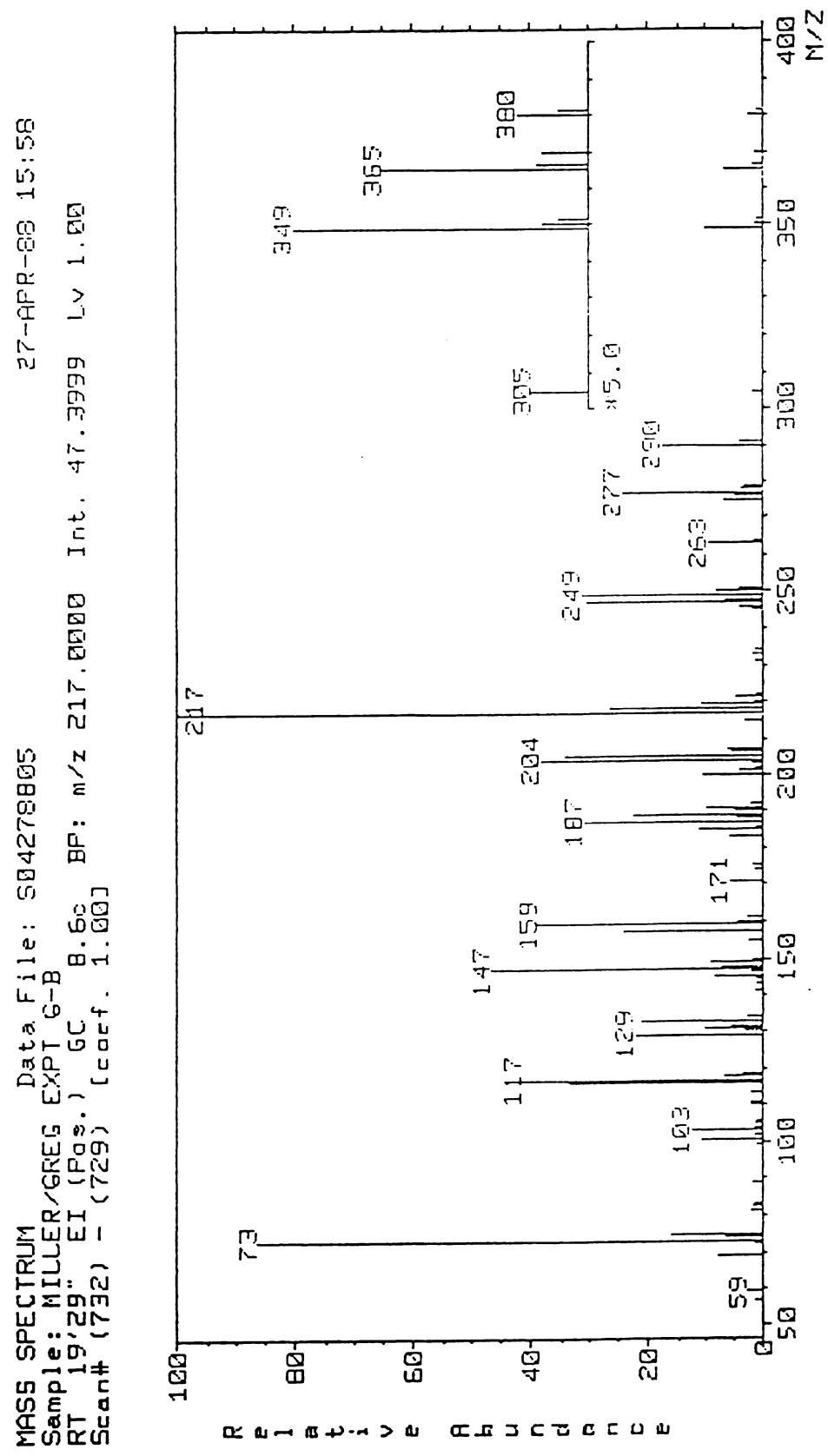

Figure A-17. Mass Spectrum of Peak 19:27, m/z 380

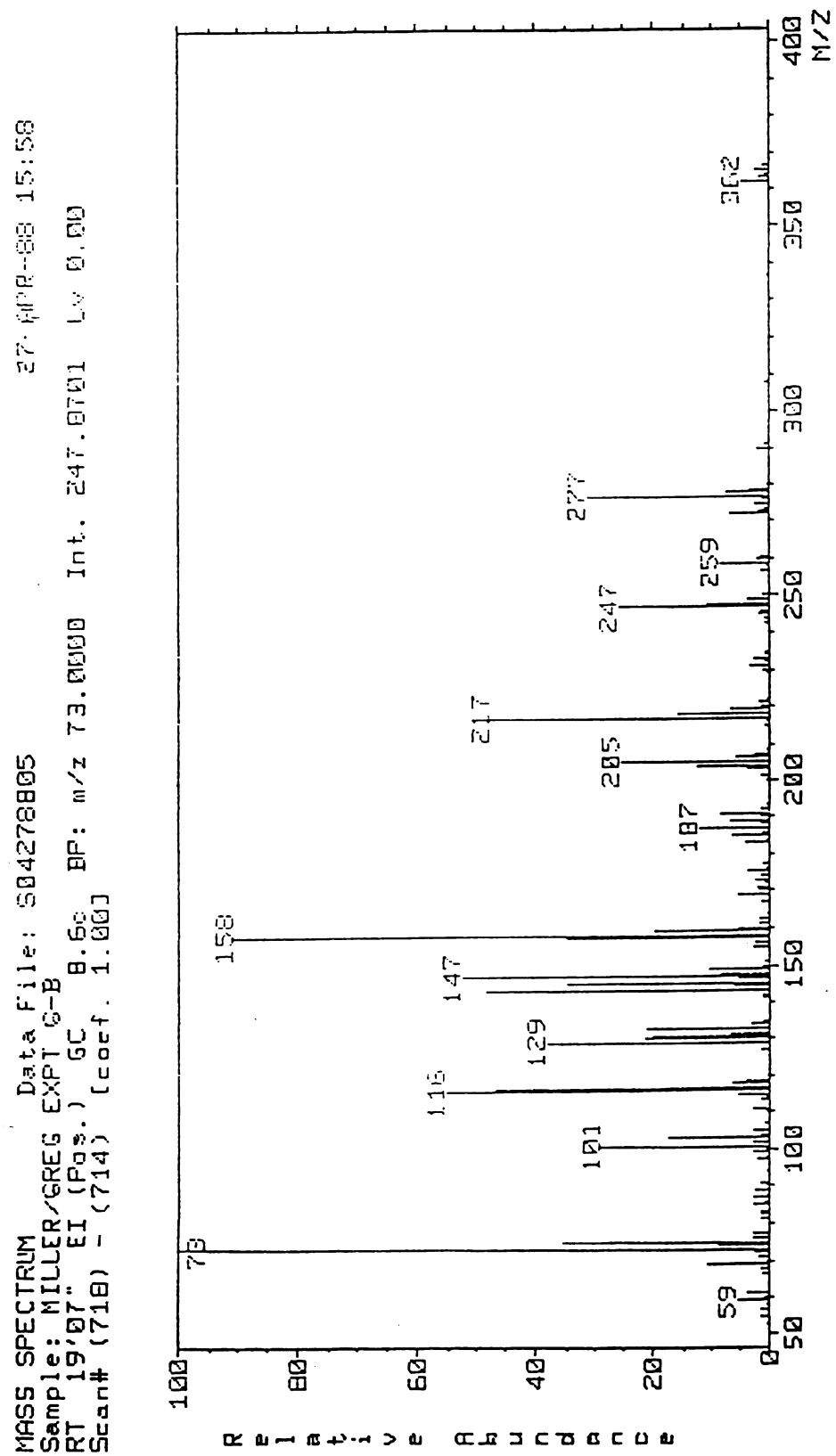

Figure A-18. Original Mass Spectrum of Peak 19:07

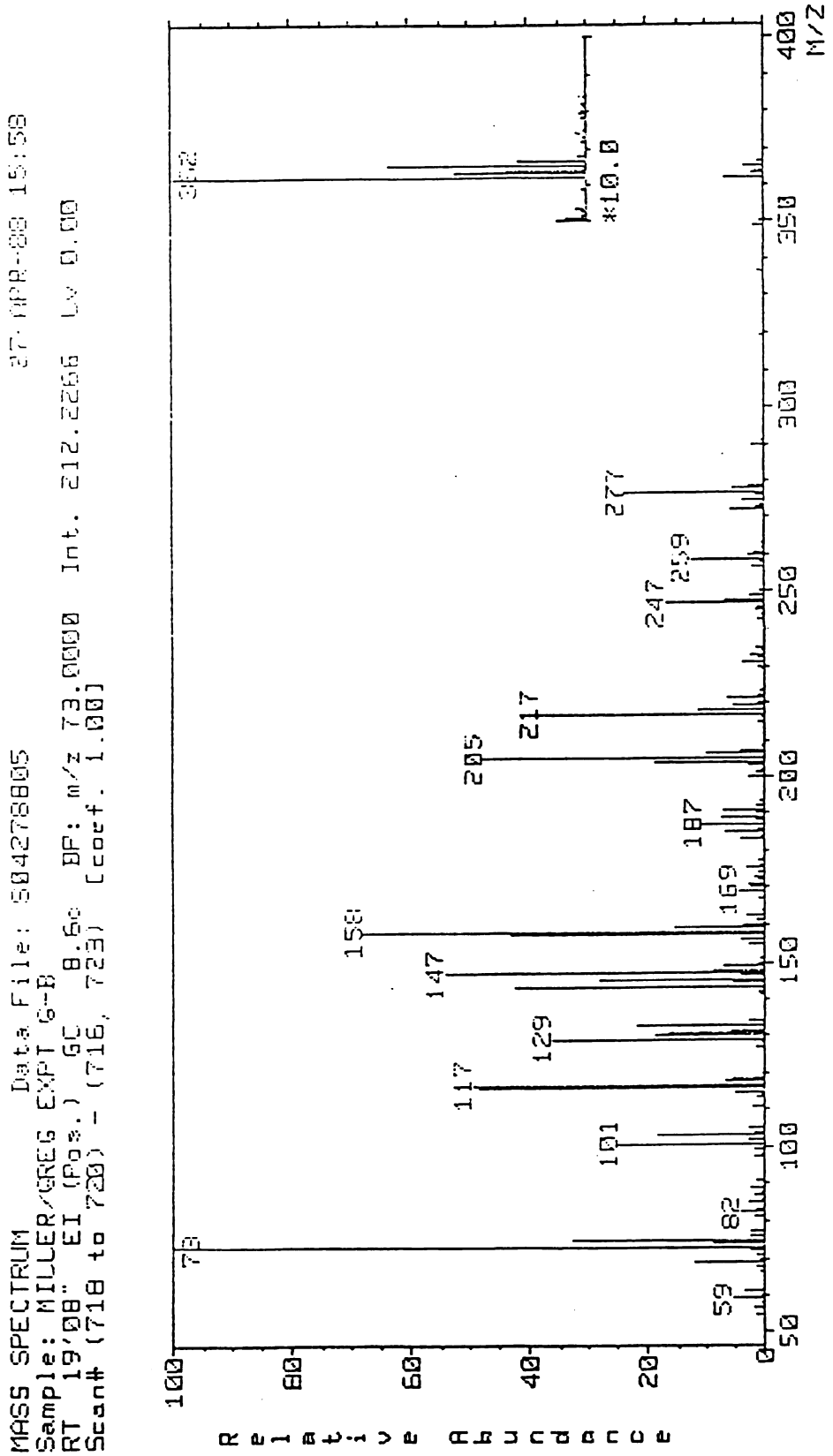

Figure A-19. Mass Spectrum of Peak 19:07, m/z 380

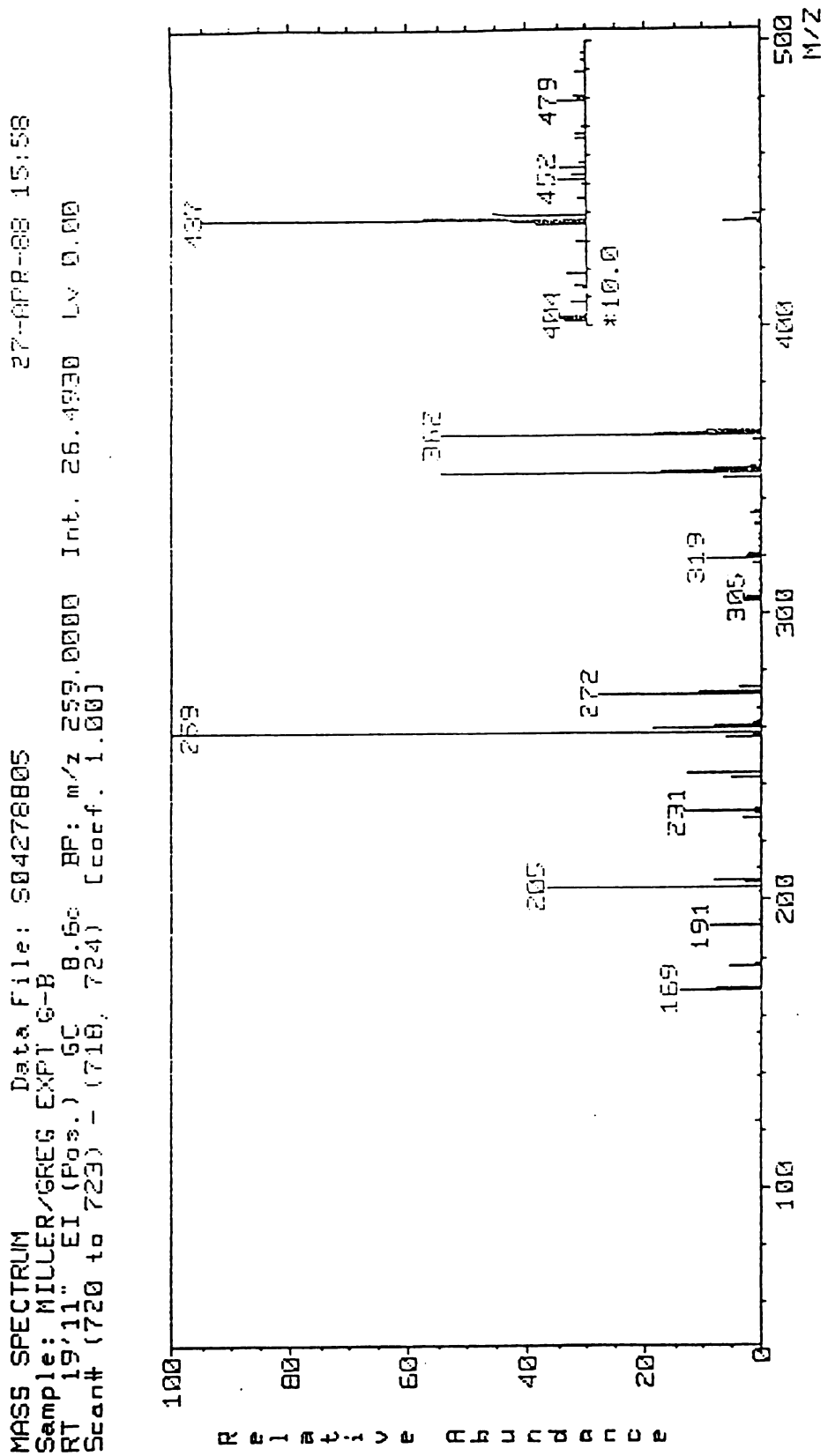

Figure A-20. Mass Spectrum of Peak 19:07, m/z 452

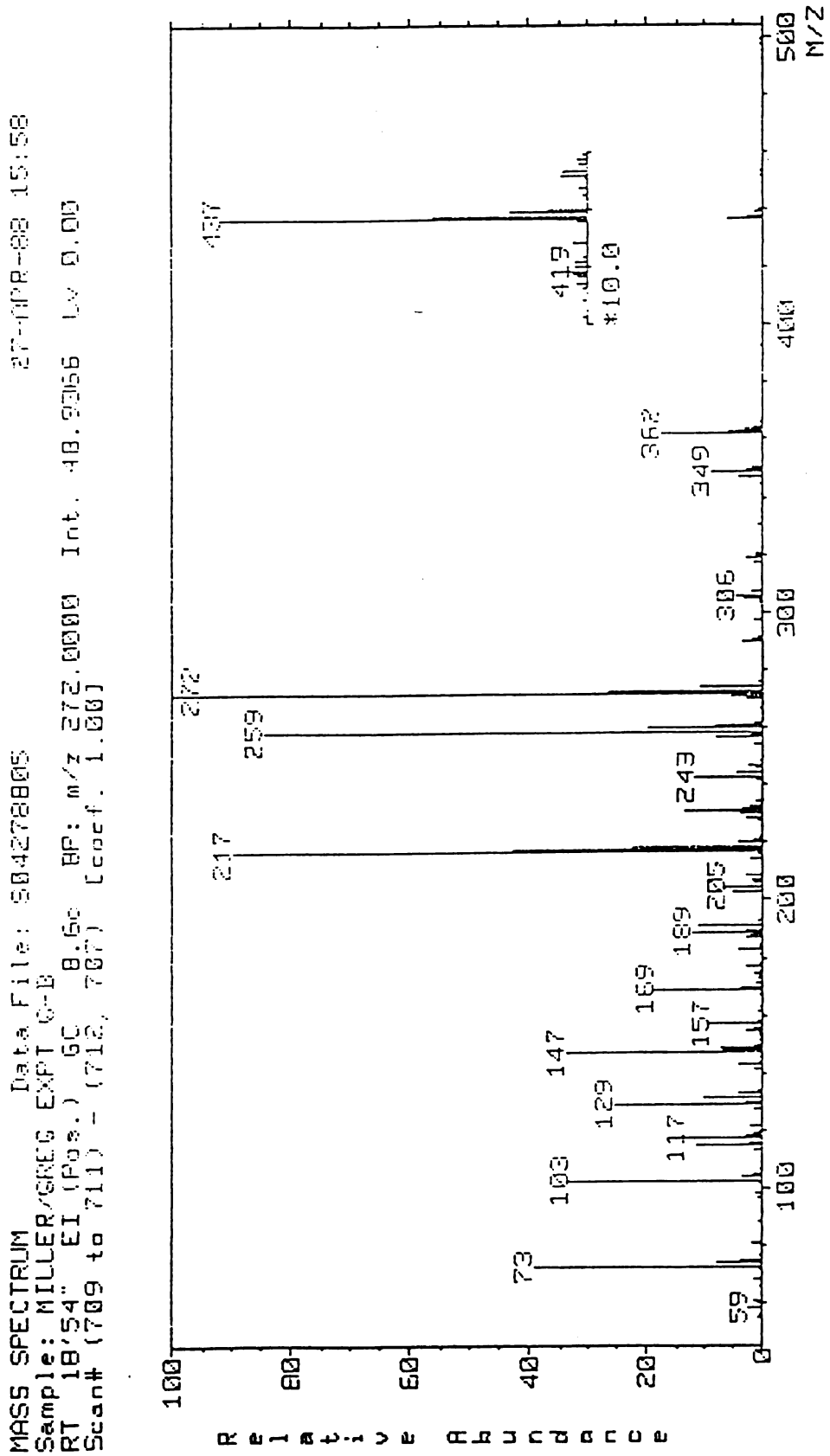

Figure A-21. Mass Spectrum of Peak 18:54

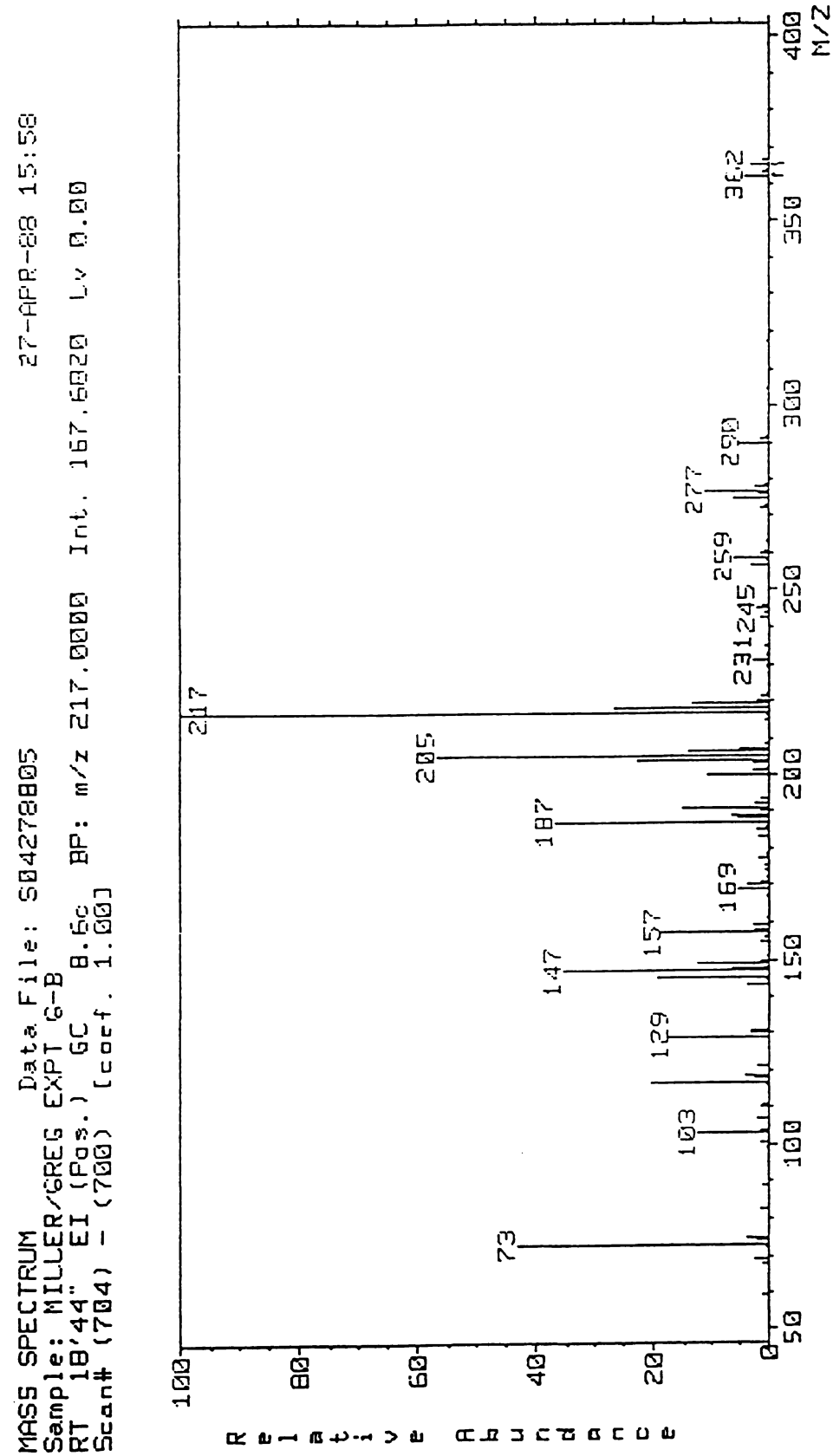

Figure A-22. Mass Spectrum of Peak 18:44

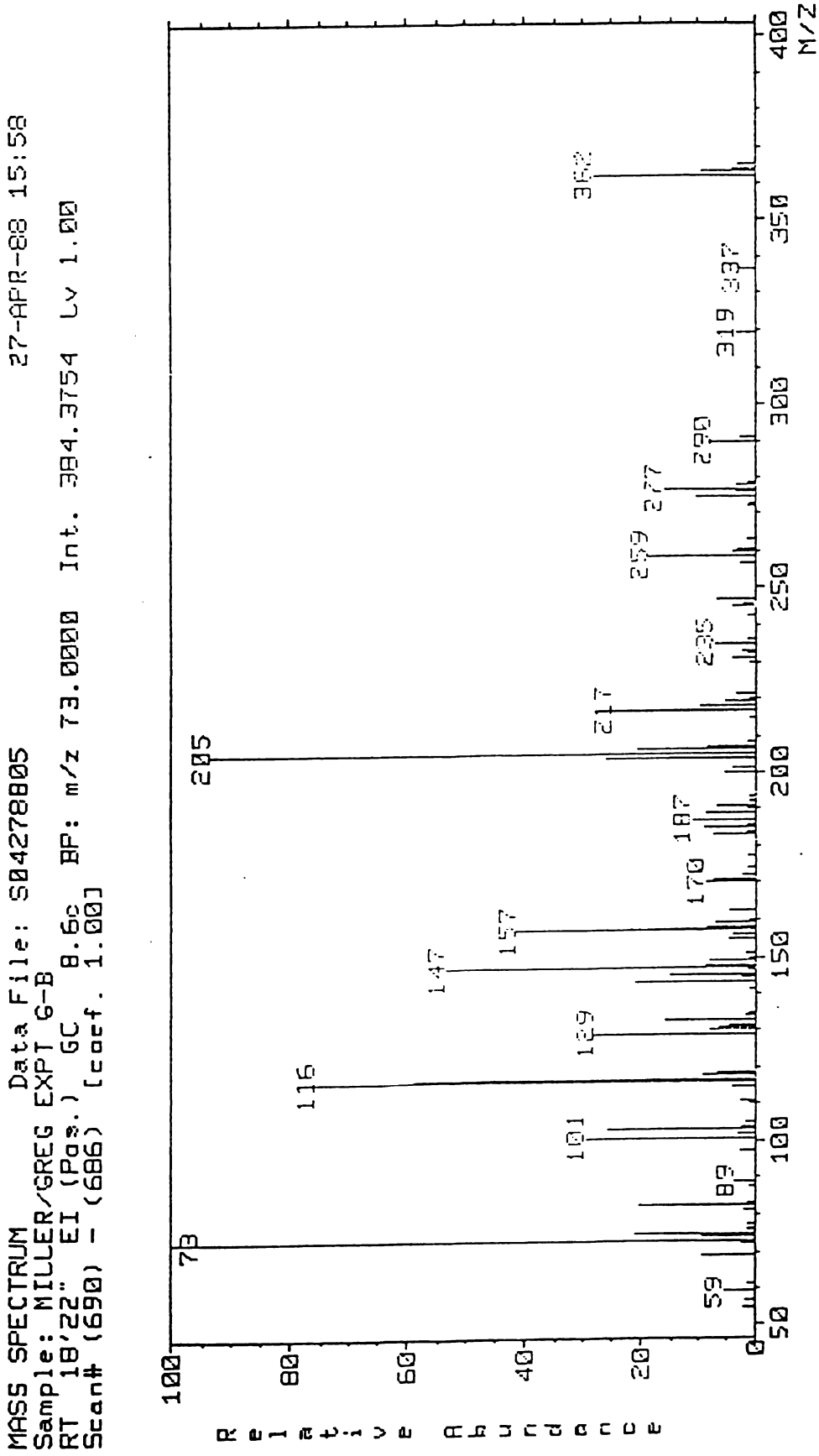

Figure A-23. Mass Spectrum of Peak 18:20, m/z 362

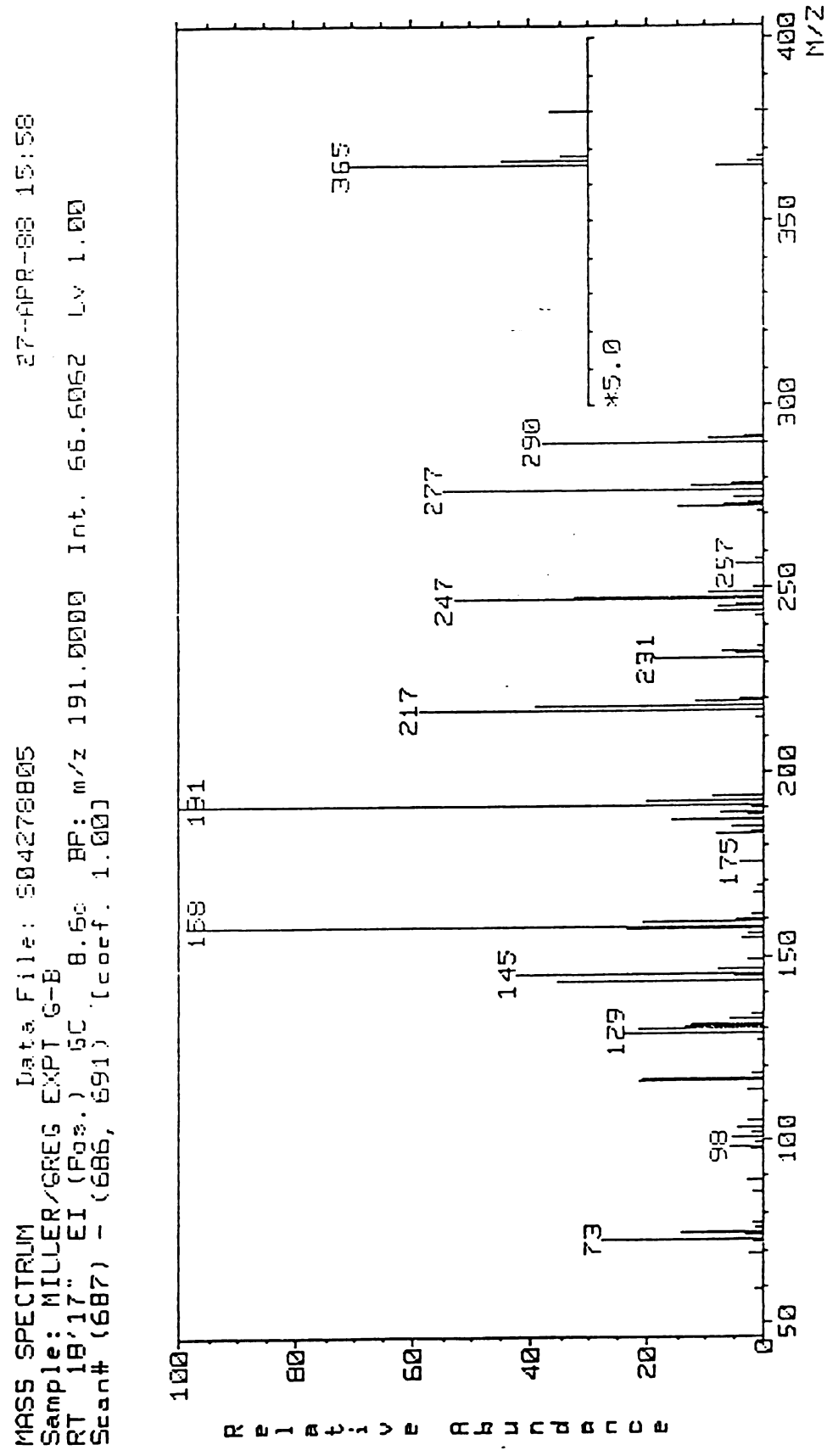

Figure A-24. Mass Spectrum of Peak 18:20, m/z 380

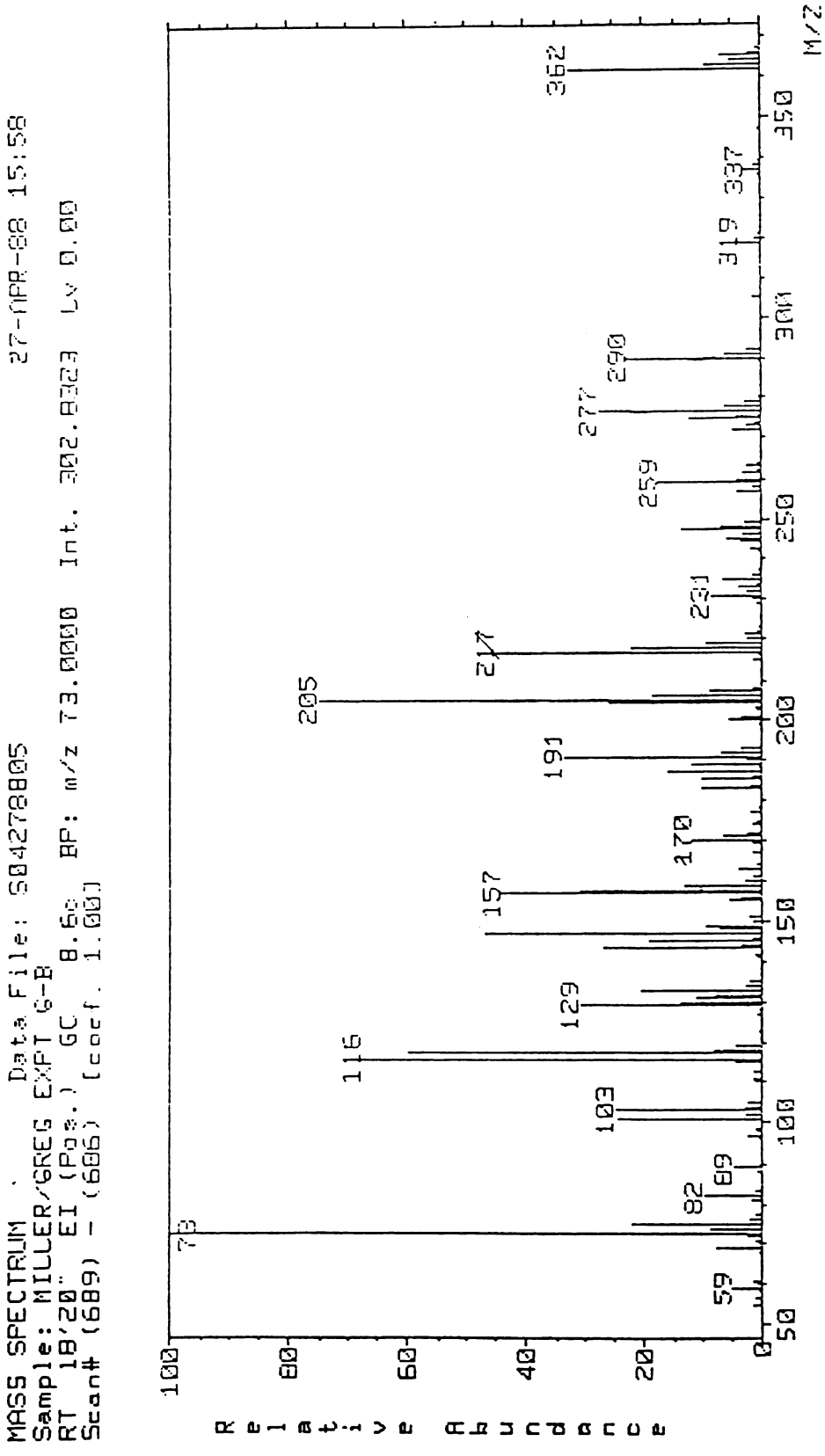

Figure A-25. Original Mass Spectrum of Peak 18:20

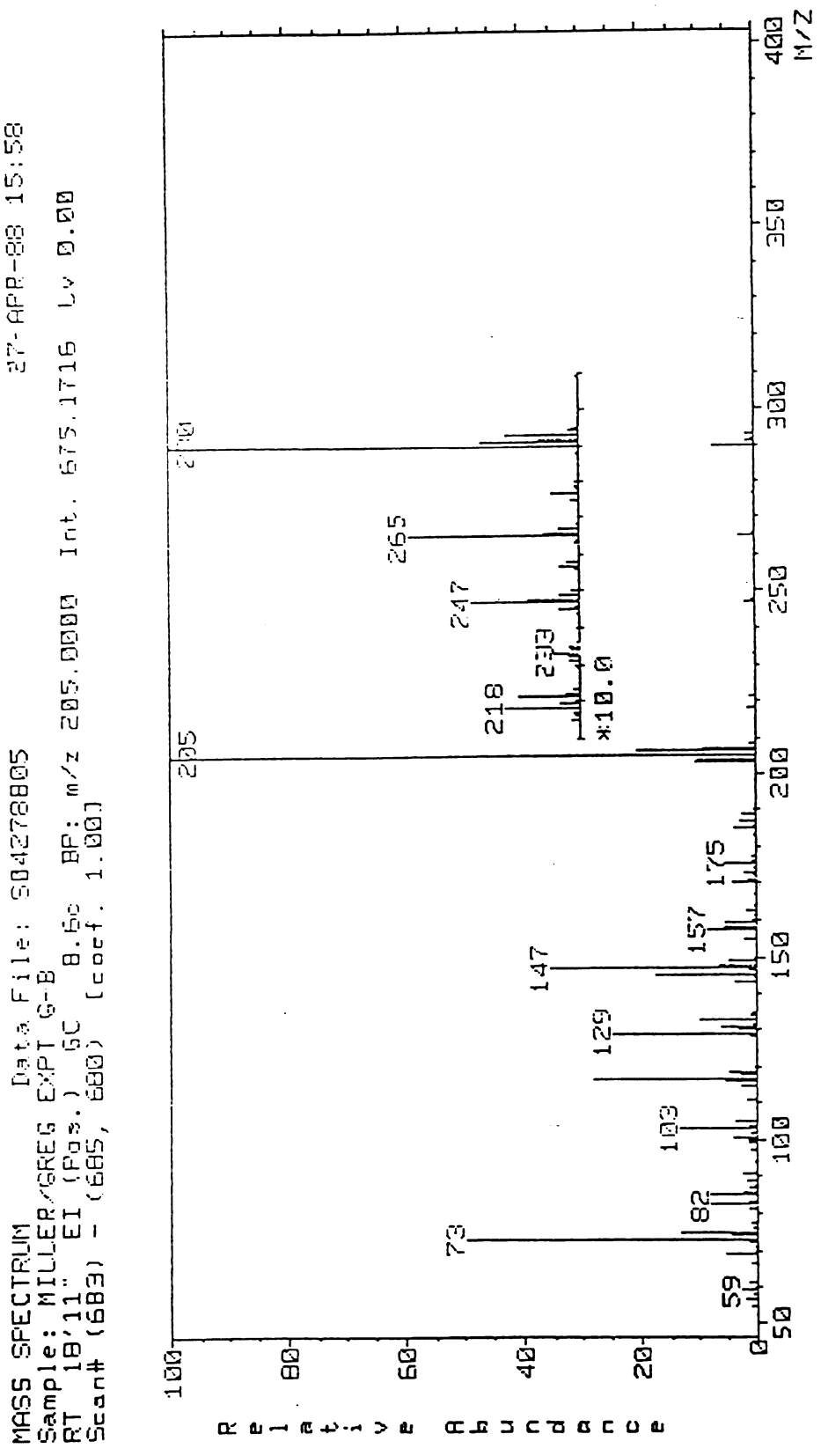

Figure A-26. Mass Spectrum of Peak 18:09, m/z 290

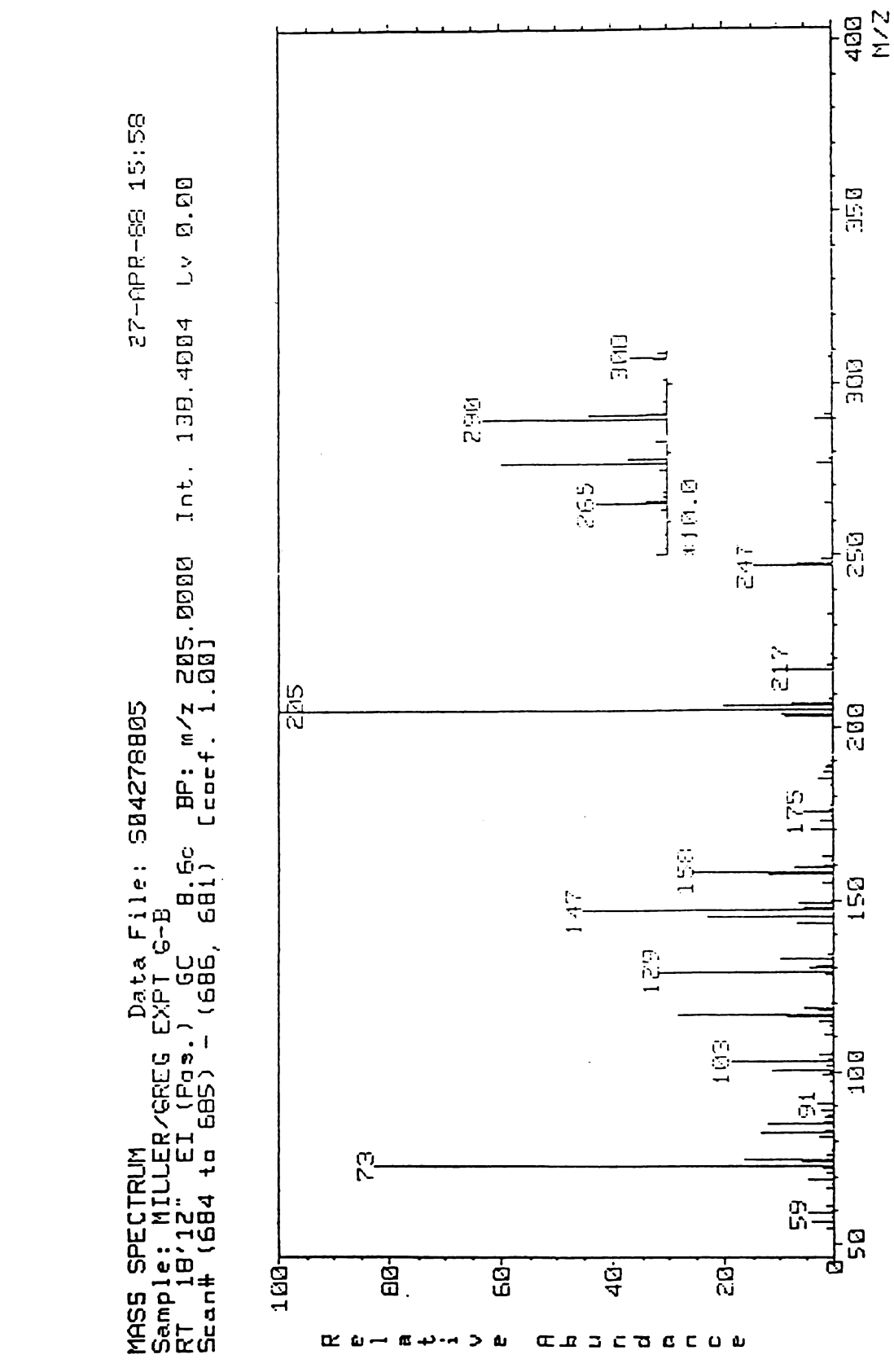

Figure A-27. Mass Spectrum of Peak 18:09, m/z 308

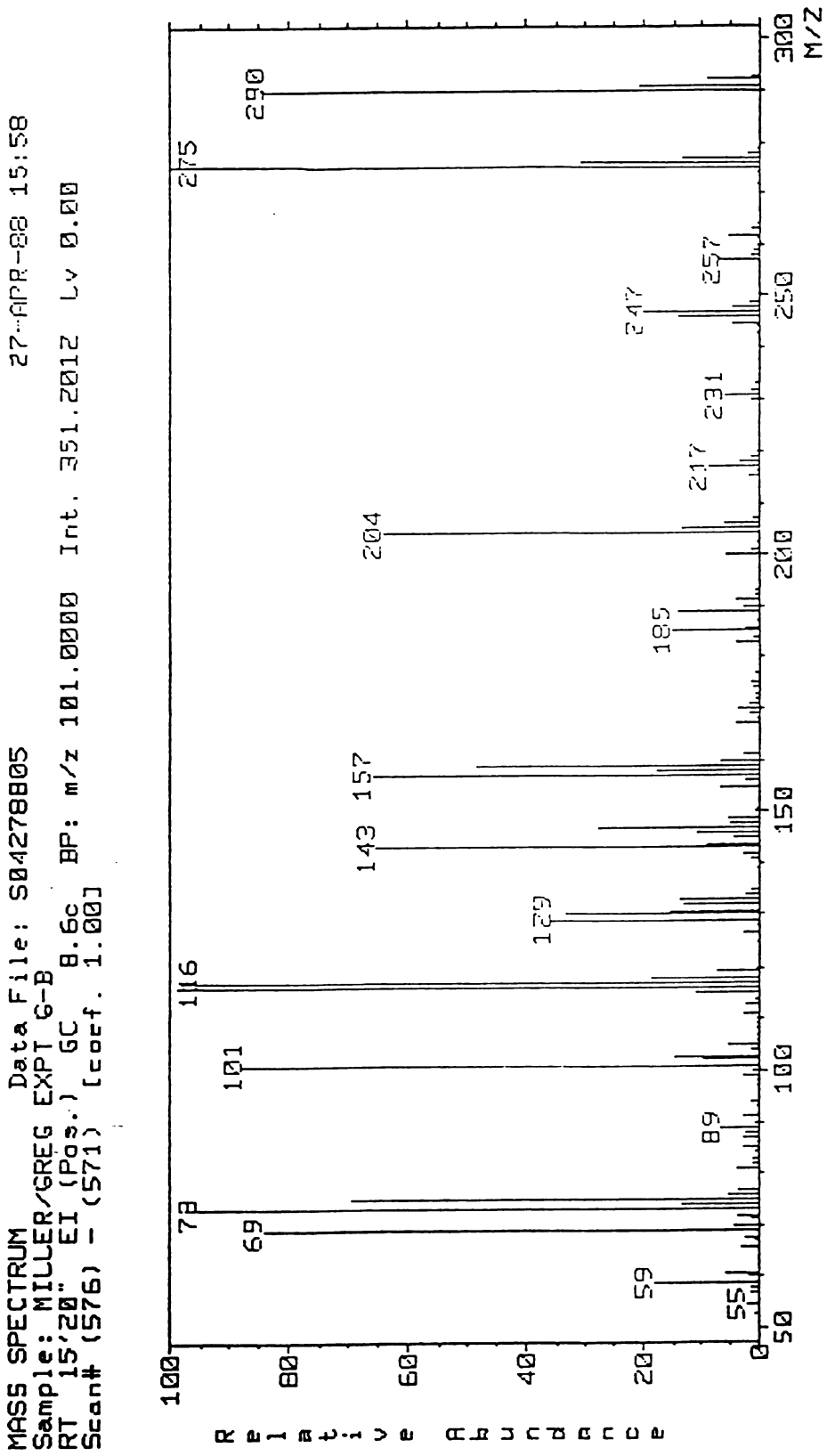

Figure A-28. Mass Spectrum of Peak 15:20

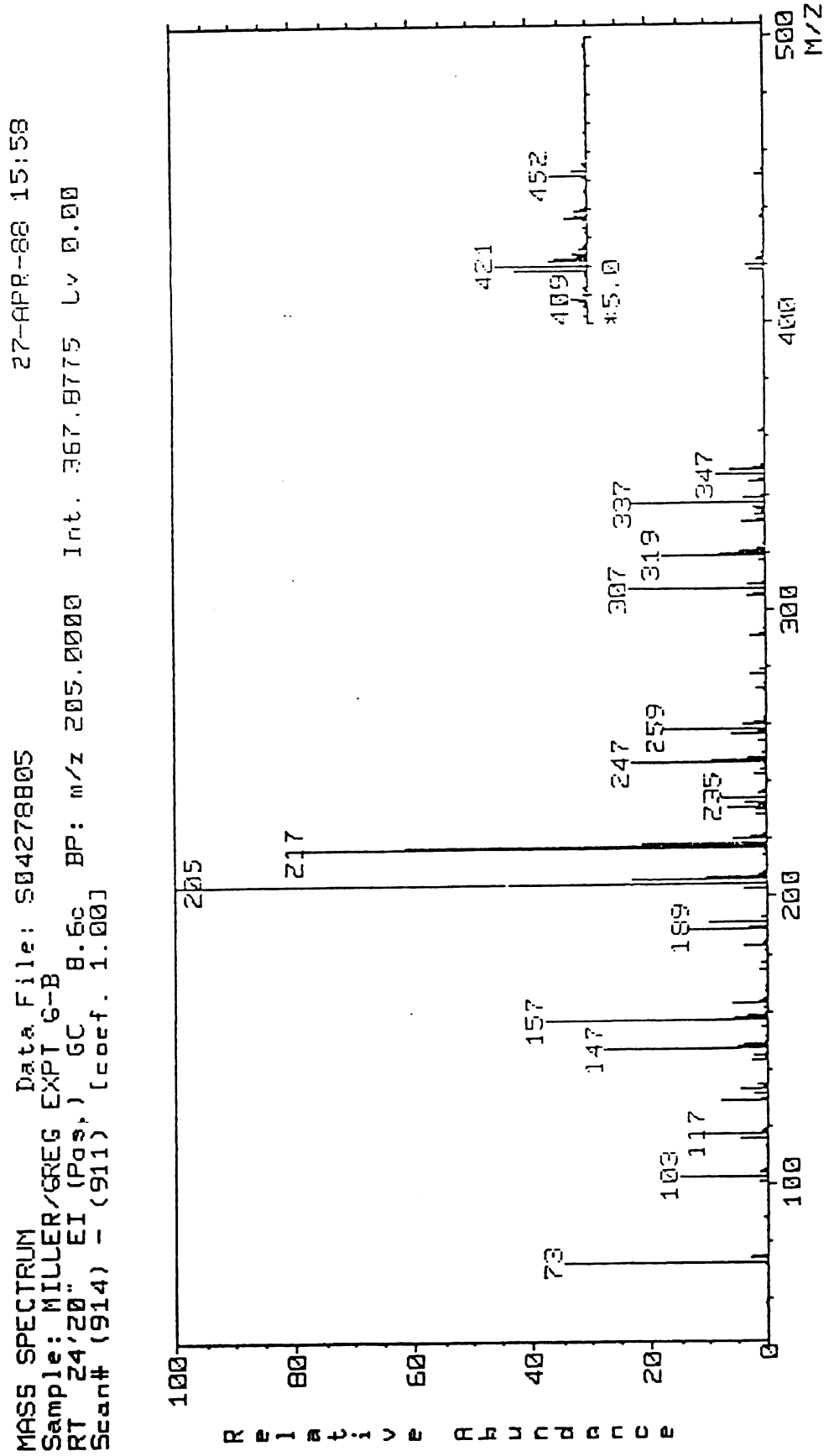

Figure A-29. Mass Spectrum of Peak 24:20

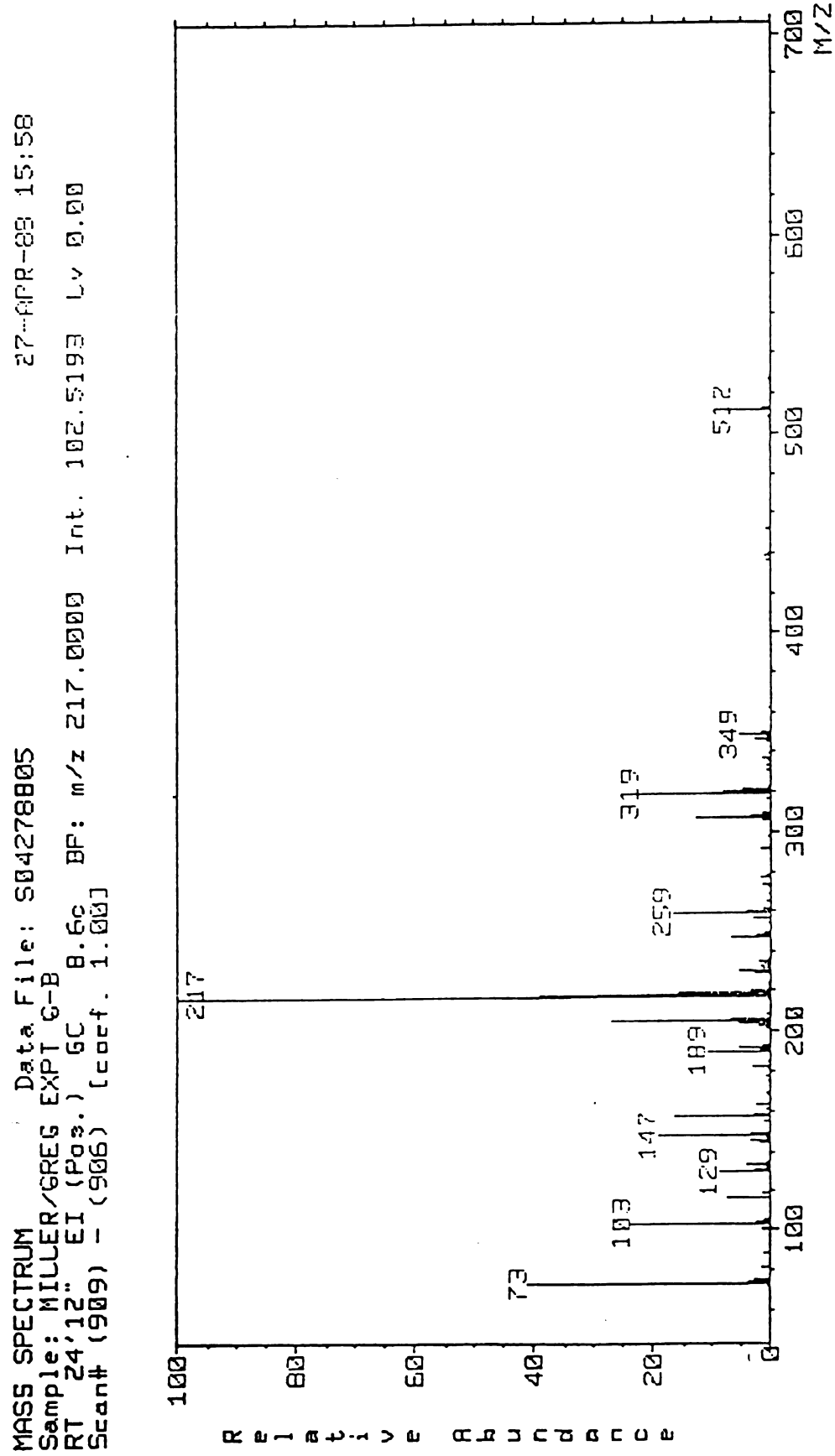

Figure A-30. Mass Spectrum of Peak 24:12

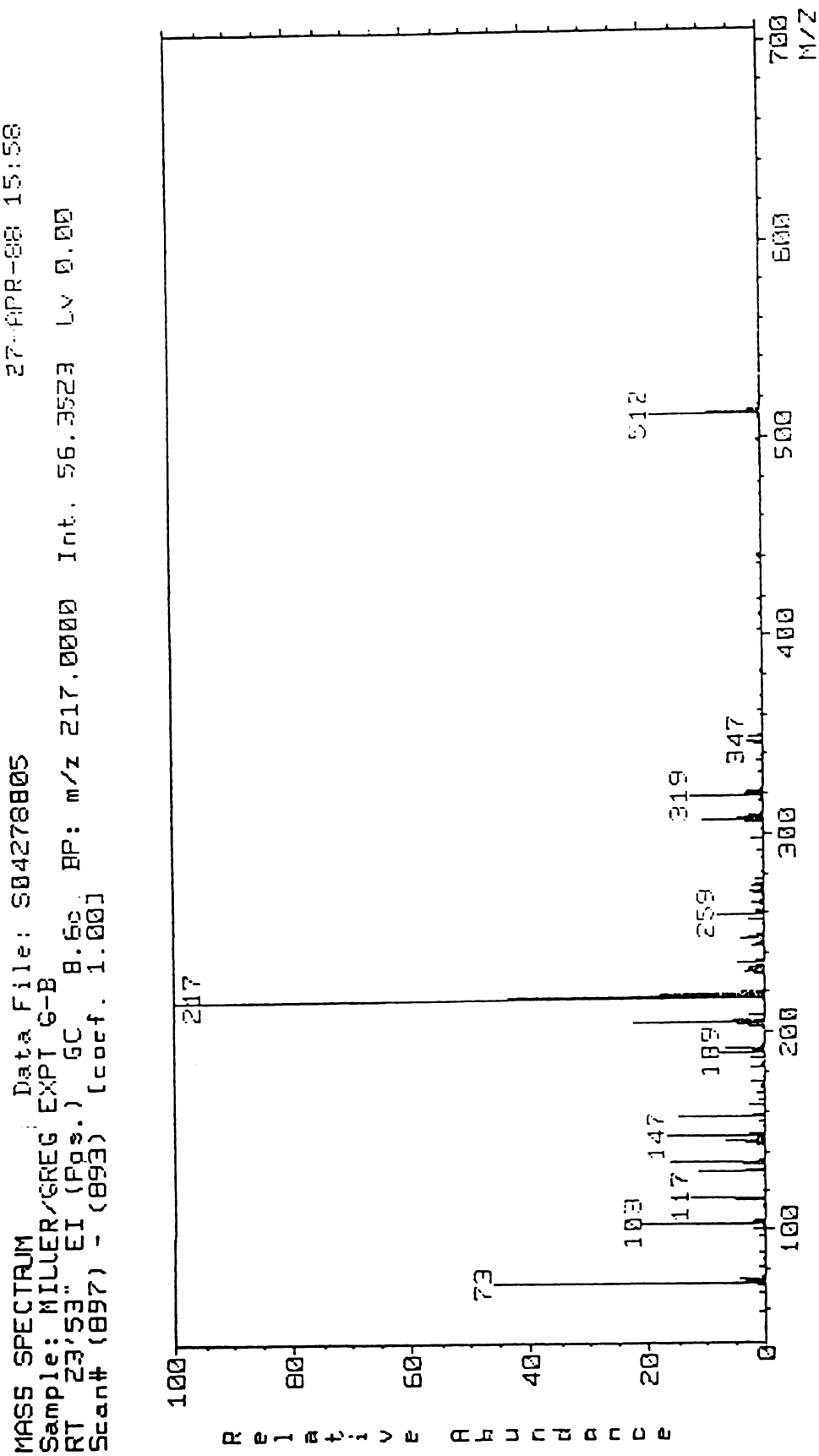

Figure A-31. Mass Spectrum of Peak 23:53

APPENDIX B

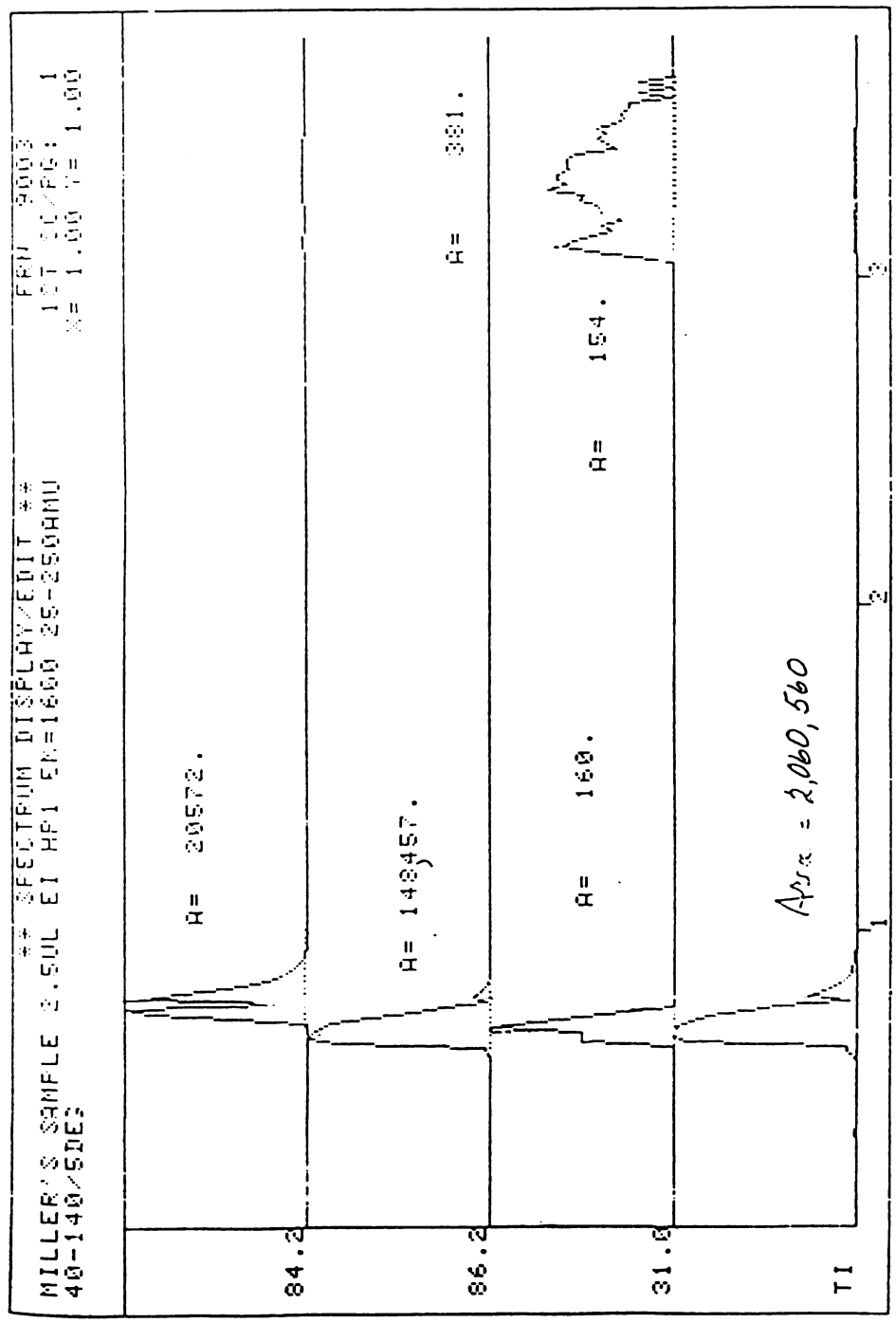

Figure B-1. Specific Ion Traces for Hexanol Experiment

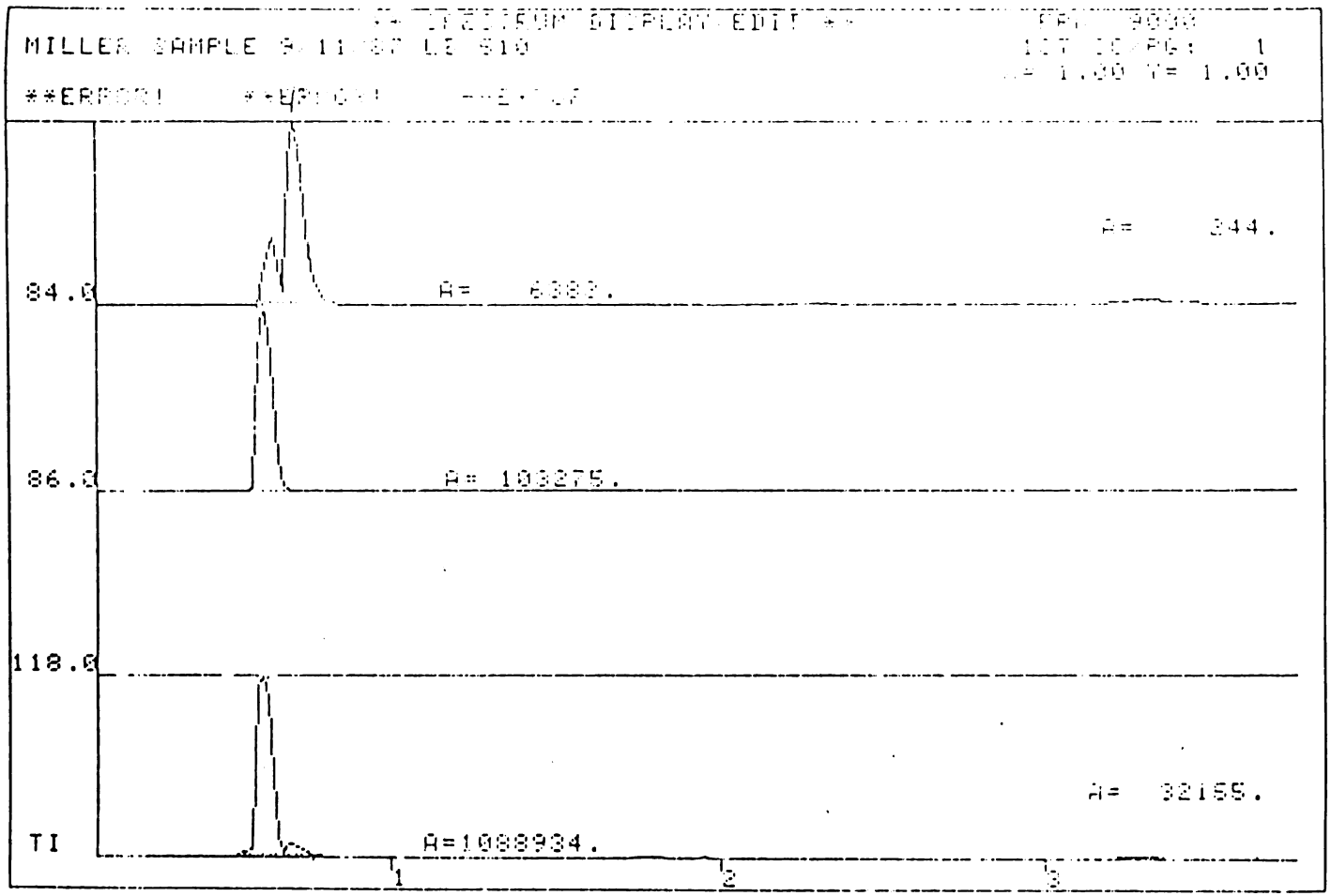

Figure B-2. Specific Ion Traces for 1,2-Hexanediol Experiment

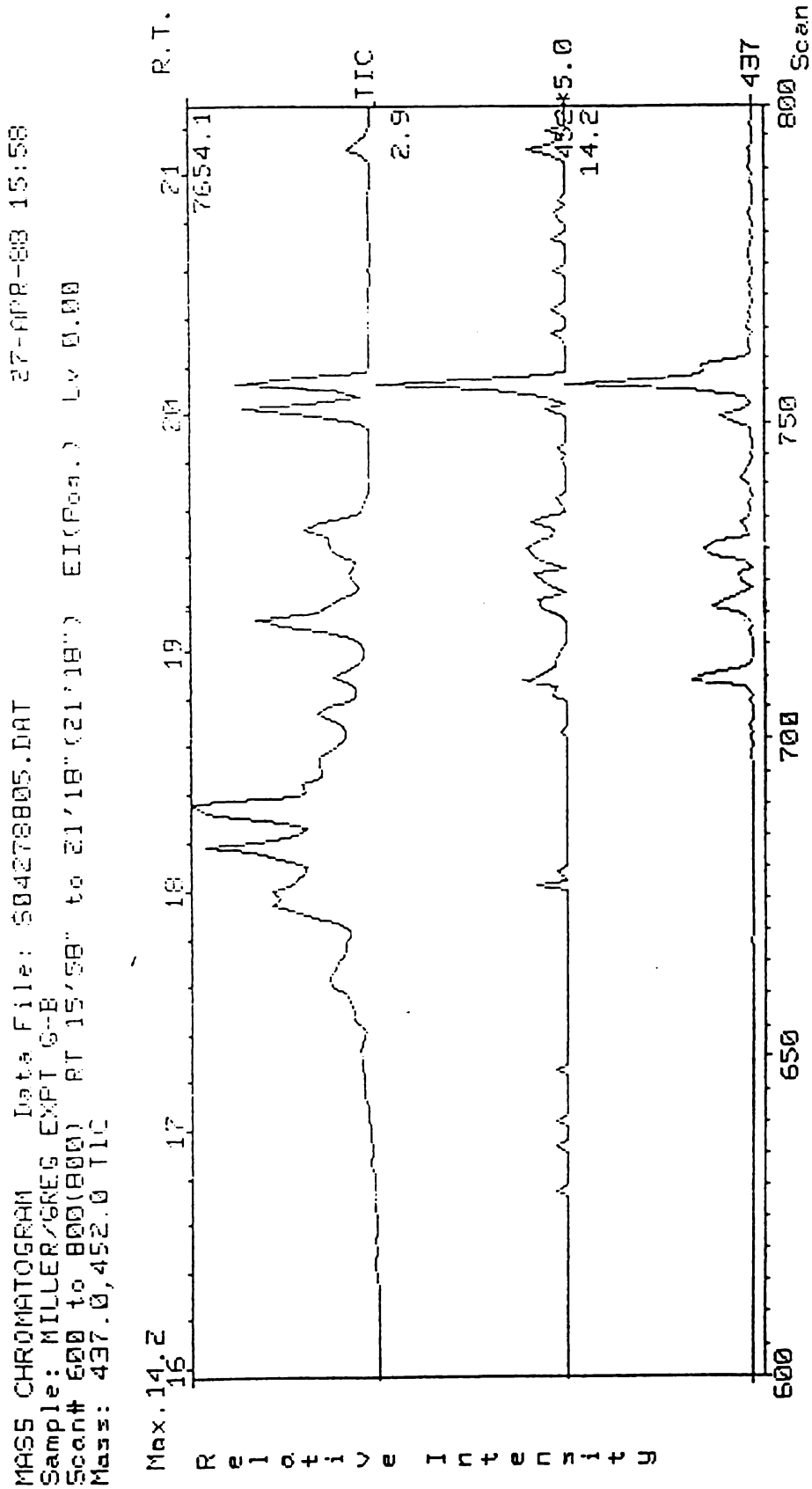

Figure B-3. Specific Ion Traces for m/z 452 and m/z 437

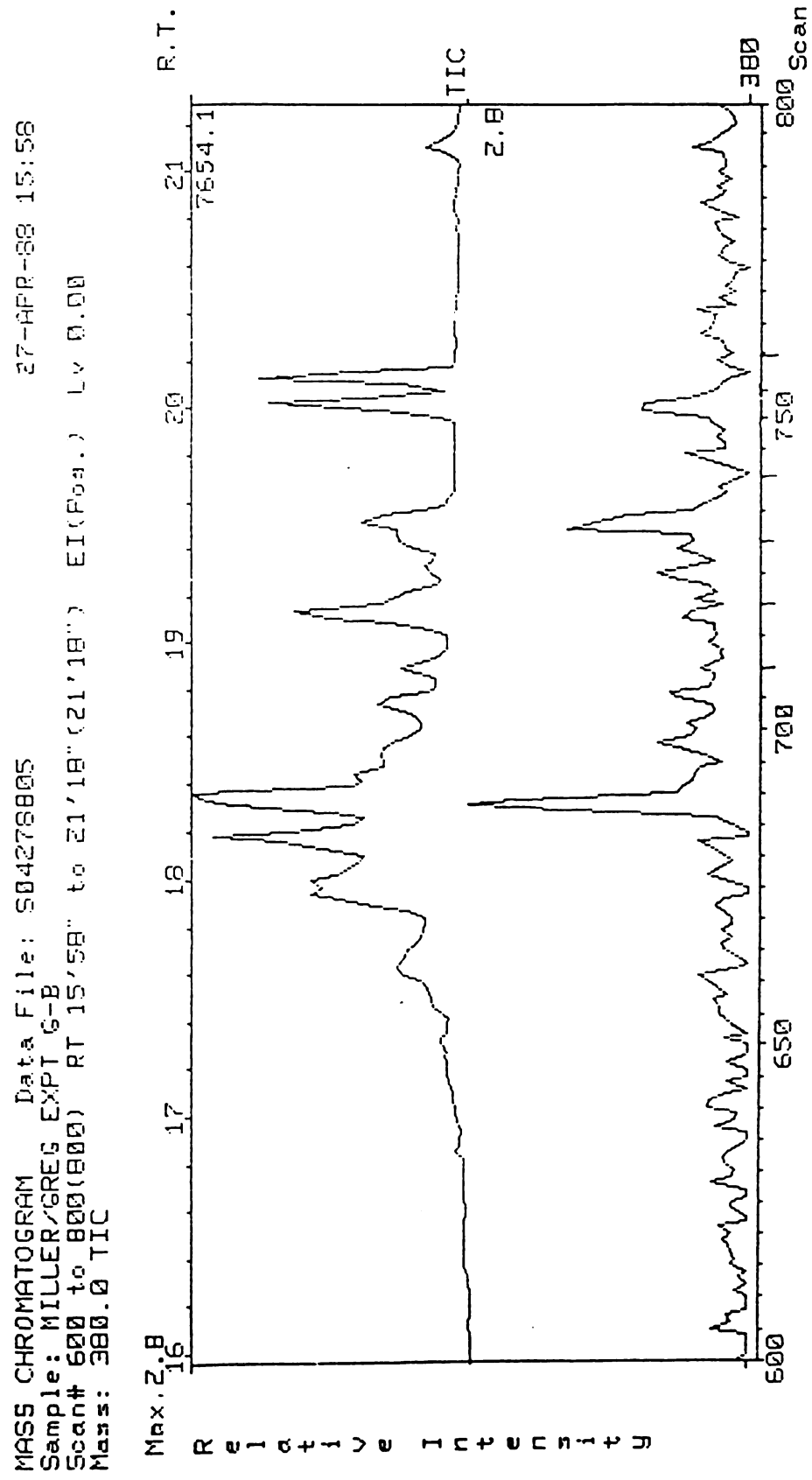

Figure B-4. Specific Ion Trace for m/z 380

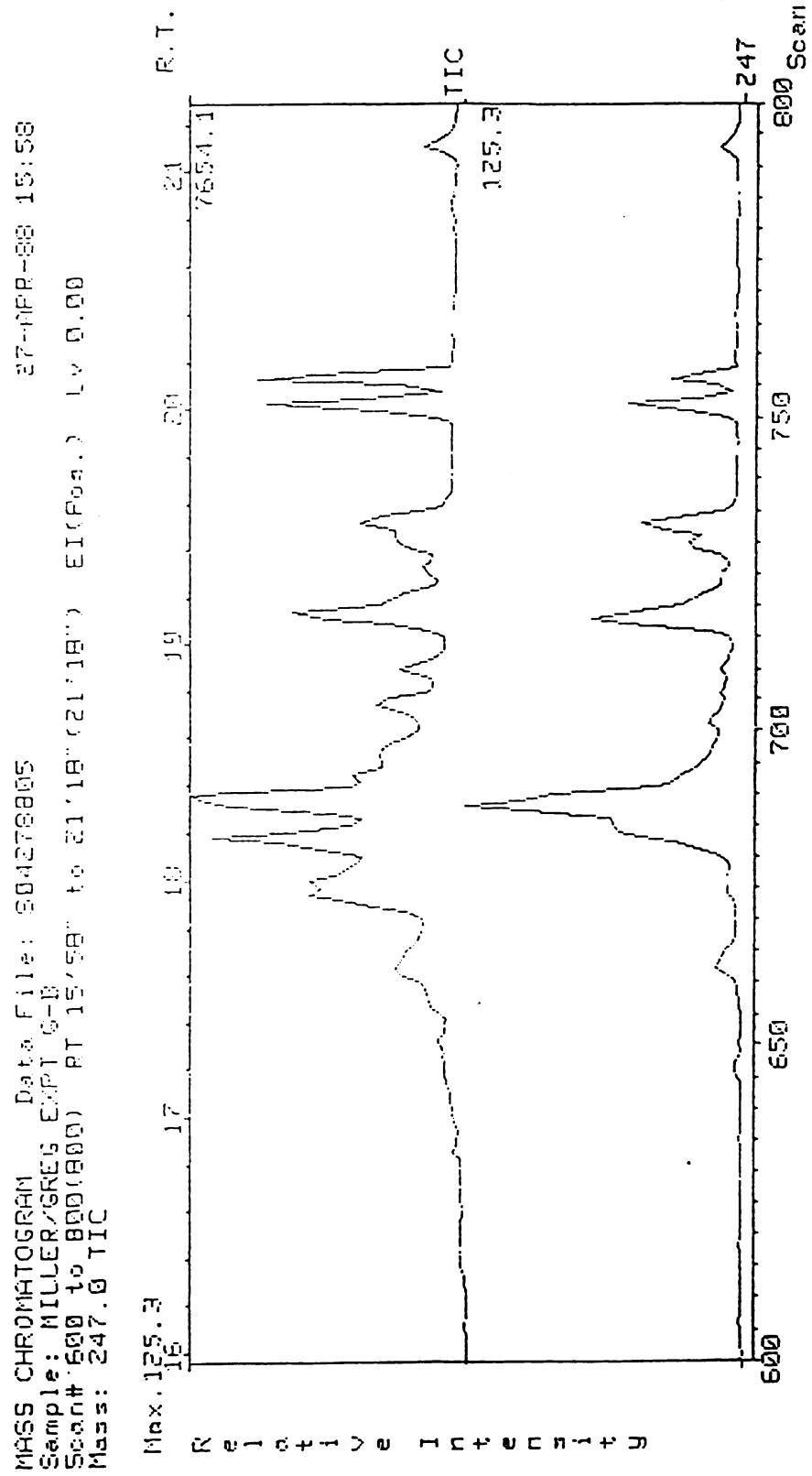

Figure B-5. Specific Ion Trace for m/z 247

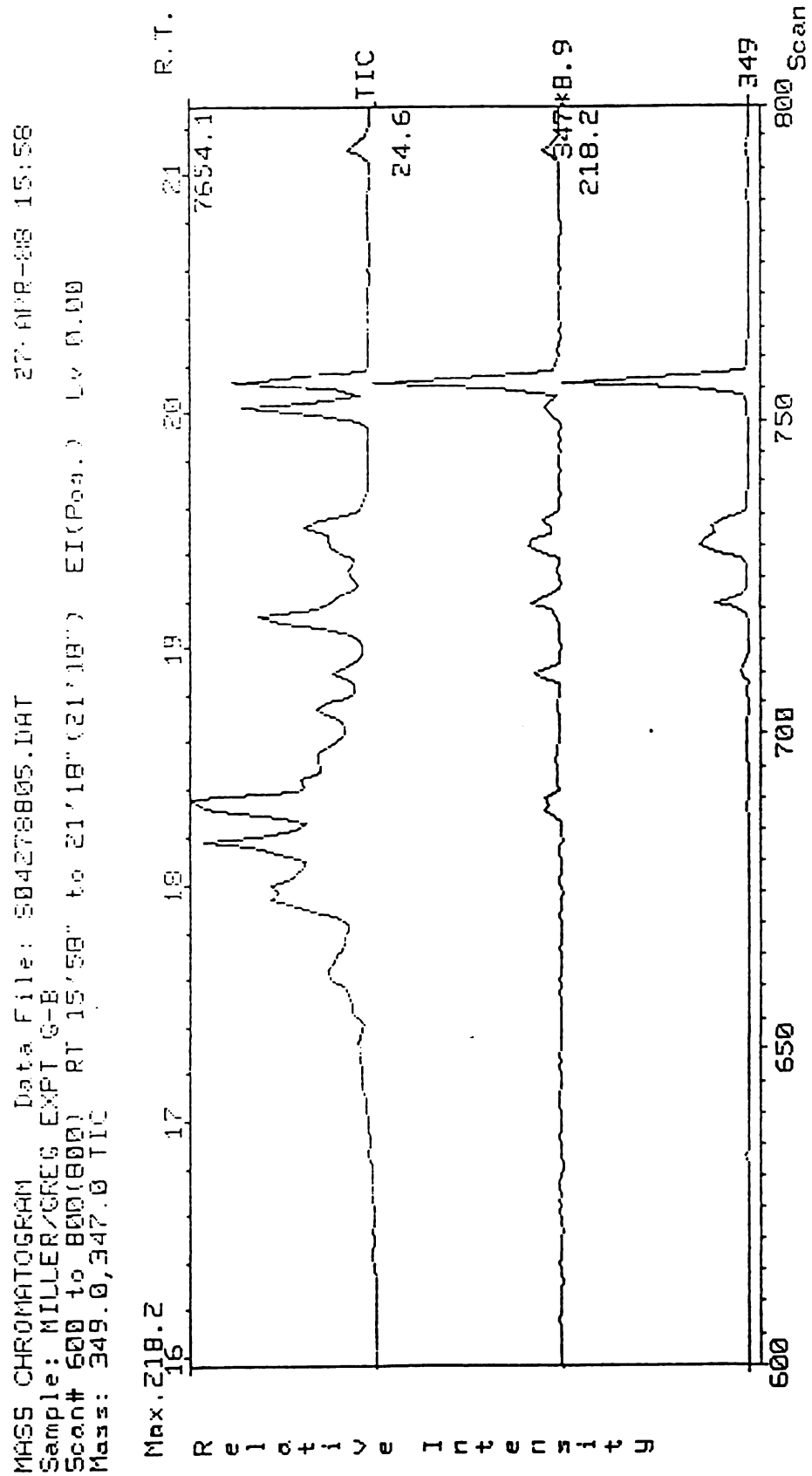

Figure B-6. Specific Ion Traces for m/z 349 and m/z 347

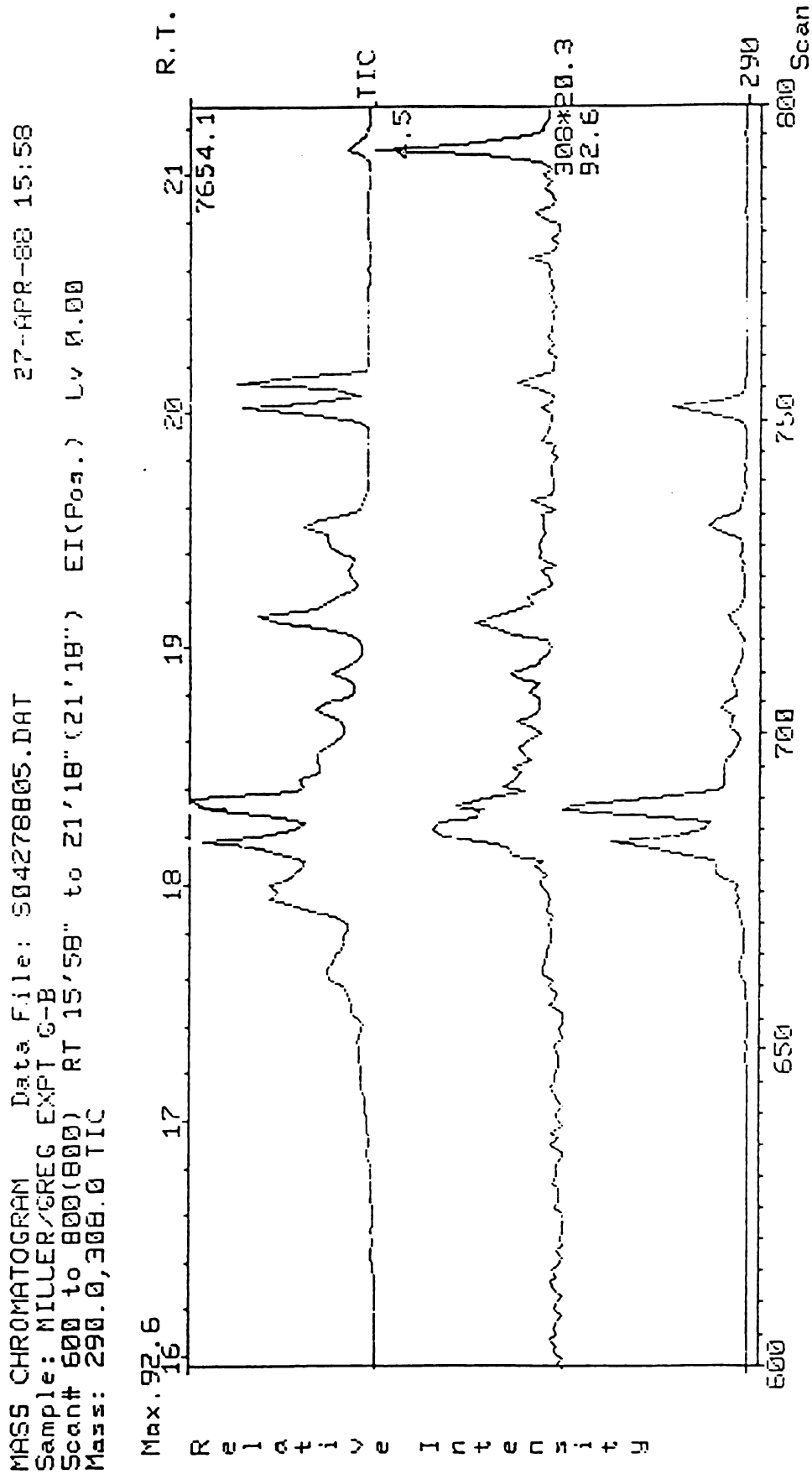

Figure B-7. Specific Ion Traces for m/z 290 and m/z 308

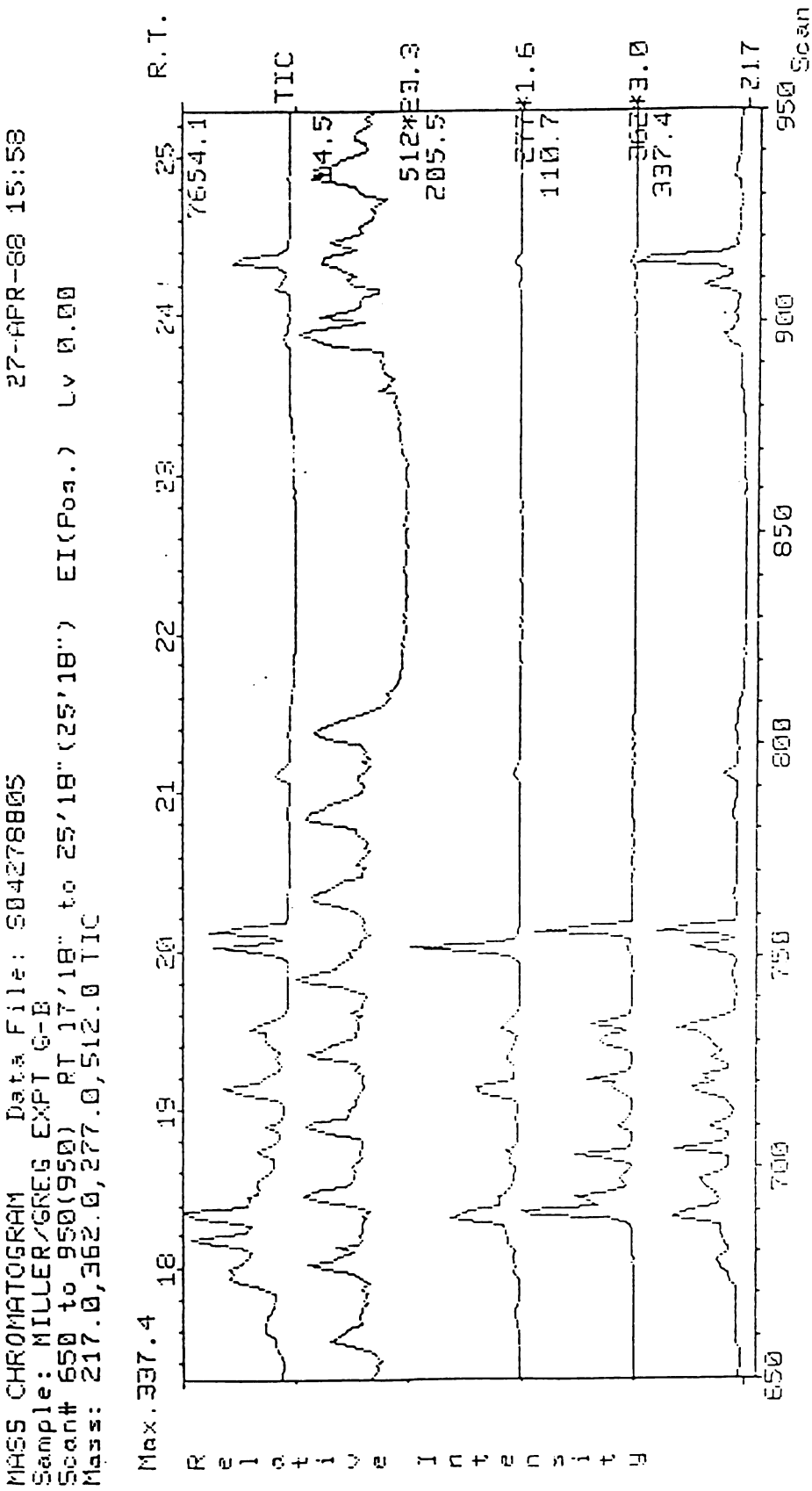

Figure B-8. Specific Ion Trace for m/z 512